

cy 3

See the



PARAMETERS AFFECTING LASER VELOCIMETER TURBULENCE SPECTRA MEASUREMENTS

J. A. Asher, P. F. Scott, and J. C. Wang

RESEARCH AND DEVELOPMENT CENTER
GENERAL ELECTRIC COMPANY
SCHENECTADY, NEW YORK 12301

October 1974

Final Report for Period June 1, 1972 — April 30, 1973

Approved for public release; distribution unlimited.

PROPERTY OF U. S. AIR FORCE
AEDC LIBRARY
F40600-75-C-0001

Prepared for

ARNOLD ENGINEERING DEVELOPMENT CENTER
AIR FORCE SYSTEMS COMMAND
ARNOLD AIR FORCE STATION, TENNESSEE 37389

NOTICES

When U. S. Government drawings specifications, or other data are used for any purpose other than a definitely related Government procurement operation, the Government thereby incurs no responsibility nor any obligation whatsoever, and the fact that the Government may have formulated, furnished, or in any way supplied the said drawings, specifications, or other data, is not to be regarded by implication or otherwise, or in any manner licensing the holder or any other person or corporation, or conveying any rights or permission to manufacture, use, or sell any patented invention that may in any way be related thereto.

Qualified users may obtain copies of this report from the Defense Documentation Center.

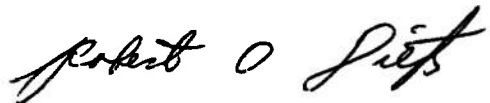
References to named commercial products in this report are not to be considered in any sense as an endorsement of the product by the United States Air Force or the Government.

APPROVAL STATEMENT

This technical report has been reviewed and is approved.



MELVIN L. GUIOU
Captain, USAF
Research and Development
Division
Directorate of Technology



ROBERT O. DIETZ
Director of Technology

UNCLASSIFIED

SECURITY CLASSIFICATION OF THIS PAGE (When Date Entered)

REPORT DOCUMENTATION PAGE		READ INSTRUCTIONS BEFORE COMPLETING FORM
1. REPORT NUMBER AEDC-TR-74-54	2. GOVT ACCESSION NO.	3. RECIPIENT'S CATALOG NUMBER
4. TITLE (and Subtitle) PARAMETERS AFFECTING LASER VELOCIMETER TURBULENCE SPECTRA MEASUREMENTS		5. TYPE OF REPORT & PERIOD COVERED Final Report for Period 6/1/72 to 4/30/73
		6. PERFORMING ORG. REPORT NUMBER
7. AUTHOR(s) J. A. Asher, P. F. Scott, and J. C. Wang		8. CONTRACT OR GRANT NUMBER(s) F40600-72-C-0013
9. PERFORMING ORGANIZATION NAME AND ADDRESS Research and Development Center General Electric Company Schenectady, New York 12301		10. PROGRAM ELEMENT, PROJECT, TASK AREA & WORK UNIT NUMBERS Program Element 65802F
11. CONTROLLING OFFICE NAME AND ADDRESS Arnold Engineering Development Center (DYFS) Air Force Systems Command Arnold Air Force Station, Tennessee 37389		12. REPORT DATE October 1974
		13. NUMBER OF PAGES 89
14. MONITORING AGENCY NAME & ADDRESS (if different from Controlling Office)		15. SECURITY CLASS. (of this report) UNCLASSIFIED
		15a. DECLASSIFICATION/DOWNGRADING SCHEDULE N/A
16. DISTRIBUTION STATEMENT (of this Report) Approved for public release; distribution unlimited.		
17. DISTRIBUTION STATEMENT (of the abstract entered in Block 20, if different from Report)		
18. SUPPLEMENTARY NOTES Available in DDC		
19. KEY WORDS (Continue on reverse side if necessary and identify by block number) Laser velocimeter Turbulence spectra measurements		
20. ABSTRACT (Continue on reverse side if necessary and identify by block number) This investigation developed a random sampling theory appropriate to utilizing the laser velocimeter optical technique for measurement of turbulence velocity spectra. The theory developed indicates that while undistorted turbulence spectra may be obtained from such a sampling technique, a wideband noise is superimposed on these spectra. The magnitude of this noise was found to be indirectly proportional to the mean particle arrival rate. The required data acquisition rate was found to be dependent on the spectral dynamic		

UNCLASSIFIED

SECURITY CLASSIFICATION OF THIS PAGE(When Data Entered)

20. ABSTRACT (cont'd)

range and bandwidth of the flow phenomena. As part of this investigation, various other parameters were studied to define their effect on spectra measurements derived from the laser velocimeter technique. These include the studies of particle relaxation times and processor-borne errors.

APSC
Arnold AFB Tex

UNCLASSIFIED

SECURITY CLASSIFICATION OF THIS PAGE(When Data Entered)

PREFACE

This technical report covers work performed under Contract No. F40600-72-0013 for the Arnold Engineering Development Center, Arnold Air Force Station, Tennessee. The work was performed between June 1, 1972 and April 30, 1973 by the Research and Development Center of the General Electric Company in Schenectady, New York. The program was under the direction of Lt Col J. R. Taylor, Arnold Engineering Development Center, DYR.

The reproducibles used in the reproduction of this report were supplied by the authors.

TABLE OF CONTENTS

<u>Section</u>		<u>Page</u>
1	INTRODUCTION	9
2	THEORETICAL AND EXPERIMENTAL STUDY OF PARTICLE DYNAMICS	11
	Fluid-Particle Dynamics in Turbulent Flow	11
	Theoretical Investigation of Shock-Particle Relaxation Times	15
	Experimental Investigation of Shock-Particle Relaxation Times	17
3	LASER VELOCIMETER PROCESSOR ACCURACY	28
	Doppler Burst Signature Modeling	28
	Signature Model in the Frequency Space.	33
	Pedestal Removal Filter Errors	34
	Limiter Threshold Error	36
	Summary of Laser-Velocimeter Criteria	38
4	VELOCITY POWER SPECTRA ESTIMATION FROM LASER VELOCIMETER DATA.	40
	Random Sampling Probability Model	40
	Spectra Theory Based on Random Sampling	40
	Spectra Measurements at High Data-Acquisition Rates	42
	Practical Interpretation for Turbulence Spectra Measurement	47
	Applicability of Counter and Frequency Tracker Laser Velocimeter Processors to Spectral-Analysis Measurement Theory	49
5	EXPERIMENTAL CONFIRMATION OF LASER- VELOCIMETER SPECTRAL ANALYSIS THEORY	50
	Verification of Sampling Probability Distribution Assumption	50
	Experimental Determination of Signal Properties of Doppler Burst	58
	Electronic Simulation of Spectra Analysis by Random Sampling	62
	Experimental Attempt to Obtain Laser Velocimeter Turbulence Spectra Measurements	63
	Experimental Setup for Spectra Analysis	67
	Effect of Sample-and-Hold Output Circuit on Spectra Measurements	72
	Monitoring Data Acquisition Rate.	75

TABLE OF CONTENTS (Cont'd)

<u>Section</u>		<u>Page</u>
6	SUMMARY AND CONCLUSIONS	77
7	REFERENCES	78
<u>Appendix</u>		
I	LASER-VELOCIMETER OPTICAL SETUP AND PROCESSOR	80
	Dual-Scatter Optical Method	80
	Laser-Velocimeter Processor	81

LIST OF ILLUSTRATIONS

<u>Figure</u>		
1	Particle Turbulence-Velocity Response for AEDC Tunnel A ($P_o = 51$ psia; $T_o = 680^\circ\text{R}$) at Mach Numbers 3.2 and 5.7, Particle Specific Gravity 3.5 (Alumina Powder).	14
2	Particle Turbulence-Velocity Response for AEDC Tunnel B ($P_o = 850$ psia; $T_o = 1350^\circ\text{R}$) at Mach Number 7.9 and Particle Specific Gravity 3.5 (Alumina Powder) . . .	14
3	Particle Turbulence-Velocity Response Forecast for AEDC Tunnel C ($P_o = 2000$ psia; $T_o = 2350^\circ\text{R}$) at Mach Number 10.6 and Particle Specific Gravities = 3.5 and 0.5	15
4	Determination of Relaxation Time Constant for a Step Change in Velocity	16
5	Laser Shadowgraph of 0.75-Inch-Diameter Underexpanded Air Jet. Stagnation Pressure = 80 Psig; Jet Mach Number = 1.87	17
6a	Experimental Setup for Particle Relaxation Investigation .	18
6b	Jet and Reservoir for Particle Relaxation Investigation. .	19
7	Experimental Results of Mach Disk Breadth, s , Versus Jet Mach Number ($P_{\text{ambient}} = 14.6$ psia)	20
8	Experimental Results of Mach Disk Standoff Distance, l , Versus Jet Mach Number ($P_{\text{ambient}} = 14.6$ psia).	20
9	Theoretical Fluid Velocity Change Across Mach Disk Versus Jet Mach Number ($P_{\text{ambient}} = 14.6$ psia).	23

LIST OF ILLUSTRATIONS (Cont'd)

<u>Figure</u>		<u>Page</u>
10	Schematic of Particle Relaxation Behavior at Mach Number = 1.72 (Assuming No Axial Velocity Acceleration Upstream of Mach Disk).	23
11	Fluidized Particle Bed	24
12	Particle-Shock Experimental Results: Colloidal Alumina (2μ) -- Relaxation Time = $40\ \mu\text{sec}$; Axial Relaxation Distance = 0.60.	25
13	Particle-Shock Experimental Results with Linde Type A Alumina (0.3μ) -- Relaxation Time = $0.65\ \mu\text{sec}$; Axial Relaxation Time = 0.01	25
14	Particle-Shock Experimental Results: Cab-O-Sil (0.05μ) -- Relaxation Time = $0.02\ \mu\text{sec}$; Axial Relaxation Distance = 0.002	26
15	Schematic of Laser Velocimeter Counter Processor (Time Domain)	28
16a	Geometry of Beam Intersection	31
16b	Disk Integration on y Axis	31
17	Gain Factor of Cosine Term	32
18	Fourier Transform of Laser Doppler Velocimeter Burst	33
19	Graph of High-Passed Filter Pulse of the Form e^{-t^2} Where $\omega = \alpha$ (Cutoff).	34
20	Baseline Ripple Error in High-Pass Filter	36
21	Origin of Phase Error in Measuring Zero Crossing of Doppler Modulation.	37
22	Schematic of Continuous Velocity and Laser-Velocimeter Sampled Signals	41
23	Laser-Velocimeter Spectral Analysis for Various Seeding Rates	44
24	Example of Required Seeding for Narrowband Spectral Information	45
25	Example of Required Wideband Spectra Information	46
26	Signal Analysis Scheme for Laser Velocimeter Spectra	47
27	Probability of Particle Multiplicity	48

LIST OF ILLUSTRATIONS (Cont'd)

<u>Figure</u>		<u>Page</u>
28	Schematic of Instrumentation for Experimental Verification of Random Sampling Assumption	50
29a	Exponential Transformation of Particle Interarrival Time ($\tau = 1 \mu\text{sec}$; $\lambda = 143.3 \text{ K/sec}$).	53
29b	Exponential Transformation of Particle Interarrival Time ($\tau = 1 \mu\text{sec}$; $\lambda = 138.6 \text{ K/sec}$).	53
29c	Exponential Transformation of Particle Interarrival Time ($\tau = 1 \mu\text{sec}$; $\lambda = 132.4 \text{ K/sec}$).	54
29d	Exponential Transormation of Particle Interarrival Time ($\tau = 1 \mu\text{sec}$; $\lambda = 112.0 \text{ K/sec}$).	54
30a	Autocorrelation of Particle Interarrival for Record in Figure 29a	55
30b	Autocorrelation of Particle Interarrival for Record in Figure 29b	55
30c	Autocorrelation of Particle Interarrival for Record in Figure 29c	56
31a	Spectra of Particle Interarrival Times for Record in Figure 29a	56
31b	Spectra of Particle Interarrival Times for Record in Figure 29b	57
31c	Spectra of Particle Interarrival Times for Record in Figure 29d	57
32a	Transient Recorder Output of a Doppler Burst with High Contrast (Single Small Particle)	59
32b	Autocorrelation of Doppler Burst with High Contrast . . .	59
32c	Magnitude of Fourier Coefficients with Doppler Burst of High Contrast	60
33a	Transient Recorder Output of a Doppler Burst with Fair Contrast.	60
33b	Autocorrelation of Doppler Burst with Fair Contrast . . .	61
33c	Magnitude of Fourier Coefficients with Doppler Burst of Fair Contrast	61
34	Experimental Setup	62

LIST OF ILLUSTRATIONS (Cont'd)

<u>Figure</u>		<u>Page</u>
35	Electronic Simulation of Laser-Velocimeter Spectra Measurements from Random-Time Sampled White Noise of Bandwidth 158 Hertz	64
36	Electronic Simulation of Laser-Velocimeter Spectra Measurements from Random-Time Sampled White Noise of Bandwidth 468 Hertz	65
37	Electronic Simulation of Laser-Velocimeter Spectra Measurements from Random-Time Sampled White Noise of Bandwidth 165 Hertz	65
38	Electronic Simulation of Laser-Velocimeter Spectra Measurements from Random-Time Sampled White Noise of Bandwidth 6485 Hertz.	66
39	Electronic Simulation of Laser-Velocimeter Spectra Measurements from Random-Time Sampled White Noise of Bandwidth 25,700 Hertz	66
40	Schematic Diagram of Laser-Velocimeter Turbulence Spectra Measurements Setup.	67
41	Typical Laser-Velocimeter Sample-and-Hold Output at Two Data Acquisition Rates	68
42	Hot-Wire-Turbulence Power Spectrum Results from 3/4-Inch-Diameter Air Jet ($M = 0.15$; $X/D = 2$; $Y/D = 0.2$)	69
43	Hot-Wire-Turbulence Power Spectrum Results from 3/4-Inch-Diameter Air Jet ($M = 0.15$; $X/D = 2$; $Y/D = 0.4$)	69
44	Hot-Wire-Turbulence Power Spectrum Results from 3/4-Inch-Diameter Air Jet ($M = 0.15$; $X/D = 6$; $Y/D = 0.2$)	70
45	Hot-Wire-Turbulence Power Spectrum Results from 3/4-Inch-Diameter Air Jet ($M = 0.15$; $X/D = 6$; $Y/D = 0.2$)	70
46	Hot-Wire-Turbulence Power Spectrum Results from 3/4-Inch-Diameter Air Jet ($M = 0.15$; $X/D = 6$; $Y/D = 0.4$)	71
47	Hot-Wire-Turbulence Power Spectrum Results from 3/4-Inch-Diameter Air Jet ($M = 0.15$; $X/D = 10$; $Y/D = 0$)	71
48	Typical Laser-Velocimeter Narrowband Power Spectra Output from HP5451 Fourier Analyzer (Sample-and-Hold Bias Present)	72
49	Typical Laser Velocimeter One-Third-Octave Power Spectra Output from General Radio Analyzer (Sample-and-Hold Bias Present)	73

LIST OF ILLUSTRATIONS (Cont'd)

<u>Figure</u>		<u>Page</u>
50	Spectra of Unsampled Narrowband Process for Study of Sample-and-Hold Bias	74
51	Spectra of Narrowband Process Sampled by a Poisson Impulse Sequence for Study of Sample-and-Hold Bias . . .	74
52	Same Process and Sampling as Figure 51 with the Addition of a Sample-and-Hold Simulation to Study its Low-Frequency Bias of Spectra Data	75
53	Schematic Setup of Turbulence-Power Spectra System . .	76
54	Dual-Scatter or Differential Doppler Arrangement	80
55	Interference Fringes Formed by Two Coherent Crossed Beams	81
56	Laser Velocimeter Data Reduction	82
57	Timing Diagram for Laser Velocimeter Processor . . .	84
58	Typical Computer Readout from a Laser Doppler Velocimeter Signal Processor	86

LIST OF TABLES

<u>Table</u>		
1	Theoretical Particle Dynamics in High-Speed Flow Facilities at Arnold Engineering Development Center. . .	13
2	Results of Particle-Shock Interaction.	22
3	Tabulation of Filtered Noise Data	64
	Nomenclature	87

Section 1

INTRODUCTION

This report describes a study to define the feasibility of using the laser velocimeter optical technique (LV) to measure the turbulence-velocity power spectra.

Until recently, hot-wire anemometry was virtually the only means of measuring the turbulence level and associated turbulence power spectra under a variety of flow conditions. However, this technique becomes increasingly difficult to employ at Mach numbers above 0.7 and requires a probe immersed in the flow which often causes disturbances, may be difficult to deploy, and is prone to breakage.

The laser Doppler velocimeter offers the possibility of quantity measurement of mean and turbulence flow at Mach numbers limited primarily by the tracking particle dynamics. Further, no penetration into the flow is required; this can be of crucial importance in many applications. For these reasons, there has been widespread interest among research organizations in exploring the utility of the laser Doppler technique for a variety of flow situations.

At the General Electric Company, laser velocimetry has been under continuous development since 1966. This work has involved the development of a high data rate, counter-type LV processor (Refs. 1 to 3) and its utilization in varied applications (Refs. 4 to 7). A description of the laser velocimeter optical setup and LV processor which were employed in the investigation reported here is found in Appendix I, "Laser Velocimeter Optical Setup and Processor."

The study described here represents a natural outgrowth of this previous work where the time-dependent nature of the velocity data is now utilized to provide a measurement of the turbulence power spectra. This is a marked departure from the relatively simple method of obtaining time-averaged mean and turbulence velocity measurements. For deducing the turbulence power spectra, the velocity data train is recorded and utilized in the same time sequence in which it occurred. The simple reduction of these data to turbulence frequency spectra and power spectra is complicated for the following reasons:

- Measurement of velocity results only when a particle passes through the scattering volume (beam intersection volume).
- This particle passage may be expected to be randomly spaced in time.
- The average number of particle passages depends on the concentration of the particle seed. The percent of processor borne inhibits because of poor-quality input signals and the optical setup, which defines the spatial resolution of the scattering volume.

- Particle dynamics may degrade the ability of the particle to follow turbulent or accelerating flow.

Thus, the turbulence spectra as obtained from the LV technique are many-faceted in the parameters which affect their measurement. These include the particle dynamics, LV optical setup, and electronic processor for the measurement of the instantaneous velocity as well as the postprocessor for spectrum analysis. This investigation dealt with each of these. The necessary guidelines on which accurate LV spectra measurements may be based were developed. In particular, this study involved the analytical and experimental determination of particle relaxation times to quantify the ability of the seed to follow the fluid. The LV processor accuracy is analyzed from the standpoints of the high-pass filter and voltage limiter responses.

The major emphasis of this study concerned development of the theoretical analysis for measurement of turbulence frequency and power spectra.

This analysis takes into account the randomly time-spaced LV velocity measurements and provides the expected form and associated error of the resulting output spectra. The primary thrust of this theory involves high data rates, with commensurately high seed concentrations. It will also be shown that, based on the same analysis, spectra measurements may be made from far lower data rates. In such a case, the test time is significantly longer and the form of the spectral estimator and its variance has not yet been identified.

An electronic simulation confirming this theory is also provided. An attempt was made to compare the power spectra of the hot-wire and LV techniques in a subsonic jet flow. That experiment could not be satisfactorily completed within the course of this contract; various difficulties uncovered during the course of the experimental work are reported here. One such problem concerns the lower frequency bias of the sample-and-hold output circuit which is found on most LV processors. The determination of the average data rate for the slice of data being spectrum-analyzed was found to be necessary. These problems have since been overcome, and their solutions are reported here.

From this study one may be confident that with proper precautions (care in choice of seed particles and sufficient data rate) the laser velocimeter optical technique is feasible for the measurement of the turbulence power spectra.

Section 2

THEORETICAL AND EXPERIMENTAL STUDY OF PARTICLE DYNAMICS

FLUID-PARTICLE DYNAMICS IN TURBULENT FLOW

Use of the laser Doppler velocimeter to measure fluid velocity requires that seed particles in the flow act as light scatterers. If the flow is accelerating or turbulent, the question arises as to whether the particles are actually traveling at the fluid velocity. For gas flows, a gross density mismatch usually exists between the particle and the gas, with the result that very small particles must be used to follow the flow. The upper limit to the particle size is determined by the degree of accuracy that the particle must follow in the flow. For turbulent flow, the upper size limit is set by the maximum frequency of unsteadiness in the flow that is to be measured.

To assume that a particle follows the flow fairly accurately implies that the relative velocity of the fluid, v_f , and the particle, v_p , are small. In turn, this implies a low Reynolds number ($R < 1$) may be assumed and that Stokes' drag law applies. For a spherical particle of density, ρ_p , and diameter, d , in a fluid of dynamic viscosity, μ_f , the equation of motion may be written

$$\frac{\pi}{6} d^3 \rho_p \frac{dv_p}{dt} = 3\pi\mu_f d (v_f - v_p)$$

or

$$\frac{dv_p}{dt} + \gamma v_p = \gamma v_f \quad (1)$$

where $\gamma = 18\mu_f/\rho_p d^2$ and can be thought of as an inverse measure of the particle relaxation time, t_r .

The resultant equation of motion (Equation 1) has been simplified by the following additional assumptions:

- Transverse pressure gradients are negligible
- External potential forces (gravity, E-M, etc.) are negligible
- Transverse velocity gradient is negligible
- Inertia force of fluid is small
- Effect of acceleration on viscous drag is negligible

In most cases these assumptions are quite valid and the resultant linearized equation can be readily solved.

It is appropriate to discuss one other aspect of Equation 1 which is often overlooked. This equation is written in the Eulerian reference frame, where

an observer is stationary and watches the particle move relative to a moving fluid. Most instrument techniques, the laser velocimeter included, takes on an Eulerian point of view. On the other hand, the turbulent particulate movement or particle dynamics in the fluid has perhaps the greatest meaning in the Lagrangian reference frame, where the fluid is stationary and the particle moves.

It appears that the Eulerian approach is on the conservative side in establishing the particle frequency response. Therefore the results of the turbulence/particle interaction cited in this report are perhaps too stringent if this is the only criterion placed on the particle dynamics. As will be shown, a more significant problem in particle dynamics exists in the measurement of the mean and turbulence velocity, not to mention the power spectra, where shock waves exist in the flow.

Typically in a high-Mach-number tunnel facility, the gas in the test section is at a low density. Thus the isentropic expansion to high-Mach-number conditions, even with a high stagnation density (high stagnation pressure and temperature) yield rarefied conditions at high supersonic and hypersonic conditions. This may be seen in Table 1, where the flow conditions of typical wind tunnels at the Arnold Engineering Development Center are provided (Refs. 8 and 9). For a hypersonic Mach number of 10.6 in Tunnel C, the mean free path (average distance between intermolecular collisions) has increased two orders of magnitude. The force balance generated between the particle inertia and drag results from the fluid molecule-particle interaction. In a rarefied gas where a large mean free path exists, the particle inertia dominates the subsequent particle movement. This is accounted for by the Cunningham Correction to Stokes' drag law, where the relaxation time for rarefied conditions becomes (Ref. 10)

$$\gamma = \frac{18\mu_r}{\rho_p d_p^2 \left(1 + \frac{KL}{d_p}\right)} = \frac{1}{t_r} \quad (2)$$

Here K is equal to 1.8 for air, and L is the mean free path. It may be seen that for a small mean free path, as in the case of a continuum, the relaxation time, t_r , approaches that given by the equations of motion and the Stokes drag law.

A solution to Equation 1 may be obtained by defining the fluid velocity as

$$v_f = v_o + v_f^i \sin \omega t$$

where the v_f^i and ω are the turbulent magnitude and angular frequency of the fluid, respectively. It may be shown that the turbulence velocity/amplitude ratio (equal to one when the particle fully follows the flow) is given as:

$$\left[\frac{v_p^i}{v_f^i} \right]_{\max} = \frac{1}{1 + \left(\frac{\omega}{\gamma} \right)^2}^{1/2} \quad (3)$$

Table 1

**THEORETICAL PARTICLE DYNAMICS IN HIGH-SPEED FLOW FACILITIES
AT ARNOLD ENGINEERING DEVELOPMENT CENTER**

AEDC Tunnel	Free Stream Temperature (°R)	Free Stream Mach Number	Mean Free Path λ/λ_{ref}	Particle				T _e (°R)	P _e (psia)
				Specific Gravity	Diameter (d _p)	Relaxation Time, t _r (μsec)	Associated Relaxation Distance, 0.63 U _t t _r (in.)		
C	100	10.6	107	3.5	0.05	169	6.7	2350	2000
					0.10	339	13.3		
					0.20	679	26.7		
					0.50	1,707	67.1		
					1.00	3,444	135.3		
					5.00	18,382	722.3		
C	100	10.6	107	0.5	0.05	24	1.0	2350	2000
					0.10	46	1.9		
					0.20	97	3.8		
					0.50	244	9.6		
					1.00	492	19.3		
					5.00	2,628	103.2		
C	348	5.4	5	3.5	0.05	4	0.2	2350	2000
					0.10	8	0.3		
					0.20	18	0.7		
					0.50	50	1.9		
					1.00	116	4.3		
					5.00	1,230	45.6		
D	100	4.6	19	3.5	0.05	30	0.5	530	60
					0.10	62	1.1		
					0.20	125	2.2		
					0.50	321	5.5		
					1.00	672	11.6		
					5.00	4,523	77.7		
B	348	3.8	2	3.5	0.05	1	0.0	1350	850
					0.10	3	0.1		
					0.20	7	0.2		
					0.50	22	0.6		
					1.00	60	1.6		
					5.00	953	25.0		
B	100	7.9	36	3.5	0.05	57	1.7	1350	850
					0.10	115	3.4		
					0.20	231	6.8		
					0.50	587	17.2		
					1.00	1,202	35.2		
					5.00	7,173	210.1		
A	100	5.7	20	3.5	0.05	31	0.7	750	200
					0.10	62	1.3		
					0.20	126	2.7		
					0.50	325	6.9		
					1.00	679	14.4		
					5.00	4,557	96.3		
A	348	2.4	1	3.5	0.05	0	0.0	750	200
					0.10	1	0.0		
					0.20	4	0.1		
					0.50	15	0.3		
					1.00	47	0.8		
					5.00	888	14.8		
A	225	3.2	7	3.5	0.05	7	0.1	680	51
					0.10	14	0.3		
					0.20	30	0.5		
					0.50	81	1.4		
					1.00	181	3.2		
					5.00	1,647	29.1		

The particle turbulence frequency response of the above equation is shown graphically in Figures 1 to 3 for conditions which apply directly to Arnold

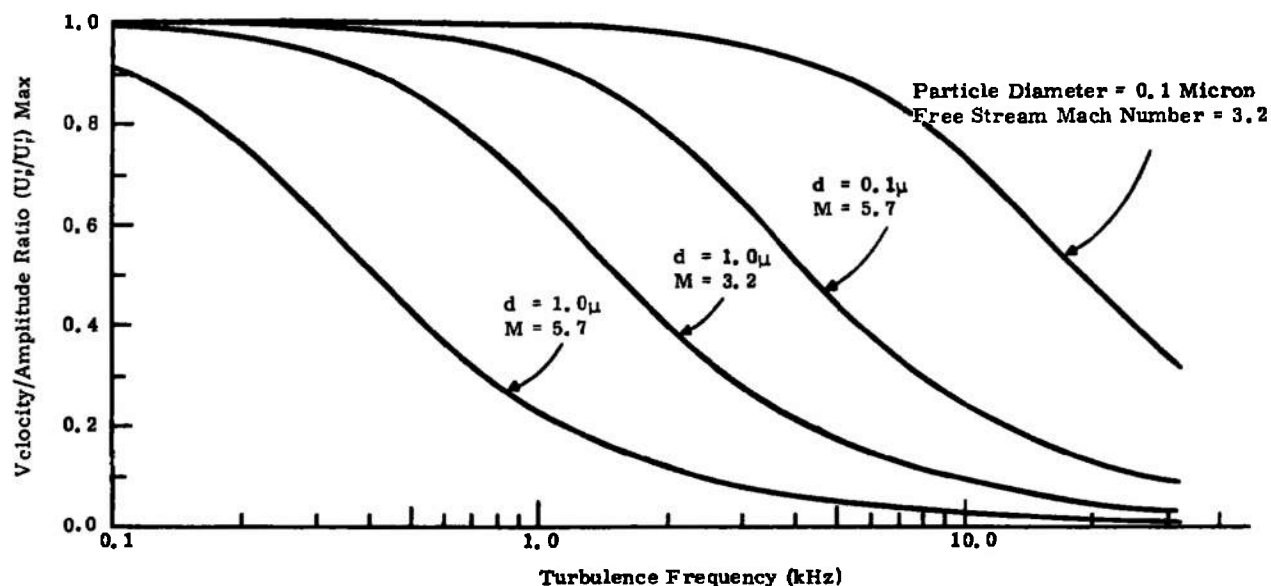


Figure 1. Particle Turbulence-Velocity Response for AEDC Tunnel A ($P_0 = 51$ psia; $T_0 = 680^\circ\text{R}$) at Mach Numbers 3.2 and 5.7, Particle Specific Gravity 3.5 (Alumina Powder)

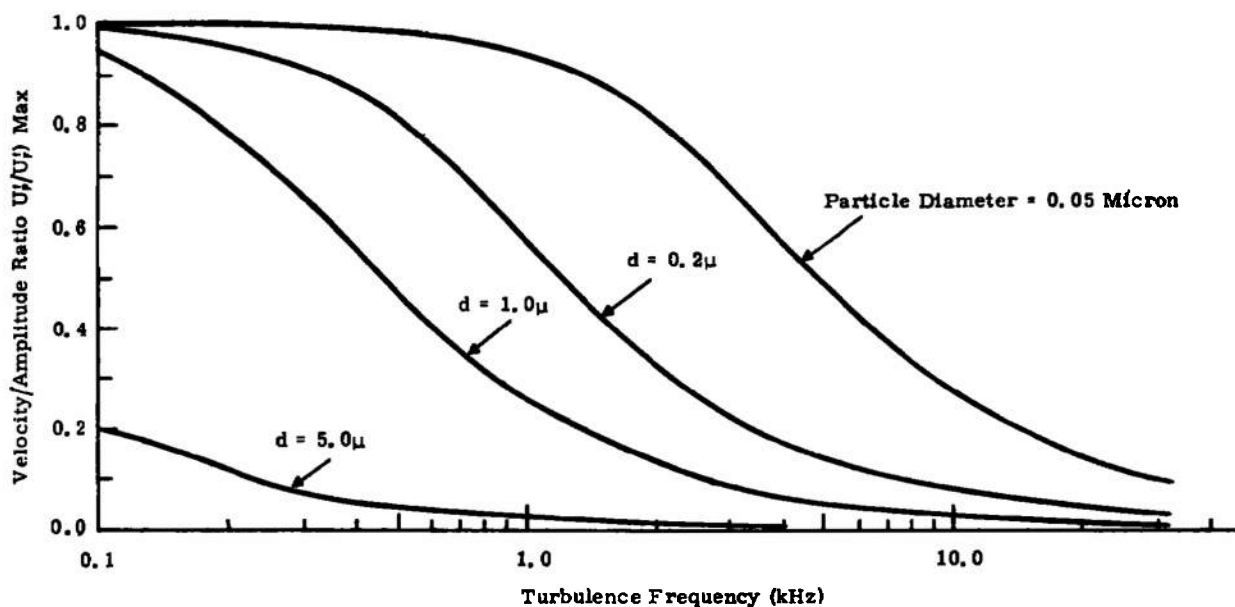


Figure 2. Particle Turbulence-Velocity Response for AEDC Tunnel B ($P_0 = 850$ psia; $T_0 = 1350^\circ\text{R}$) at Mach Number 7.9 and Particle Specific Gravity 3.5 (Alumina Powder)

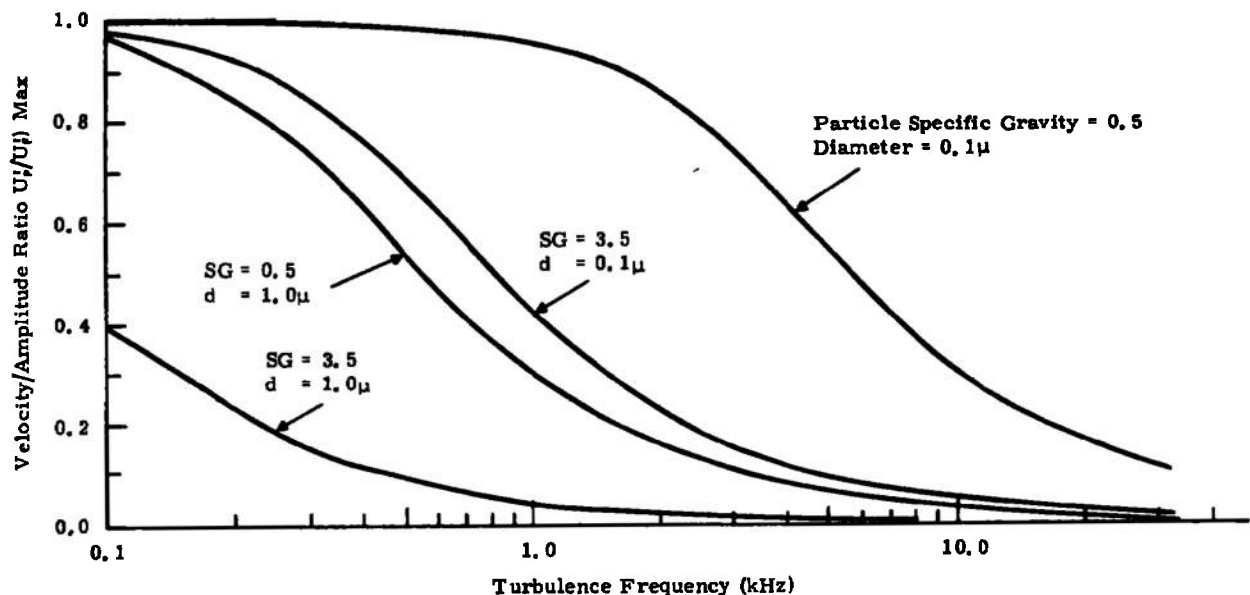


Figure 3. Particle Turbulence-Velocity Response Forecast for AEDC Tunnel C ($P_o = 2000$ psia; $T_o = 2350^\circ\text{R}$) at Mach Number 10.6 and Particle Specific Gravities = 3.5 and 0.5

Engineering Development Center super- and hypersonic facilities. The velocity/amplitude ratio is seen to drop off rapidly with increasing turbulence frequency. In Figure 1, $d_p = 0.1$, $M_\infty = 3.2$; for $[v_i'/v_i']_{\max} = 0.9$, the turbulence frequency is 5 kilohertz. The expected much-degraded frequency response in a rarefied gas (Figure 3, $M_\infty = 10.6$) is also quite apparent.

THEORETICAL INVESTIGATION OF SHOCK-PARTICLE RELAXATION TIMES

The presence of shock structure in a flow field generates a step deceleration of the fluid traversing it. The inertia of the particle serves to build in a time delay or relaxation time for the particle to once again approach the fluid velocity.

The imposition of a shock/particle interaction is the most severe condition, since it is close to a step velocity change of infinite slope. It is the definition for which the particle relaxation time, per Equation 2, applies directly. In flows of high Mach number the presence of a bluff body results in associated strong shocks. Thus, the usefulness of the relaxation time is enhanced.

The associated relaxation distance listed in Table 1 has been defined as 63 percent of the free stream velocity times the relaxation time (Figure 4). This definition would apply to a moving shock passing through a stationary fluid and thereby accelerating the fluid to U_∞ . In this case, the velocity difference is between a stationary flow and a fluid traveling at the free stream velocity. There is no need to make the assumption of a particle being initially at

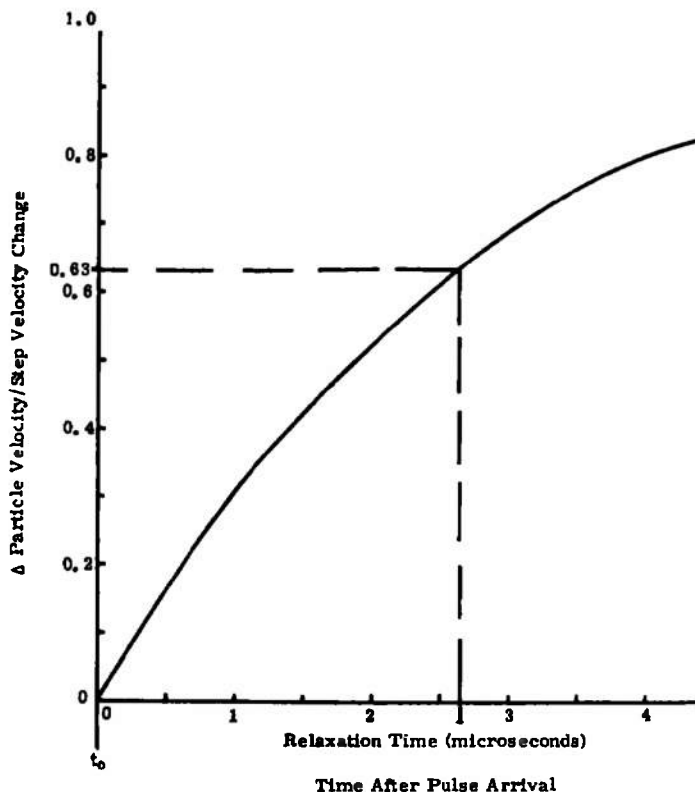


Figure 4. Determination of Relaxation Time Constant for a Step Change in Velocity

rest; the particle relaxation time refers to the particle lag associated with the magnitude of the velocity difference, not the absolute level of the velocity.

From the foregoing discussion, the particle relaxation time and distance were found for a wide range of Arnold Engineering Development Center tunnel conditions (Ref. 9). These tunnels generate continuous or intermittent flows in a Mach number range of 2.4 to 10.6. For an intermittent tunnel, the test times are the order of milliseconds, while the relaxation times are normally the order of microseconds. Thus, the fact that the intermittent tunnel flow suddenly imposes a sharp acceleration on the particle, due to startup, is an identical condition to that of a particle being accelerated through the nozzle of a continuous tunnel. As a result, the particle relaxation time imposed in the free stream is applicable to both the intermittent and the continuous tunnel conditions.

A compilation of these relaxation times and associated distances is shown in Table 1. It can be seen that even small particles of 0.5 micron or less had relaxation-length scales which would rival the axial extent of the test section. It is thus conceivable that a light-scattering particulate could pass through a tunnel nozzle having rapid flow acceleration and never approach the free stream velocity before passing out of the tunnel test section. If it is assumed that the particulate did reach the free stream velocity,

there could still be a significant difference in the fluid and particulate motion in the region around the model, caused by the particulate inertia. Therefore, for high-speed flows approaching the rarefied regime, it appears that one must either inject known seed particles (size and density) or be able to size-discriminate and use only particles which are small.

EXPERIMENTAL INVESTIGATION OF SHOCK- PARTICLE RELAXATION TIMES

It is clear from the foregoing discussions that particle dynamics is significant in the measurement of time-averaged quantities such as mean and turbulence velocities. The poor particle frequency response similarly affects the time-dependent measurement of the turbulence power spectra. As shown previously, the relaxation time, t_r , given most generally by Equation 2, infers the degree to which the particle inertia will degrade its response to both turbulence and shock-wave interactions. An investigation was therefore made to experimentally verify the theoretical predictions of the relaxation times for various particulates which are used for seeding.

To do this, a stationary Mach disk (normal shock) was created in an under-expanded, axisymmetric air jet flow (Figures 5 and 6). A brief study was made to define the shock standoff distance, S , and shock breadth, ℓ , (Figures 7 and 8).

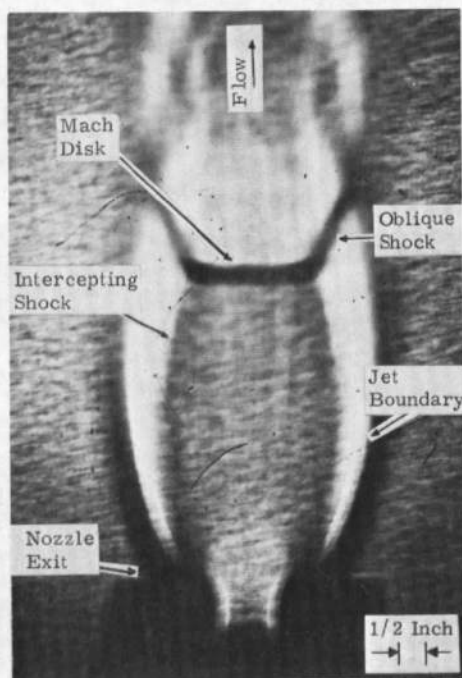


Figure 5. Laser Shadowgraph of 0.75-Inch-Diameter Underexpanded Air Jet. Stagnation Pressure = 80 psig; Jet Mach Number = 1.87

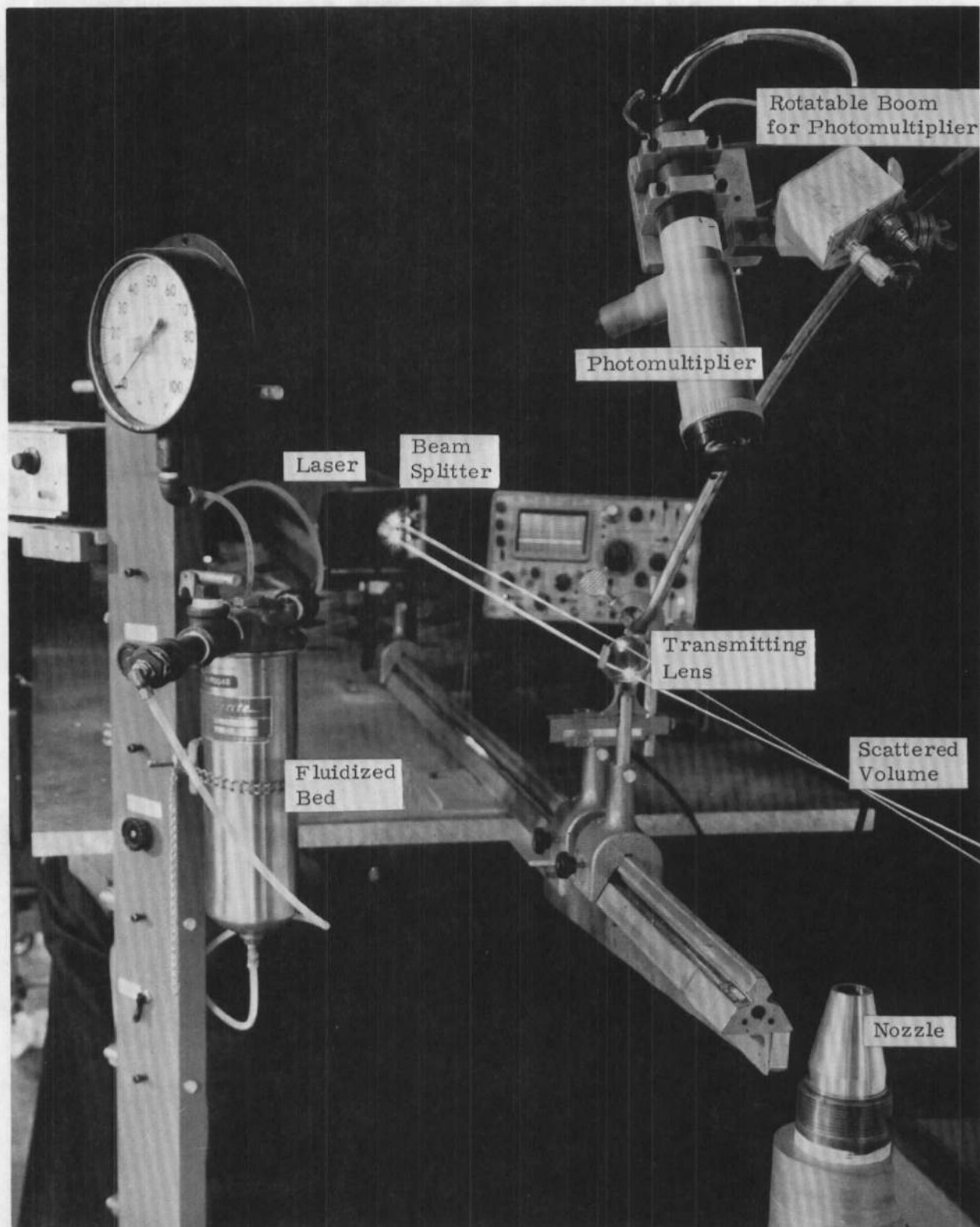


Figure 6a. Experimental Setup for Particle Relaxation Investigation

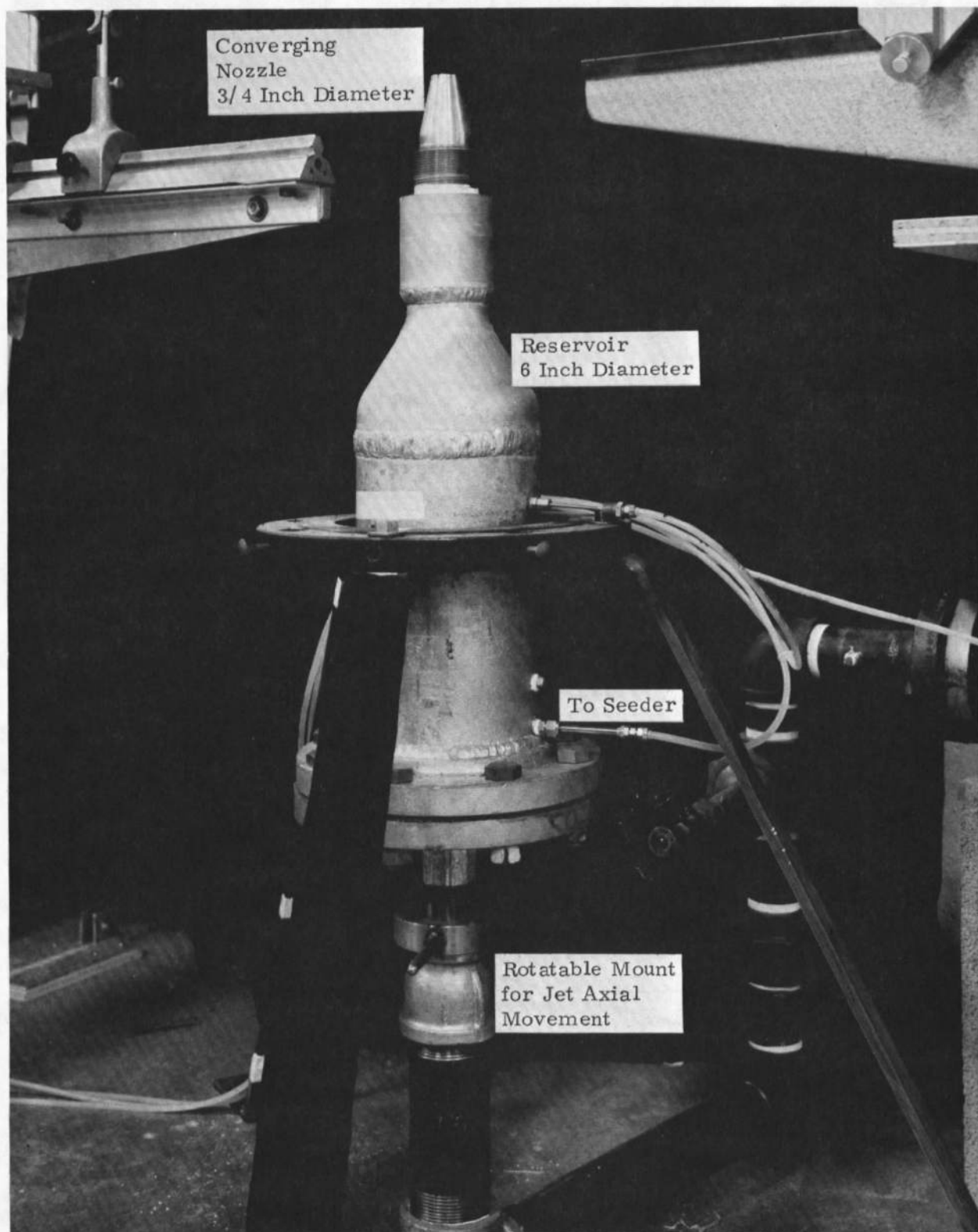


Figure 6b. Jet and Reservoir for Particle Relaxation Investigation

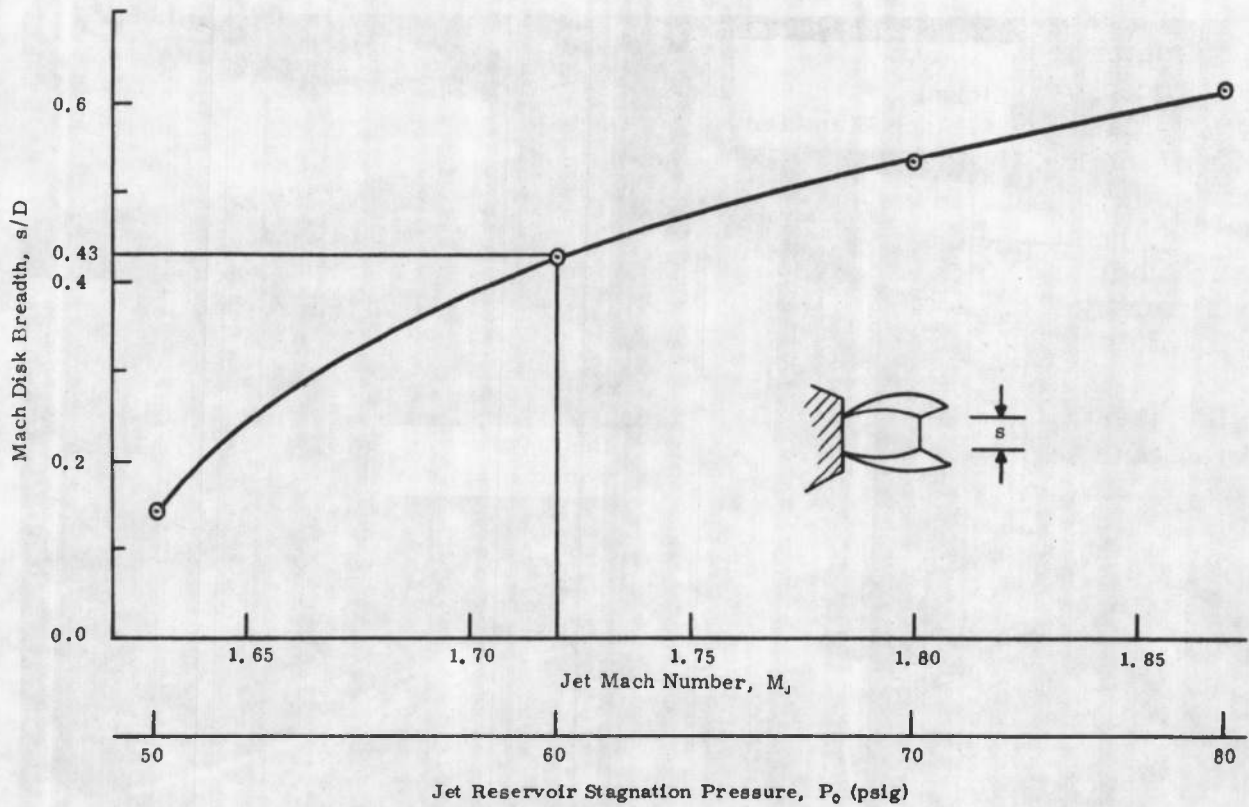


Figure 7. Experimental Results of Mach Disk Breadth, s , Versus Jet Mach Number ($P_{\text{ambient}} \approx 14.6$ Psia)

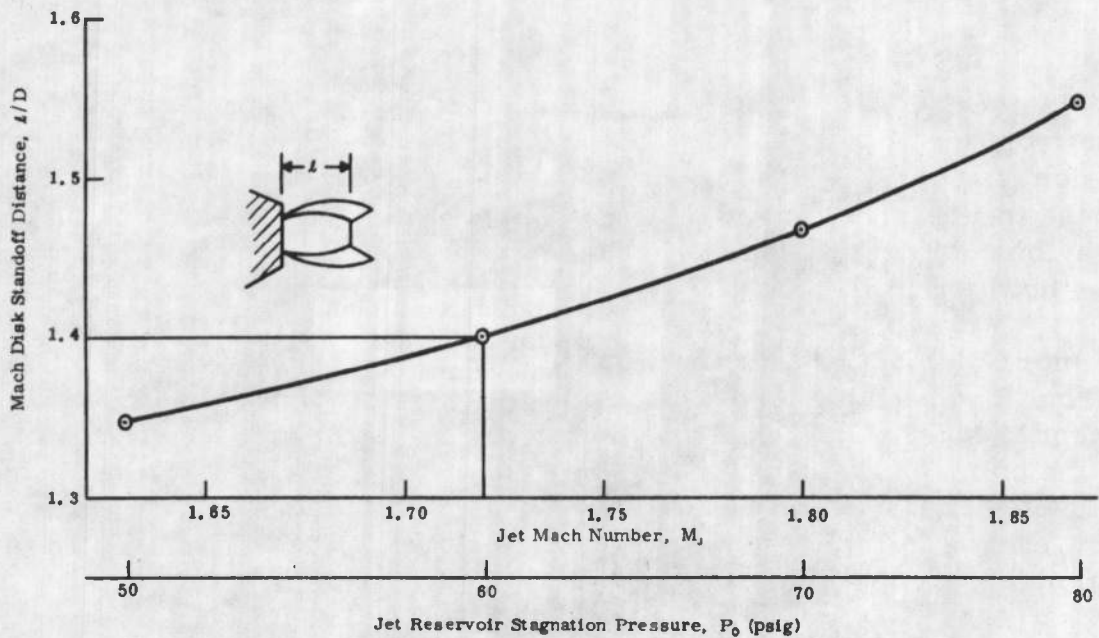


Figure 8. Experimental Results of Mach Disk Standoff Distance, l , Versus Jet Mach Number ($P_{\text{ambient}} = 14.6$ Psia)

In this experiment, the particle velocity was measured using the laser velocimeter technique (see Appendix I, "Laser-Velocimeter Optical Setup and Processor") at various upstream and downstream distances from the stationary Mach disk shock structure. The velocity results will be given as a ratio of the local measured velocity (accuracy typically 1 percent or better) to over the isentropic jet velocity, v_1 . The presentation of the velocity ratio negated the need for measurement of the local fluid velocity by use of a pitot-static tube. Such a method is known to have significant uncertainties due to the strong flow-probe interference and the existence of an axial Mach number gradient.

The isentropic free-stream Mach number, M_1 , can be defined from the following gas dynamic relation:

$$M_1 = \sqrt{\frac{2}{K-1} \left\{ \left(\frac{P_{\text{ambient}}}{P_{\text{reservoir}}} \right)^{\frac{K-1}{K}} - 1 \right\}} \quad (4)$$

and the isentropic free-stream fluid velocity, v_1 , can be obtained as

$$v_1 = M_1 a_0 \left(\frac{1}{1 + \frac{K-1}{2} M_1^2} \right)^{1/2} \quad (5)$$

By the use of normal shock relations, the anticipated flow velocity decrease across the shock can be found as:

$$\frac{v_2 - v_1}{v_1} = 1 - \frac{2}{K+1} \left[\frac{1 + \frac{K-1}{2} M_1^2}{M_1^2} \right] \quad (6)$$

This velocity ratio was used as a guide only, since the Mach number upstream from the shock was not actually measured. Thus for a truly isentropic expansion (i.e., related to the conditions just downstream from the nozzle exit), the theoretical velocity deceleration across the normal shock may in this way be computed (Figure 9). The expected particle velocity behavior for various downstream distances is shown schematically as Figure 10.

The normal shocked, subsonic flow downstream from the normal shock was seen from the shadowgraphs to persist at least one-half jet diameter. This was sufficient to track particles of even a long relaxation time. At that point, mixing of the oblique shocked, supersonic flows caused an acceleration of the centerline velocity. The subsequent diamond-structured shocks give evidence that the flow eventually becomes supersonic after passing through the oblique and normal shock structures.

It should be noted that there is an axial Mach number increase of the flow up to the normal shock, owing to the expansion waves which originate at the nozzle exit and reflect from the jet boundaries (Ref. 11). Thus, the particle velocity is seen to be greater than the velocity associated with an isentropic

expansion. As mentioned previously, either the measured upstream velocity or the velocity associated with isentropic expansion could be used for non-dimensionalization, because each is a constant for the results presented.

The experiment was carried out using a counter-type laser velocimeter processor. Various downstream positions were probed. The effective scattering volume was minimized by using a 90° scattering angle. The output data form determined to be of most interest was the velocity probability distribution, or histogram. Here the y axis represents the relative probability of a particle having a velocity of magnitude represented as the x axis. In this case, with sufficient data (normally more than 20,000 points were taken) the absolute height has little meaning. Rather, the relative heights at various velocities provides a measure of the mean and turbulence velocity, represented as the centroid and one standard deviation, respectively.

Various types of particles, their expected relaxation time, distance, and mean size are given in Table 2. It was found that the colloidal alumina

Table 2
RESULTS OF PARTICLE-SHOCK INTERACTION
(Mach Disk Location = 1.40 Diameters)

Substance	X/D_j	\bar{U}/v_1	U'/\bar{U}	$\Delta\bar{U}/v_1$
Colloidal Alumina (Dupont Baymal, 2 μ)	1.00	0.89	0.11	0.00
	1.67	0.89	0.12	0.00
	1.80	0.69	0.13	-0.20
	1.93	0.64	0.09	-0.25
	2.06	0.60	0.09	-0.29
Alumina (Linde A, 0.3 μ)	1.00	1.15	0.14	0.00
	1.67	1.21	0.16	+0.06
	1.80	0.69	0.11	-0.46
	1.93	0.65	0.08	-0.05
	2.06	0.60	0.07	-0.15
Cab-O-Sil™	1.00	1.32	0.10	0.00
	1.67	1.01	0.24	-0.31
	1.80	0.64	0.14	-0.68
Alumina (Linde C, 1.0 μ)	1.00	0.98	0.14	0.00
Alumina (Linde B, 0.05 μ)	1.00	1.10	0.14	0.00

™ Trademark of the Cabot Corporation,
Oxide Division

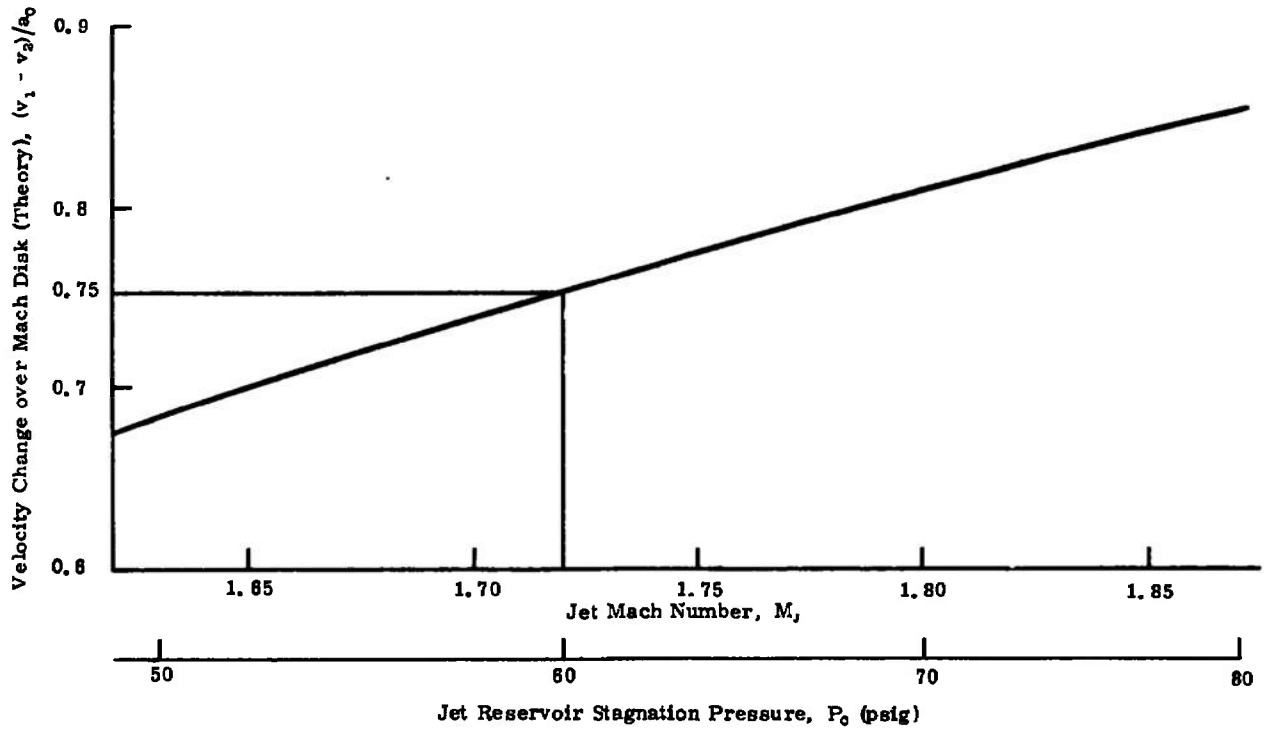


Figure 9. Theoretical Fluid Velocity Change Across Mach Disk Versus Jet Mach Number ($P_{\text{ambient}} = 14.6$ Psia)

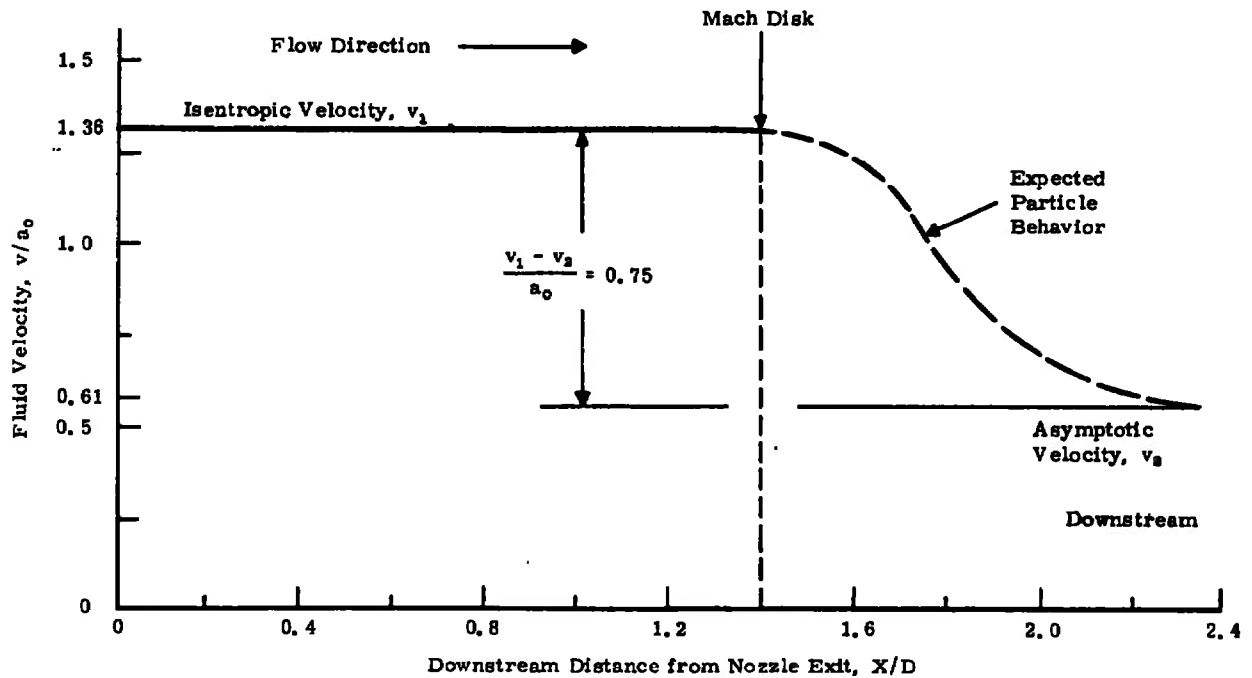


Figure 10. Schematic of Particle Relaxation Behavior at Mach Number = 1.72 (Assuming No Axial Velocity Acceleration Upstream of Mach Disk)

(duPont's Baymal) was agglomeration-free, while the Linde powder Type B, (0.05 micron) (a product of the Union Carbide Corporation's Linde Division), and Cab-O-Sil (manufactured by the Cabot Corporation, Oxide Division) tended to agglomerate before dispersal.

A fluidized particle bed was used for particulate dispersal into the flow (Figure 11). Extreme care was taken between runs with various particles to flush

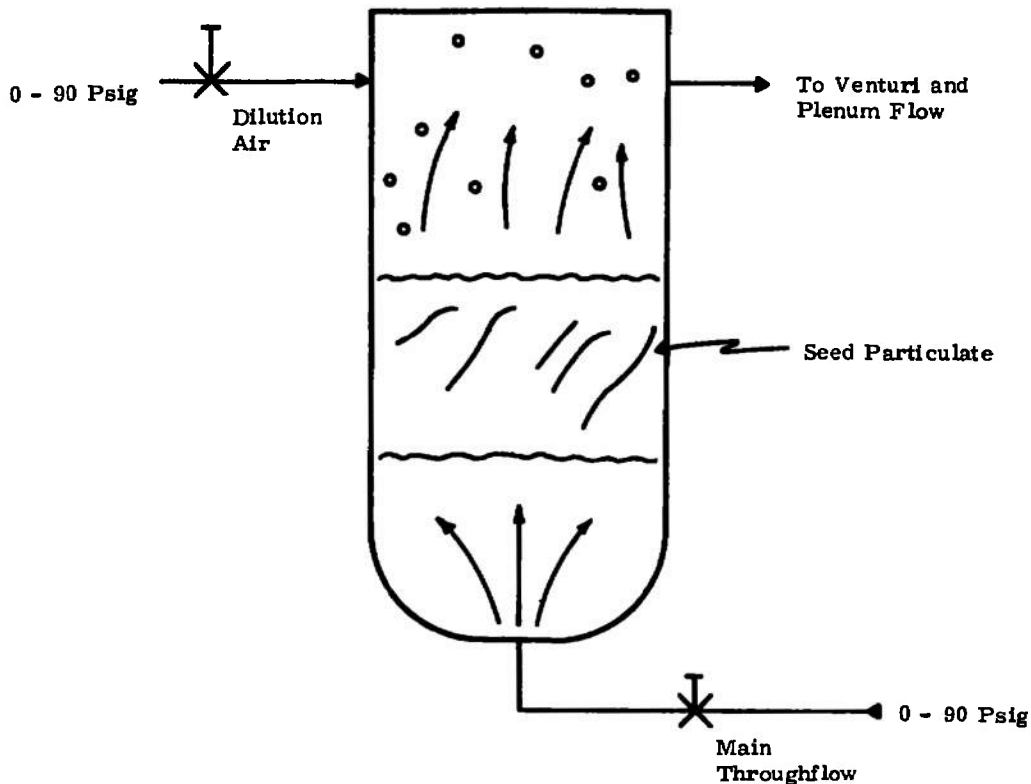


Figure 11. Fluidized Particle Bed

out all previous seeding. Oil vapor, which was a severe problem earlier in the program, was finally minimized. This was done by the use of a high-efficiency oil filter and combining clean laboratory air with the less desirable but higher-capacity air containing oil vapor. The contribution of oil vapor as scattering centers was further avoided by ensuring that the data acquisition rate approached zero before the test particles were injected into the flow. Typically the background data rate was 0 to 20 per second and the data rate during testing was between 500 and 10,000 per second.

The results of this study are compiled as Figures 12 through 14 and Table 2. The following conclusions may be made:

- A significant dispersion in size was evident for the smaller particles (Cab-O-Sil and Linde A) as shown by the wide range of velocity upstream and just downstream from the Mach disk.

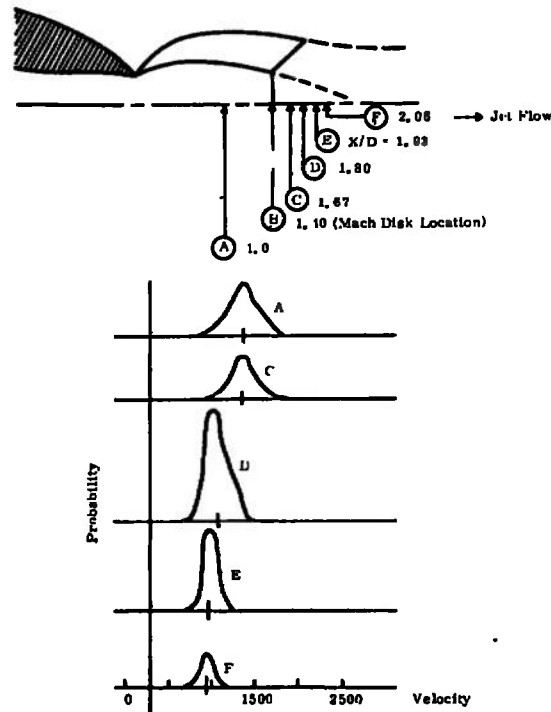


Figure 12. Particle-Shock Experimental Results: Colloidal Alumina (2μ)
Relaxation Time = $40\mu\text{sec}$; Axial Relaxation Distance = 0.60

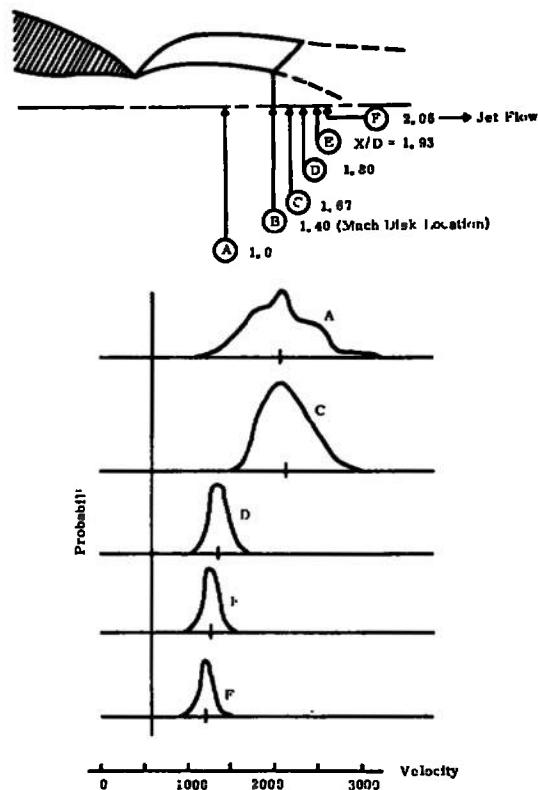


Figure 13. Particle-Shock Experimental Results with Linde Type A Alumina (0.3μ)
-- Relaxation Time = $0.65\mu\text{sec}$; Axial Relaxation Distance = 0.01

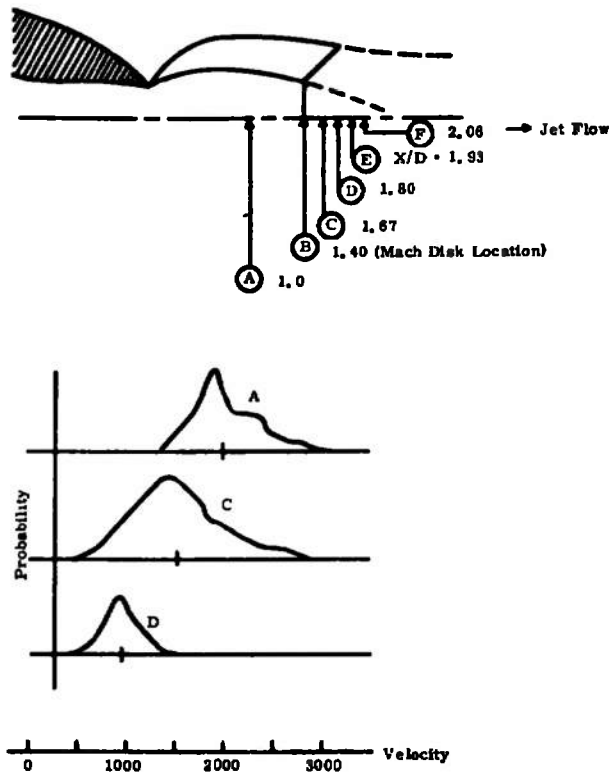


Figure 14. Particle-Shock Experimental Results: Cab-O-Sil (0.05μ) -- Relaxation Time = $0.02 \mu\text{sec}$; Axial Relaxation Distance = 0.002

- Owing to the particle acceleration through the nozzle exit, the apparent mean velocity upstream from the Mach disk also varied widely. Generally the smaller the particle size, the higher the mean velocity.
- For the colloidal alumina the relaxation time and associated distance were close to that which was expected. Significantly greater relaxation times than were anticipated were found for the Linde A and Cab-O-Sil particulates. This is ascribed to agglomeration and the fact that these particulates are nonspherically shaped. From electron photomicrographs these latter particles tended to be ragged platelets whose effective diameter and drag coefficient are not easily established. The colloidal alumina, on the other hand, resembled smooth spheres or ellipsoids.
- As expected, the velocity distribution narrowed markedly at a distance sufficiently downstream from the normal shock. At this position the particle inertia effects no longer dominated the measured particle velocity. In this region, the particle size range did not unduly influence the degree to which the seed followed the flow, since axial velocity gradients are small.
- The measure of the turbulence level by deducing the standard deviation of the velocity probability distribution was significantly influenced by the particle size. This may be seen from the Figures 12 to 14 and

Table 2, where the broadening of the histogram is caused principally by varying degrees of particle lag; this is due to size range rather than to the turbulence.

In summary, it has proved critical in the use of the laser velocimeter that seed particulates be chosen on the basis of their ability to follow the flow as well as their effectiveness as scattering centers. In high-speed flows, where a significant power spectrum exists at high frequency, this choice becomes more severe. Furthermore, in rarefied flow and/or flows with shock structure, the associated relaxation distance may rival the length of the test section or model size. Using the same argument, care should be taken to utilize a method and/or type of particles which are not agglomerated when dispersed in the flow. An agglomeration of one or more particles yields an increase in the seed's apparent diameter and an associated square of that increase in the relaxation time.

It is evident from this study that even small particles can generate significant discrepancies in the measurement of the mean and turbulence velocities. The measurement of the turbulence power spectra is likewise affected. The lag associated with larger or heavier particles is akin to employing a low-pass filter at the output of a fast-response velocimeter or hot-wire anemometer. The characteristic cutoff frequency and filter response at cutoff are dictated by the particle dynamics. Power spectra deduced with an "effective" low-pass filter would correspondingly show a bias away from the high-frequency flow energy.

Section 3

LASER VELOCIMETER PROCESSOR ACCURACY

A study was made to determine the accuracy of criteria for the design and adjustment of the electronic components of the laser velocimeter system as shown in Figure 15. To accomplish this, a model was developed for the LV signal burst which was explored in both the time and frequency domains. This model was then used to determine the errors caused by the pedestal removal filter and the threshold of the limiter used in determining the Doppler frequency (and hence the particle velocity). These results were formulated into design rules which are summarized at the end of this section.

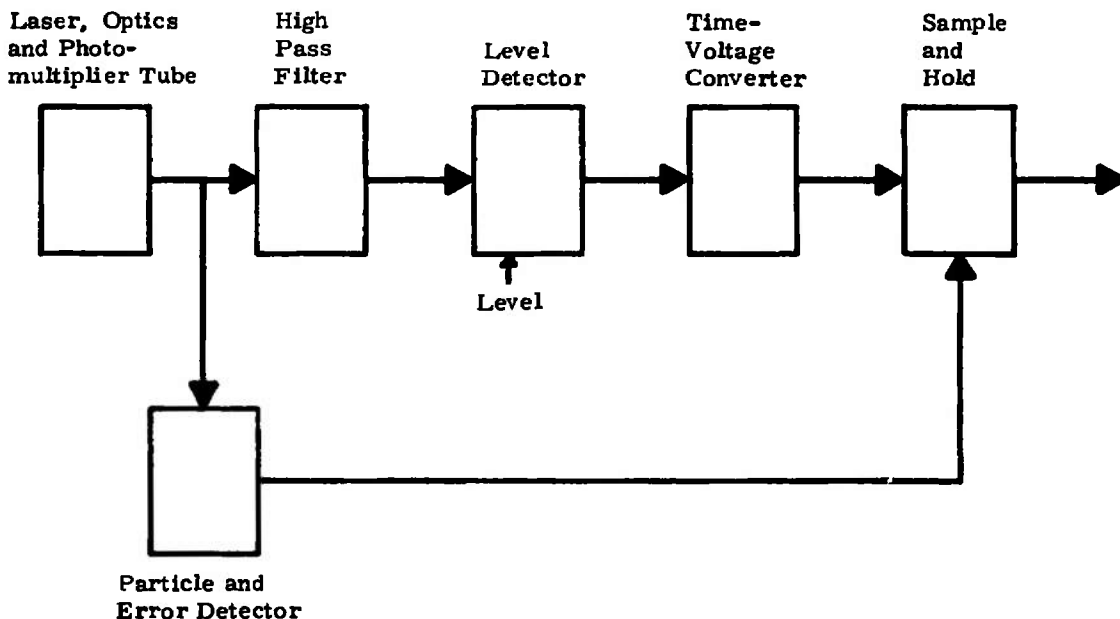


Figure 15. Schematic of Laser-Velocimeter Counter Processor (Time Domain)

DOPPLER BURST SIGNATURE MODELING

To obtain a generalized and useful analysis of a laser-velocimeter processor it is necessary to obtain first a model of the ensemble, or set of signals, available at the photodetector output. Such an analysis has been conducted by Farmer (Ref. 12), and his results are briefly reconstructed below.

The ensemble model is based on essentially three assumptions:

- For a particular particle the photodetector output for forward- or back-scatter radiation is proportional to the average intensity of the light incident upon a disk whose radius is that of the particle.
- The beams are of equal amplitude with Gaussian profiles and the apparatus is perfectly aligned.

- The particle can be considered spherical and is considerably smaller than the laser beam width.

If Assumption 1 is accepted, then

$$V_p = H(E_1 + E_2)^2 \quad (7)$$

where H is a function of the particle reflectivity and geometry, the photodetector placement and gain, and E_1 and E_2 are the fields of the two beams. V_p is the output voltage from the photodetector from the light incident upon any infinitesimal point on the particle.

To agree with Assumption 2, one has the instantaneous intensity,

$$E_N = e^{-R_N^2/\beta^2} \cos(\omega t - KX_N) \quad (8)$$

where β is the radial position at which the local intensity of the laser beam is $1/e$, the centerline value, and

$\omega = 2\pi c/\lambda$, the natural frequency of the light

K = wave number of the light

X_N = distance along the axis of the beam

R_N = distance perpendicular to that axis

By inserting beams of the form of Equation 8 into Equation 7, one obtains

$$\begin{aligned} V_p = & H(G_1^2 \cos^2(\omega t - KX_1) + G_2^2 \cos^2(\omega t - KX_2) \\ & + G_1 G_2 \cos(2\omega t - KX_1 - KX_2) \\ & + G_1 G_2 \cos(-KX_1 + KX_2)) \end{aligned} \quad (9)$$

where $G_N = e^{-R_N^2/\beta^2}$

The output of the photodetector does not respond at the speed of light, but instead averages these terms. Thus,

$$V_p = H \left[\frac{G_1^2}{2} + \frac{G_2^2}{2} + G_1 G_2 \cos(K[X_2 - X_1]) \right] \quad (10)$$

If X_N and R_N are transformed to a common coordinate system X , Y , and Z , as shown in Figure 16a, and insert these in Equation 10, simple algebra leads to

$$\begin{aligned} V_p = & H e^{-2(Z^2 + X^2 \sin^2 \theta + \cos^2 \theta Y^2)/\beta^2} \\ & \cdot \left[\cos(2Y \sin \theta K) + \cosh(2X \sin(2\theta)Y/\beta^2) \right] \end{aligned} \quad (11)$$

Note that this expression consists of three terms. The first of these is a common multiplier of a symmetric exponential form whose argument is an ellipsoid. This term determines the shape of the probe volume. The other two terms are the "cos" and "cosh" expressions. The cos expression, which contains only spatial coordinate Y, is the fringe field information. It is the frequency of this cosine that the laser-velocimeter processing electronics must determine. Finally, the cosh term represents what is called the pedestal level. The argument of the cosh term varies at a rate comparable with the probe volume as it contains the $1/\beta^2$ term. Thus the argument of the cosh term will never greatly exceed $10 \sin(2\theta)$ and, since this quantity is very small, the approximate result is

$$\cosh(2X \sin(2\theta)Y/\beta^2) \approx 1 \quad (12)$$

and V_p becomes

$$V_p = H e^{-2(Z^2 + X^2 \sin\theta + \cos^2\theta Y^2)/\beta^2} \cdot [1 + \cos(2Y \sin\theta K)] \quad (13)$$

The latitude of Assumptions 1 and 3 is now applied to obtain the photodetector output, V, for a particle of finite size. This gives

$$V = \frac{\int_{\text{Disk}} V_p dA}{A} \quad (14)$$

where only Y in the cosine terms is allowed to vary during the integration, as the other spatial terms will vary only slightly if the particle is small. It is thus found that

$$V = H e^{-2(Z^2 + X^2 \sin\theta + \cos^2\theta Y^2)/\beta^2} \times \frac{\int_0^a \int_{-\pi}^{\pi} [1 + \cos(2Y \sin\theta K)] r d\theta dr}{4\pi a^2} \quad (15)$$

As can be seen from Figure 16b,

$$y = y_0 + r \cos\theta$$

where y_0 is the value of y at the center of the particle.

The integral is performed with the help of the tables, to obtain

$$V = H e^{-2(Z^2 + X^2 \sin\theta + \cos^2\theta Y^2)/\beta^2} \times \left[1 + \frac{J_1(2Ka \sin\theta)}{Ka \sin\theta} \cos(2(\sin\theta)Ky) \right] \quad (16)$$

where J_1 is the first-order Bessel function.

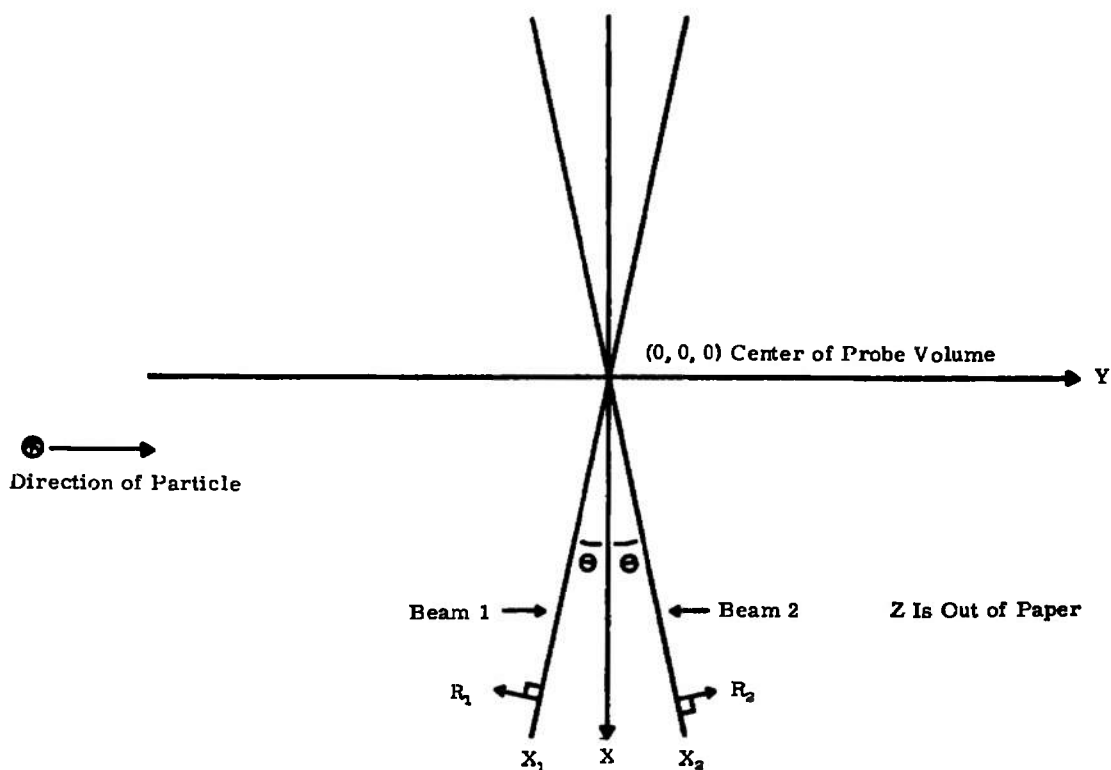
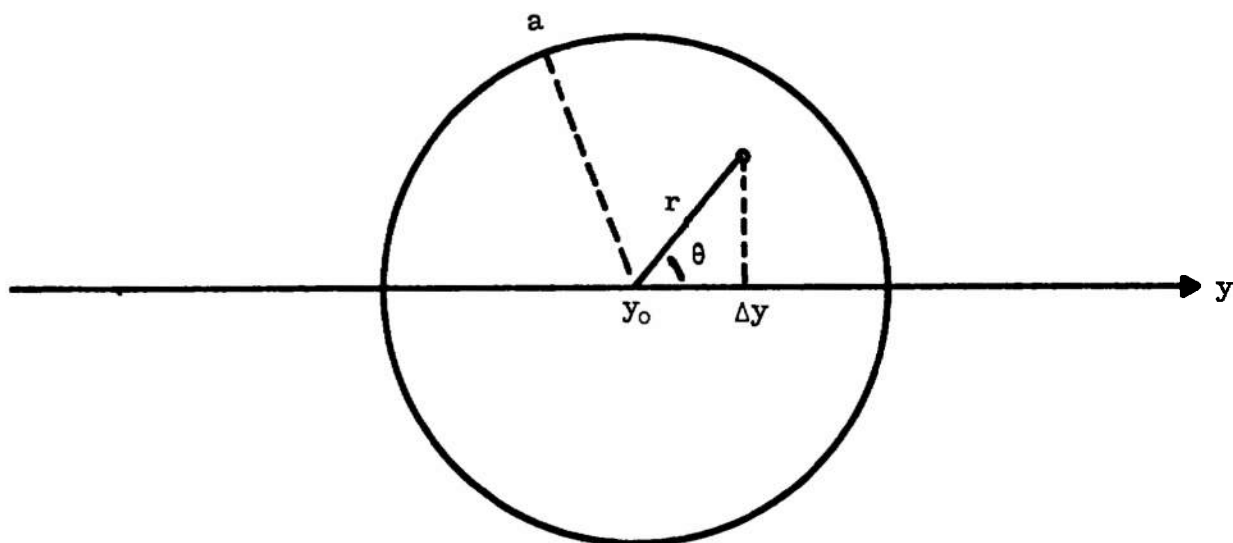


Figure 16a. Geometry of Beam Intersection



Disk of Integration

$$y = y_0 + 2y = y_0 + r \cos \theta$$

Figure 16b. Disk Integration on y Axis

Under these assumptions the effect of particle size is to add a gain term in front of the cosine which is a function of the particle radius, a . For small particles (as $a \rightarrow 0$) this result becomes the expression for the intensity scattered from a small point in space. A plot of $J_1(2X)/X$ is submitted as Figure 17.

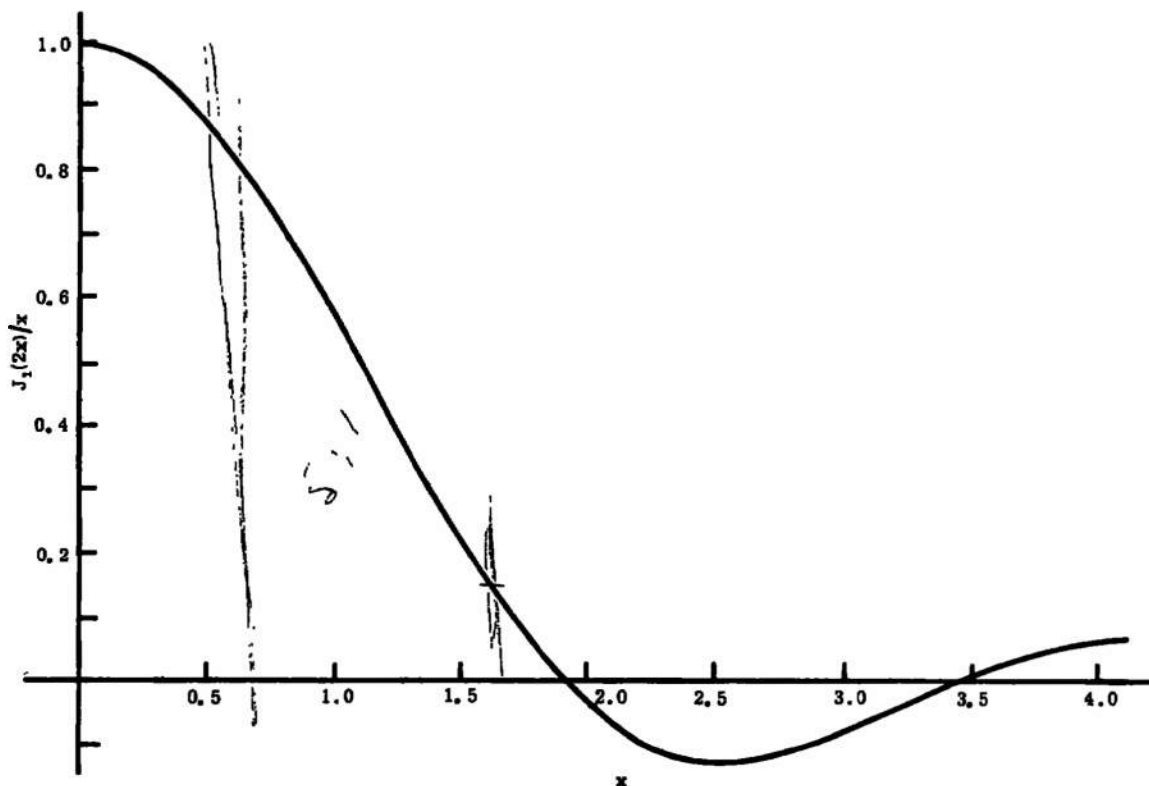


Figure 17. Gain Factor of Cosine Term

The study of Equation 16 reveals that if a period measurement is used to determine the velocity, a minimal error is achieved when the pedestal is perfectly removed and the period is measured at the occurrence of the zero crossings. When a particle is not present in the probe volume, however, the system will be very susceptible to noise unless it is disabled during these intervals.

Further examination of Equation 16 suggests that information about the particle size might be obtained from the burst signature. However, examination of Figure 17 shows that in a practical system with a total error of 5 percent, the particle size could be determined unambiguously only over a 5:1 range. This is considerably smaller than the size range of particles available to the detector. Thus the employment of some ratio between pedestal and Doppler voltage is deemed impractical for particle size measurement. Note, however, that for particles where

$$a < (1/2K\theta) \quad (17)$$

are used, ample output will be available from the detector.

SIGNATURE MODEL IN THE FREQUENCY SPACE

In examining Equation 16 in the frequency domain, it is convenient to convert the result to the time domain by substituting

$$y = vt \quad (18)$$

where v is the velocity of the particle, and, since θ is very small, replace $\sin\theta$ by θ and $\cos\theta$ by 1. Thus is found the Fourier transform of

$$V(t) = He^{-2(Z^2 + X^2\theta^2)/\beta^2} \left[e^{-2(vt)^2/\beta^2} \left(1 + \frac{J_1(2Ka\theta)}{Ka\theta} \cdot \cos(2\theta Kvt) \right) \right] \quad (19)$$

Performing the Fourier integral, Equation 20 is obtained:

$$V(\omega) = He^{-2(Z^2 + X^2\theta^2)/\beta^2} \sqrt{\pi\beta^2/2v^2} \cdot \left[e^{-\beta^2\omega^2/8v^2} + \frac{1}{2} \left(\frac{J_1(2Ka\theta)}{Ka\theta} \right) \left(e^{-\beta^2(\omega - \omega_0)^2/8v^2} + e^{-\beta^2(\omega + \omega_0)^2/8v^2} \right) \right] \quad (20)$$

where $\omega_0 = 2\theta Kv$.

Note again that the result of Equation 20 consists of two terms: a frequency packet centered around direct current and a pair of frequency packets centered around the Doppler frequency. If these are to be successfully separated by filtering it is clear that

$$\theta K\beta \gg \sqrt{5/2} \quad (21)$$

Otherwise these packets would overlap. This measure should be applied to the design of a laser-velocimeter system.

Figure 18 shows the burst transform for a system meeting the criteria of Equation 20.

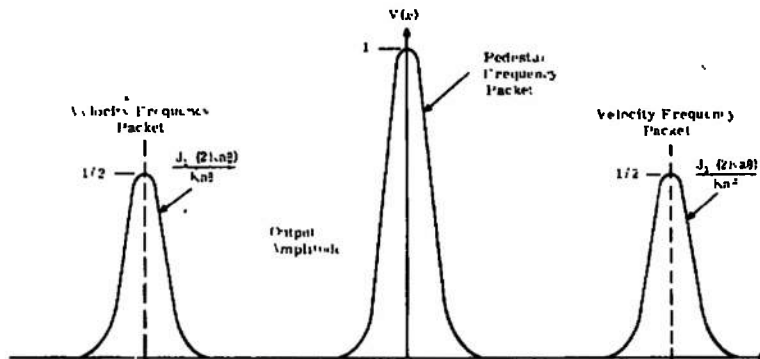


Figure 18. Fourier Transform of Laser Doppler Velocimeter Burst

PEDESTAL REMOVAL FILTER ERRORS

There are two error sources associated with the adjustment of the cutoff frequency of the high-pass pedestal removal filter. If the cutoff frequency is adjusted too high, then at low particle velocities the side bands of the velocity frequency packet are distorted by the filter and measurement of its center frequency; thus the velocity of the fluid is impeded. On the other hand, if the cutoff frequency is set too low, then at high velocities pedestal energy passes through the filter, causing distortion of the velocity frequency packet. The spectra of the laser-velocimeter burst was shown in Figure 18.

To determine the response of an arbitrary high-pass filter to the laser-velocimeter burst is an arduous task and is not essential to this analysis. If the high-pass filter is assumed to be ideal, a solution may be obtained to guide the adjustment of a realizable filter. A simple computer program was written to evaluate the response of an ideal high-pass filter with cutoff frequency $\omega = \alpha$ to the input (where $\alpha = 0$ is the zero frequency cutoff)

$$x(t) = e^{-t^2} \quad (22)$$

This can be viewed as a normalized version of the pedestal signal. The predicted responses agree with the approximation given in Equation 12, as can be seen by evaluating Figure 19. The amplitude of the pedestal is reduced

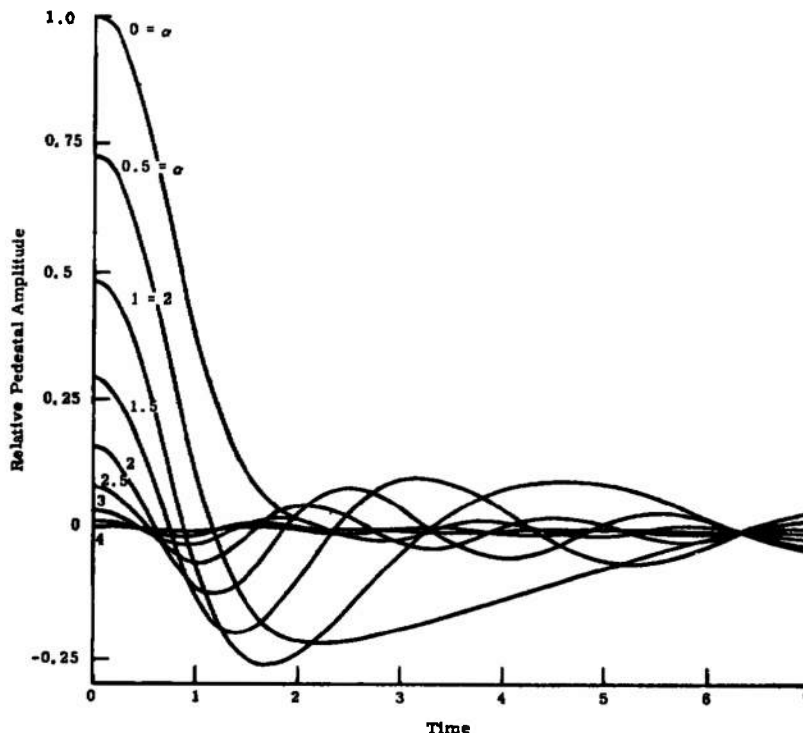


Figure 19. Graph of High-Passed Filter Pulse of the Form e^{-t^2}
Where $\omega = \alpha$ (Cutoff)

as the cutoff frequency is reduced, while the length of the response in time increases. By noting that the maximum value of this response occurs at $t = 0$, the amount of pedestal ripple present in the filtered laser-velocimeter burst as a fraction of the maximum of the velocity cosine component may be bounded by

$$R_A \leq \frac{1}{\pi} \int_0^{\omega_0} \frac{\beta}{v} \sqrt{\pi/2} e^{-\beta \omega^2} 8v^2 d\omega \quad (23)$$

If it is assumed that the radius of the particle, a , is

$$a \ll 1/(2K\theta) \quad (24)$$

and ω_0 = the filter cutoff frequency, the result becomes

$$R_A \leq 1 - \text{ERF}\left(\frac{\tau_p \omega_0}{2\sqrt{2}}\right) \quad (25)$$

where $\tau_p = \frac{\beta}{v}$, which is proportional to the particle transit time across the probe volume, and 2β = the e^{-1} beam width of the laser.

Figure 20 is a graph of R_A as a function of $\tau_p \omega_0$. If

$$\omega_0 \tau_p > 4 \quad (26)$$

this error will be reduced to a negligible level. Thus

$$\omega_0 > \frac{4v_h}{\beta} \quad (27)$$

or

$$f_0 > \frac{2v_h}{\pi\beta} \quad (28)$$

where f_0 is the filter cutoff frequency in hertz and v_h is the highest velocity to be determined.

Since the velocity frequency packet has the same envelope function as the pedestal frequency packet, the low velocity error may be bounded in the same manner. By a parallel analysis

$$f_0 < \left(2\theta K - \frac{2}{\pi\beta}\right) v_l \quad (29)$$

where, as before, 2θ is the angle between the two laser beams, K is the wave number ($2\pi/\lambda$) of the laser, and v_l is the lowest velocity to be measured.

Combining these results,

$$\frac{2}{\pi\beta} v_h < f_0 < \left(2\theta K - \frac{2}{\pi\beta}\right) v_l \quad (30)$$

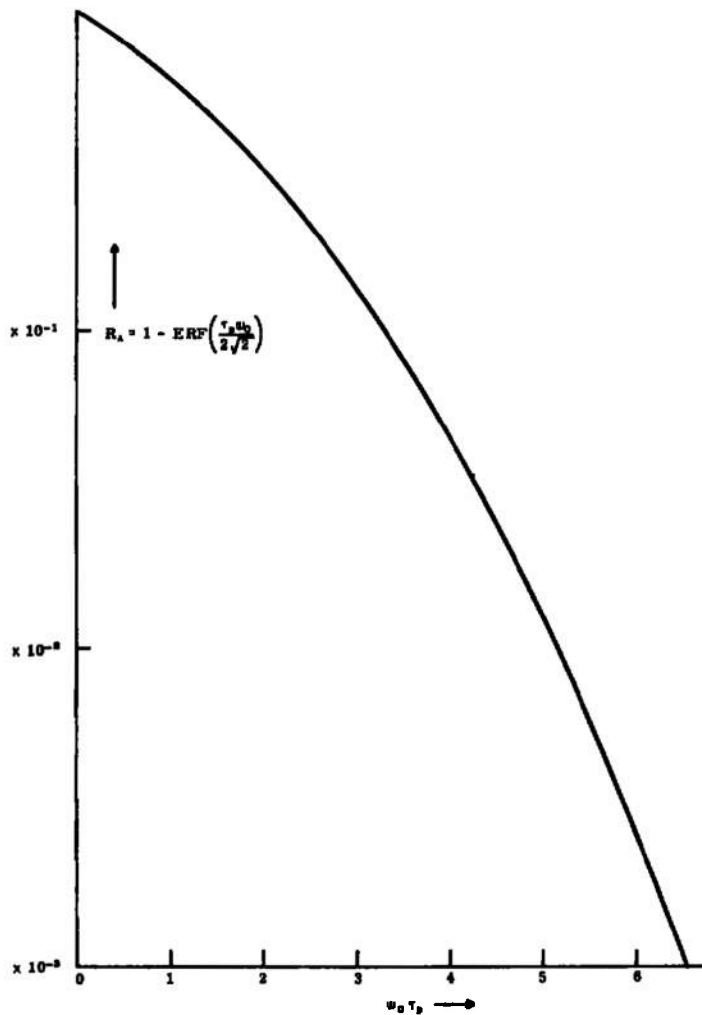


Figure 20. Baseline Ripple Error in High-Pass Filter

This result may be applied to nonideal filters by allowing the transition region of the filter to occur in the region bound by v_h and v_l in Equation 30. Thus, for

$$f > \left(20K - \frac{2}{\pi\beta} \right) v_l \quad (31)$$

the filter should have its passband gain and minimal phase shift, and for

$$f < \frac{2}{\pi\beta} v_h \quad (32)$$

the filter should have ample attenuation (say 40 decibels below its passband value).

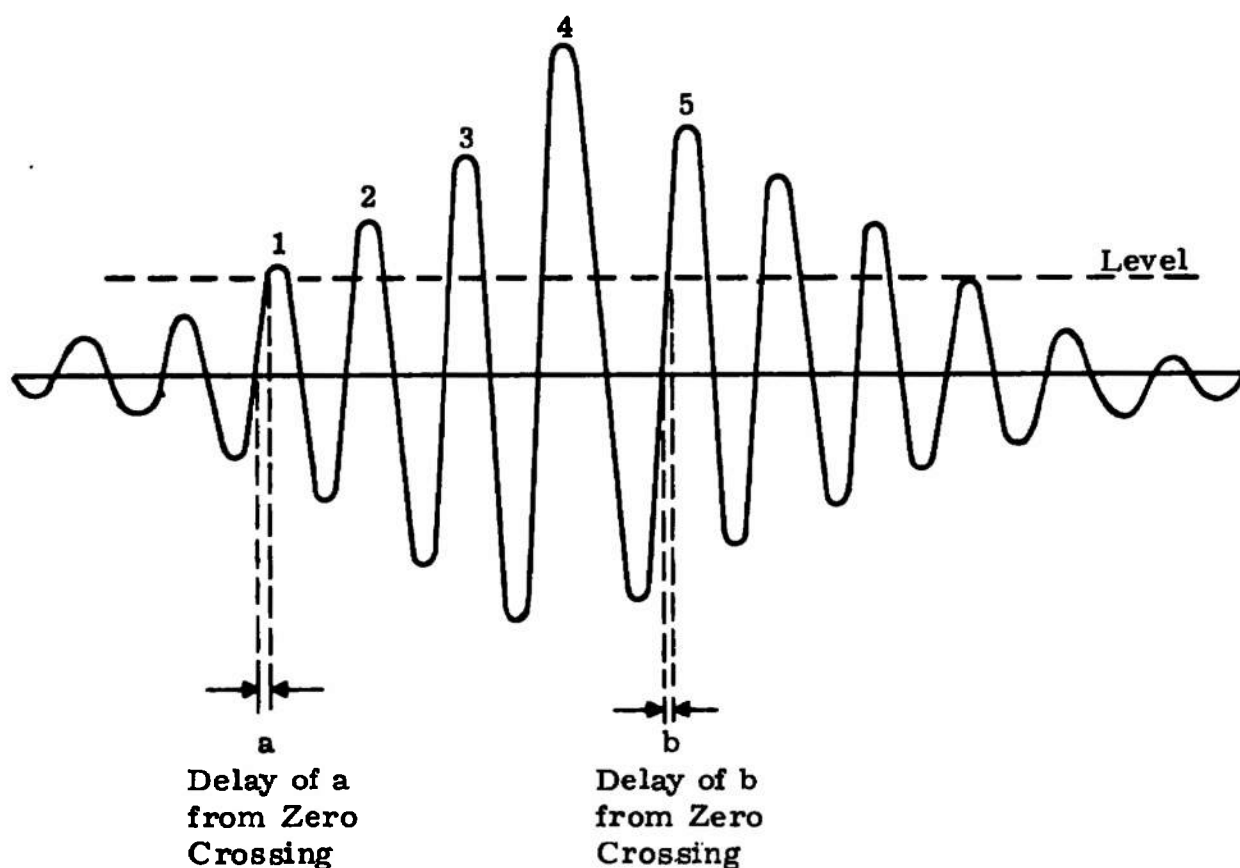
LIMITER THRESHOLD ERROR

Minimal error in the velocity measurement is achieved by determining the period of the velocity cosine at its zero crossings. To avoid noise errors, however, the laser-velocimeter processor developed by the General Electric

Research and Development Center estimates the frequency of the cosine velocity signal by measuring the time between N low-to-high crossings of a fixed threshold level by the signal (see "Laser-Velocimeter Counter Processor," in Appendix I). The timing process is initiated when the signal crosses this threshold the first time. As can be seen in Figure 3, an error is induced in the measurement because the starting and stopping points of the measurement are at different phase distances from the zero crossing. Examination of Figure 21 yields

$$E \begin{cases} \leq +0 \\ \geq -100(1/4N) \end{cases} \quad (33)$$

where E is the percent error and N is the number of cycles over which the period is measured.



$$a > b$$

$$a - b \leq \pi/2$$

Figure 21. Origin of Phase Error in Measuring Zero Crossing of Doppler Modulation

Thus, if five cycles are used to determine the period of the velocity cosine, the error is bounded by

$$E \begin{cases} \leq +0 \\ \geq -5\% \end{cases} \quad (34)$$

Experience shows that the presence of noise and envelope distortion in the return burst can cause the processor to begin the count on the downward side of a cycle or finish a count on an upward side. Therefore, a conservative upper bound on the error is

$$E^+ = 100(1/4N) \quad (35)$$

One should keep in mind that the higher likelihood of minus error to plus error will cause a measurement bias in the estimate of the velocity: the mean measured value will be lower than the actual value.

It may also be noted that the ratio of the limiter threshold to the signal amplitude, α , determines the number of cycles of the velocity cosine which are above the limiter threshold. If the threshold is set too high, a high percentage of particle passages will be ignored by the processor.

$$\begin{aligned} \text{For } 1 > \alpha > e^{-(2\pi)^2/\mu^2} & \quad \text{there is 1 limiter crossing,} \\ \text{for } e^{-(2\pi)^2/\mu^2} > \alpha > e^{-(4\pi)^2/\mu^2} & \quad \text{there are 3 limiter crossings,} \\ \text{for } e^{-(4\pi)^2/\mu^2} > \alpha > e^{-(6\pi)^2/\mu^2} & \quad \text{there are 5 limiter crossings,} \\ \text{or, for } e^{-(z-1)^2(2\pi)^2/\mu^2} > \alpha > e^{-z^2(2\pi)^2/\mu^2} & \quad \text{there are } 2z - 1 \\ & \quad \text{limiter crossings} \end{aligned}$$

where $\mu \cong \sqrt{2} \theta K \beta$. If $2z - 1 = M$, the maximum number of limiter crossings, M , is

$$M = \text{Int} \left(\frac{\mu}{\pi} \sqrt{\ln(1/\alpha)} \right) + 1 \quad (36)$$

where Int denotes the integer value of the bracketed expression.

SUMMARY OF LASER-VELOCIMETER PROCESSOR CRITERIA

To ensure proper operation of a laser-velocimeter apparatus, the following conditions as derived in the previous sections of this report should be established:

- For maximum light intensity and fringe variation, the particles should be as large as possible but meeting the condition that

$$d < \frac{1}{K\theta}$$

where d = diameter of the particles

K = wave number of the laser

2θ = angle between the beams intersecting to form the probe volume

- So that the pedestal may be properly removed from the bursts, it is necessary that

$$\theta K\beta > \sqrt{5/2} = 1.58$$

where β is $1/e$ intensity radius of the laser beam.

- The pedestal removal filter should be set so that

$$f_{pass} > \left(2\theta K - \frac{2}{\pi\beta}\right) v_l$$

and

$$f_{reject} < \frac{2}{\pi\beta} v_h$$

where v_h and v_l are the highest and lowest velocities of interest.

- The number of cycles in the burst used to determine the velocity, N , should be set so that

$$N < \text{Int}\left(\frac{\mu}{\pi} \sqrt{\ell_n(1/\alpha)}\right) + 1$$

where $\text{Int}(\cdot)$ = the integer value of (\cdot) ,

$$\mu \approx \sqrt{2} \theta K\beta$$

α = ratio of the threshold level in the comparator stage to the minimum acceptable burst amplitude.

- For an estimate of the velocity based on measuring over N cycles, the error (in percent) is bounded by

$$|E| \leq 100(1/4N)$$

The mean value of the estimate will always be lower than the actual value (there is some measurement bias).

Section 4

VELOCITY POWER SPECTRA ESTIMATION FROM LASER-VELOCIMETER DATA

RANDOM SAMPLING PROBABILITY MODEL

To estimate the velocity spectra from the laser-velocimeter data, the effect of random sampling (due to the random arrival of particles in the probe volume) on the turbulent velocity must be examined. If it is assumed that

- Times between successive particle arrivals are independent
- In each infinitely small time increment, Δt , the probability of one particle arrival is $\lambda \Delta t$, the probability of no arrival is $(1 - \lambda \Delta t)$ and the probability of more than one arrival is zero

then according to the theory of statistics the sampling constitutes a Poisson process. Thus λ is the expected arrival rate, and in any interval, t , the probability of K arrivals is

$$P(K, t) = \frac{(\lambda t)^K}{K!} e^{-\lambda t}$$

It will be useful to discuss a way in which the Poisson distribution may be derived. Note that the interarrival times between successive particles conform to the exponential distribution (in the theory of Poisson distributions that is often referred to as the first-order Erlang distribution). This distribution may be derived as the limit of independent trials, interval Δt apart, where the probability of arrival of a particle at the end of each interval is p . The interval time and the probability are allowed to approach zero while their ratio, $\Delta t/p$, is held constant at $1/\lambda$, the average time between arrivals. The resulting differential equation yields the exponential distribution.

SPECTRA THEORY BASED ON RANDOM SAMPLING

Using a similar proof following the method of Lorens (Ref. 13) to determine the effects of sampling a signal with a Poisson process, consider the sampling signal, $s(t)$, and the velocity signal, $m(t)$, which form a sampled signal, $g(t)$, through the relation

$$g(t) = s(t) m(t) \quad (37)$$

This is illustrated in Figure 22. Note that $s(t)$ and $m(t)$ are random variables. If it is assumed they are independent, Equation 38 may be written,

$$R_{gg}(\tau) = R_{ss}(\tau) R_{mm}(\tau) \quad (38)$$

as the relation between the autocorrelation functions, where the notation $R_{xx}(\tau)$ means the autocorrelation function of $x(t)$. Noting that the power spectra are

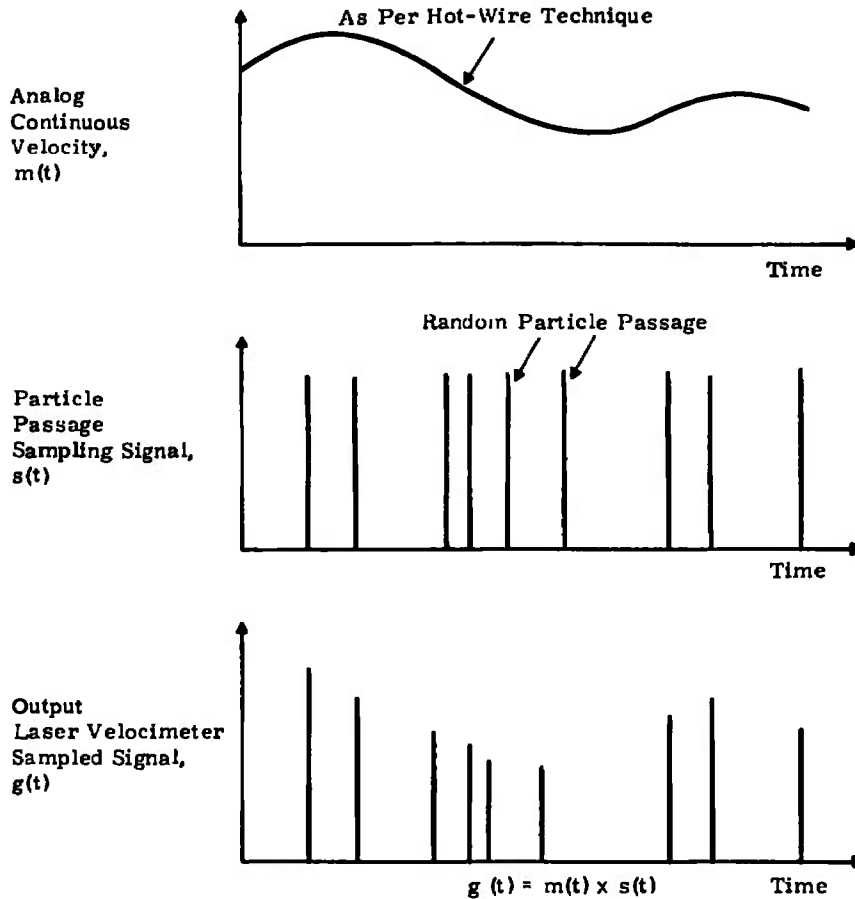


Figure 22. Schematic of Continuous Velocity and Laser Velocimeter Sampled Signals

the Fourier transform of the autocorrelation function, the spectra of $g(t)$ are written as

$$S_g(\omega) = \frac{1}{2\pi} \int_{-\infty}^{\infty} S_m(\eta) S_s(\omega - \eta) d\eta \quad (39)$$

where $S_m(\omega)$ is the spectra of the velocity signal and $S_s(\omega)$ is the spectra of the sampling signal.

Equations 38 and 39 suggest two approaches for determining the spectra of the velocity process, $S_m(\omega)$, from the output of the LV device, $g(t)$.

The first of these, the most general, suggests that $R_{mm}(\tau)$ may be recovered from estimates of $R_{gs}(\tau)$ and $R_{ss}(\tau)$ using Equation 38 as

$$\hat{R}_{mm}(\tau) = \frac{\hat{R}_{gs}(\tau)}{\hat{R}_{ss}(\tau)} \quad (40)$$

if $\hat{R}_{gg}(\tau)$ is non-zero in the region of interest. It has been shown that this condition is met by ideal random sampling (the particle arrivals are Poisson distributed).

Equation 40, however, requires special hardware for its realization. It is necessary to compute $\hat{R}_{gg}(\tau)$; this is done by passing $g(t)$ through a correlator. The autocorrelation function of the sampling sequence, $R_{gg}(\tau)$, is related to the interarrival-time probability density, which may be determined from the particle arrival signal available from most counter-type LV signal processors. It is interesting to note that theoretically this estimate may be made with any (no matter how low) particle arrival rate.

The second approach may be seen heuristically. If the velocity of a high enough rate is sampled, the signal is "fully" recovered (that is, the sampled signal and unsampled signal would look nearly identical when viewed on a scope). The spectra of the velocity sequence can then be determined by conventional techniques. This method will provide an estimate with the minimum of special hardware (unlike the first approach, which probably requires a special-purpose processor to compute the required functions).

Because of the advantages for a minimum capital investment and the potential use of conventional laboratory spectrum analyzers, the remainder of this section will pursue the criteria for spectral estimations utilizing this second approach.

SPECTRA MEASUREMENTS AT HIGH DATA-ACQUISITION RATES

This is done by the estimation of the spectra of the sampling signal as a set of impulses, $\mu_o(\omega)$, corresponding to the particle passage through the scattering volume, so that

$$S_s(\omega) \cong 2\pi \mu_o(\omega)$$

and Equation 39 reduces to

$$S_s(\omega) = \frac{1}{2\pi} \int_{-\infty}^{\infty} [2\pi \mu_o(\omega - \zeta)] \cdot S_s(\zeta) d\zeta = S_s(\omega)$$

If Poisson sampling is assumed, one may obtain a functional relationship for $S_s(\omega)$ via its autocorrelation function. For $S(t)$ of the form

$$S(t) = \sum_{\substack{\text{all} \\ N}} A \mu_o(t - N\Delta T) \quad (41)$$

where A is a random variable and

$$A = \begin{array}{l} A \text{ with probability } p \\ 0 \text{ with probability } (1 - p) \end{array}$$

a function is established which samples by a process of independent trials, ΔT apart. Recalling that for stationary processes

$$R_{ss}(\tau) = \lim_{T \rightarrow \infty} \frac{1}{2T} \int_{-T}^T S(t) S(t + \tau) dt \quad (42)$$

it is noted that

$$\begin{aligned} R_{ss}(0) &= \frac{pA^2}{\Delta T} \mu_0(0), \quad t = 0 \\ R_{ss}(N\Delta T) &= \frac{p^2A^2}{\Delta T} \mu_0(N\Delta T), \quad t = N\Delta T \neq 0 \\ R_{ss}(t) &= 0, \quad t \neq N\Delta T \end{aligned} \quad (43)$$

or, in better form,

$$R_{ss}(\tau) = \frac{(p - p^2) A^2}{\Delta T} \mu_0(\tau) + \sum_{\substack{\text{all} \\ N}} \frac{p^2 A^2}{\Delta T} \mu_0(\tau - N\Delta T) \quad (44)$$

The spectra are then found from the Fourier transform as

$$S_s(\omega) = \frac{A^2(p-p^2)}{\Delta T} + \frac{2\pi p^2 A^2}{\Delta T^2} \sum_{\substack{\text{all} \\ N}} \mu_0 \left(\omega - \frac{2\pi N}{\Delta T} \right) \quad (45)$$

The spectra of the sampled process are now found by performing the convolution of Equation 39 as

$$S_s(\omega) = \frac{A^2(p-p^2)}{\Delta T} \frac{1}{2\pi} \int_{-\infty}^{\infty} S_s(\omega) d\omega + \frac{p^2 A^2}{\Delta T^2} S_s \left(\omega - \frac{2\pi N}{\Delta T} \right) \quad (46)$$

The spectra for Poisson sampling are now determined by allowing $\Delta T \rightarrow 0$, $p \rightarrow 0$, while $\Delta T/p \rightarrow 1/\lambda$. Thus,

$$\lim_{\substack{\Delta T \rightarrow 0 \\ p \rightarrow 0 \\ \Delta T/p \rightarrow 1/\lambda}} S_s(\omega) = A^2 \lambda \frac{1}{2\pi} \int_{-\infty}^{\infty} S_s(\omega) d\omega + A^2 \lambda^2 S_s(\omega) \quad (47)$$

To further simplify the result, it is recalled from Parseval's theorem that the mean square value of $m(t)$, $\overline{m^2}$, is given by

$$\overline{m^2} = E \{m^2(t)\} = \frac{1}{2\pi} \int_{-\infty}^{\infty} S_s(\omega) d\omega \quad (48)$$

and this is used to write

$$S_s(\omega) = A^2 \lambda \overline{m^2} + A^2 \lambda^2 S_s(\omega) \quad (49)$$

Finally, recalling that A is the height of the sampling function, further simplification may be achieved with little loss of generality by making

$$A = 1/\lambda \quad (50)$$

resulting in

$$S_s(\omega) = \frac{\overline{m}^2}{\lambda} + S_a(\omega) \quad (51)$$

From Equation 51, three interesting facts are observed:

- The spectra of the original sampled signal are maintained without frequency distortions.
- There is no aliasing in the sampling process.*
- A broadband noise is added to the original spectra whose amplitude is proportional to the ratio of the average power of the sampled signal, $m(t)$, to the mean sampling rate, λ . Thus λ must be chosen to reduce this noise to an acceptable level (see Figure 23).

There are three calculations which may be made from Equation 51 to better identify the value of λ necessary for successful spectra recovery by signal reconstruction.

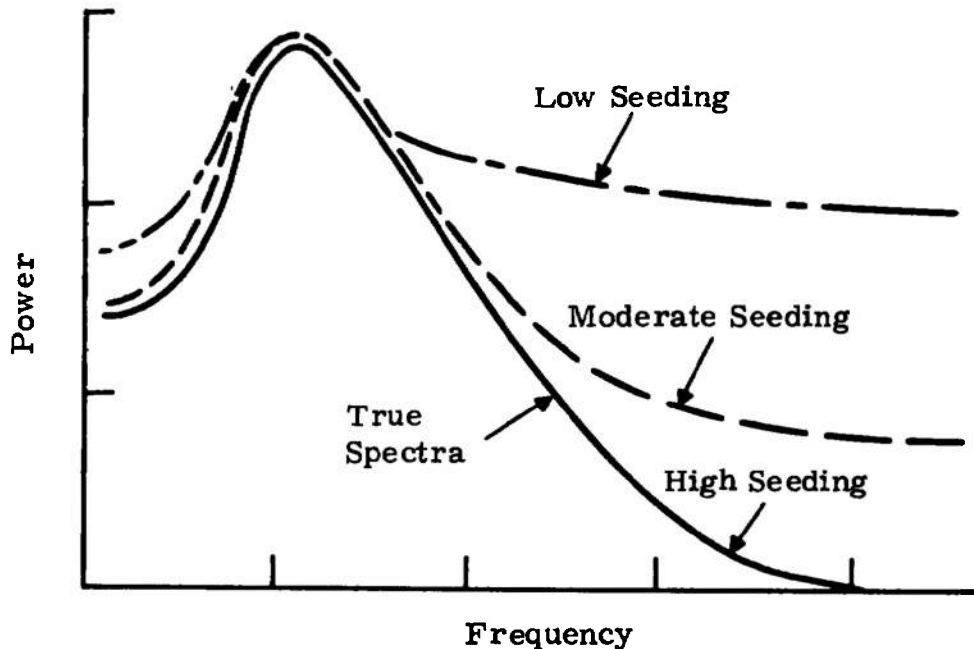


Figure 23. Laser-Velocimeter Spectral Analysis for Various Seeding Rates

*The "Shannon sampling theorem" is obtained from Equation 46 by letting $p = 1$.

To determine a spectral amplitude/noise ratio, D , defined here as the ratio of the maximum value of $S_n(\omega)$ to \overline{m}^2/λ , is an indication of one's ability to discern the shape of $S_n(\omega)$. If it is assumed that $S_n(\omega)$ is a narrowband process where

$$S_n(\omega) = \frac{a^2}{a^2 + (\omega - \omega_p)^2} + \frac{a^2}{a^2 + (\omega + \omega_p)^2} \quad (52)$$

so that the spectra are centered around ω_p with 3db bandwidth $2a$, it is found (Ref. 14) that

$$\overline{m}^2 = a \quad (53)$$

$$\text{and } S_n(\omega)_{\max} = 1. \text{ Thus } D_{NB} = \lambda/a \quad (54)$$

$$\text{Then letting } 2\pi f_{3db} = 2a \quad (55)$$

it is found that

$$D_{NB} = \frac{\lambda}{\pi f_{3db}} \quad (56)$$

Thus, to discern the spectra of a narrowband process, λ must be chosen so that

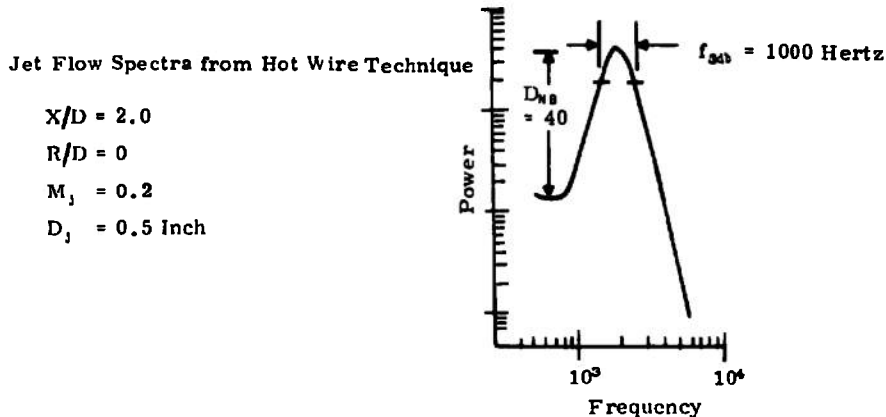
$$\lambda \geq D_{NB} \pi f_{3db} \quad (57)$$

where D_{NB} is the amount of discernibility which must be estimated qualitatively. An example of a narrowband analysis is shown in Figure 24.

Finally, a wideband process, where

$$S_n(\omega) = 1; -\omega_0 \leq \omega \leq \omega_0 \quad (58)$$

$$S_n(\omega) = 0 \text{ elsewhere}$$



$$\lambda \geq 3.14 \times 40 \times 1000 = 120,000 \frac{\text{Particles}}{\text{Second}}$$

Figure 24. Example of Required Seeding for Narrowband Spectral Information

gives
$$\overline{m}^2 = \omega_0 / \pi \quad (59)$$

and, therefore,

$$D_{WB} = \frac{\pi \lambda}{\omega_0} \quad (60)$$

Substituting

$$2\pi f_0 = \omega_0 \quad (61)$$

the result becomes

$$D_{WB} = \frac{\lambda}{2f_0} \quad (62)$$

An example of a wideband process is shown in Figure 25.

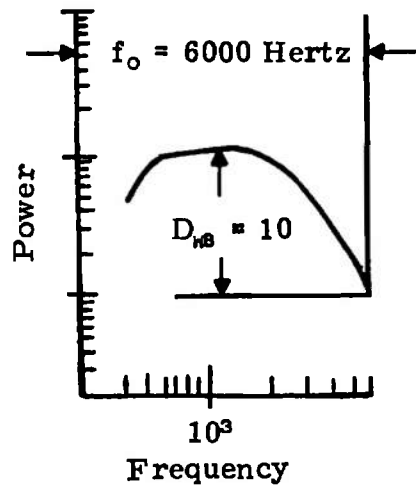
Jet Flow Spectra from Hot Wire Technique

$$X/D = 2.0$$

$$R/D = 0.4$$

$$M_j = 0.2$$

$$D_j = 0.5 \text{ Inch}$$



$$\lambda \geq 2 \times 10 \times 6000 = 120,000 \frac{\text{Particles}}{\text{Second}}$$

Figure 25. Example of Required Wideband Spectra Information

From this analysis it is seen that a system utilizing this second approach, shown schematically as Figure 26, would be suitable if sufficiently high data-acquisition rates were available. Based on the above criteria, if for a given flow situation the average seeding rate is found to be prohibitively high (as may be the case for wind tunnel flows), then the first method for spectral estimation (Equations 38 and 39) should be considered. It should be emphasized that such a choice will probably necessitate a significantly larger test time and greater capital investment in special-purpose post-LV processor hardware for computing the autocorrelation functions.

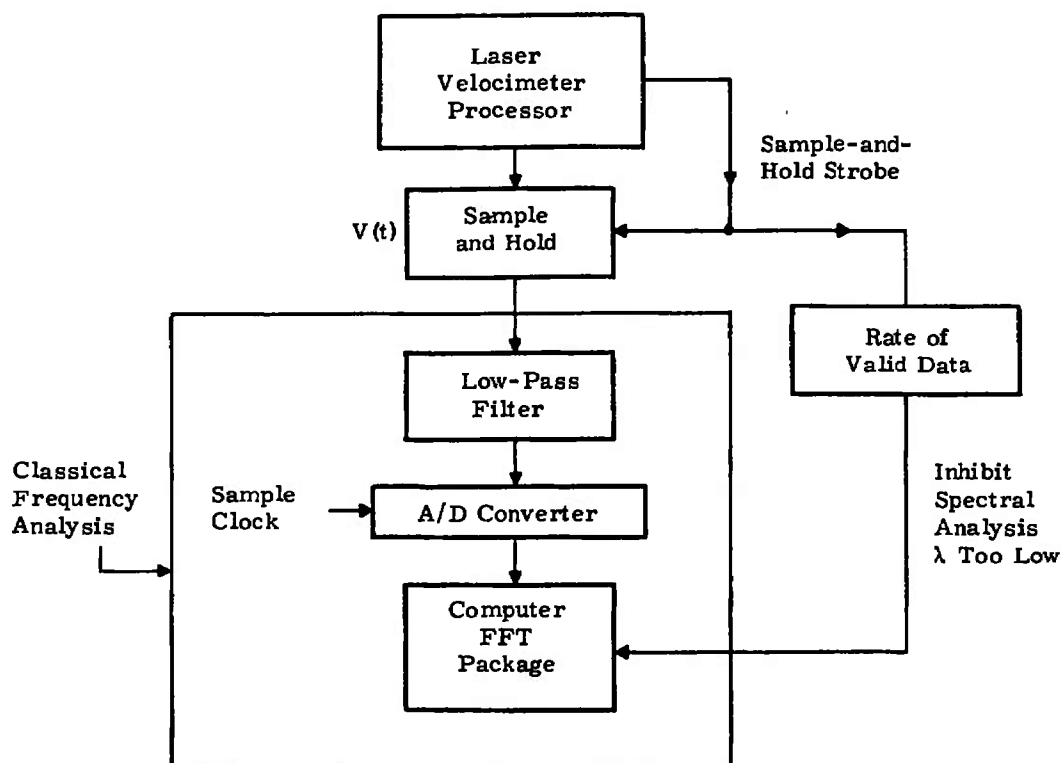


Figure 26. Signal Analysis Scheme for Laser Velocimeter Spectra

PRACTICAL INTERPRETATION FOR TURBULENCE SPECTRA MEASUREMENT

Equation 51 together with "amplitude/noise relations equations" 52, 56, and 60 provide a means for determining velocity spectra from the output of the LV. As no frequency distortion is added to the velocity spectra, the successive LV outputs may be processed directly by any conventional spectral analyzer. The only restrictions on the system are that the particle passage rate, λ , be made high enough so that the spectra are discernible in the sampling noise as determined in Equation 51 and that the probe volume be reduced to the point at which the probability of two particles in the probe volume simultaneously is reduced to a negligible level. This probability for a second length T_ℓ in time is easily derived as

$$P(T_\ell) = e^{-8\lambda^2 T_\ell \beta / v}$$

The exponent can be divided into two dimensionless numbers of physical significance:

$$\frac{8\lambda\beta}{v} = \text{average number of particles in probe volume}$$

$$T_\ell\lambda = \text{average number of particles in a data record}$$

The probability of a record with no particle multiplicity as a function of these two quantities is submitted as Figure 27.

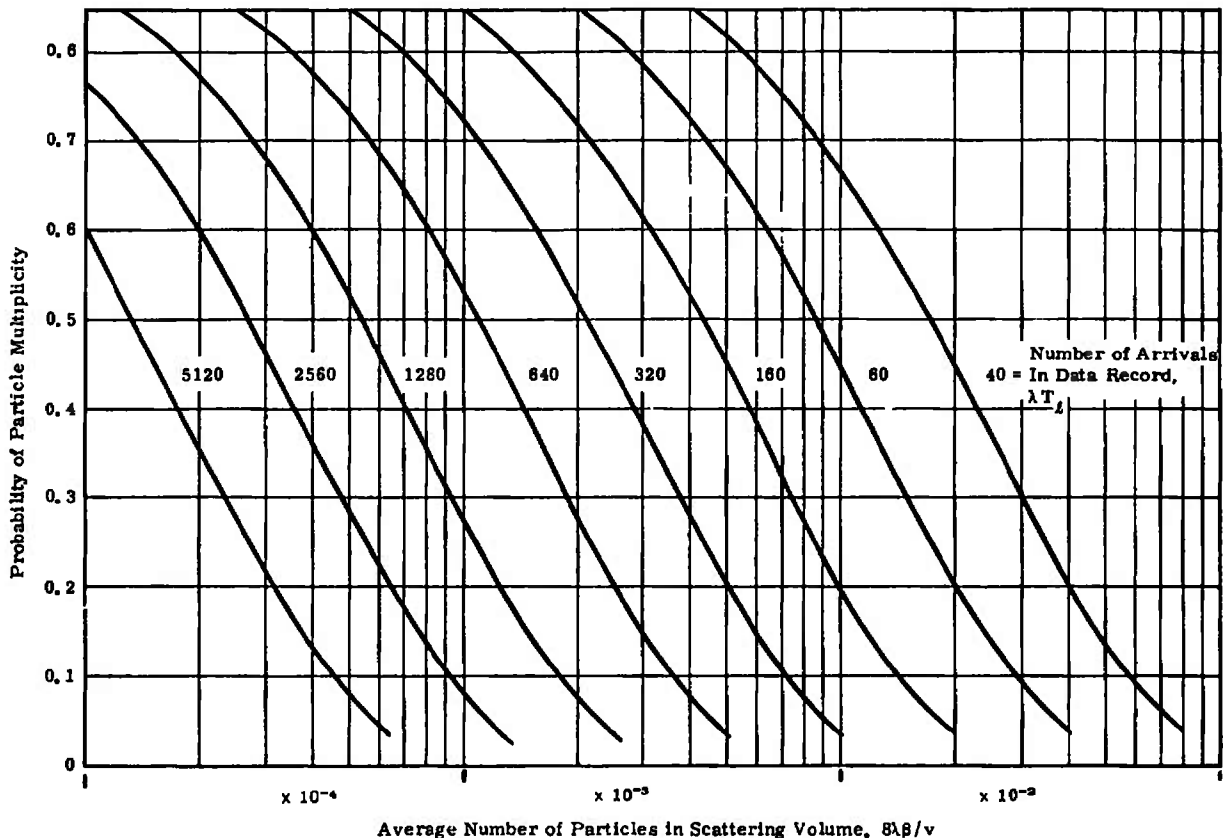


Figure 27. Probability of Particle Multiplicity

There is some debate as to the effect of the multiplicity of particles on the velocity spectra. The effect becomes more unclear if these points are detected and removed from the data. The main criteria necessary for the validity of the approach presented in this report is that the particle inter-arrival times correspond closely to an exponential distribution. Clearly, if the particle transit time through the probe volume approaches $1/\lambda$, this assumption is questionable.

The high sampling rates required by this approach may be reduced somewhat by prequalification of the data to choose those parts of the record with the highest sampling density prior to spectral analysis. The effects of this on the spectral estimate and the degree to which the rate can be reduced is a source of future work in this area. Also, the effect of using "short records" in the spectral analysis (those of length $100/\lambda$, etc.) should be investigated, particularly where the spectral estimate is accomplished using fast-Fourier-transform techniques.

APPLICABILITY OF COUNTER AND FREQUENCY TRACKER LASER VELOCIMETER PROCESSORS TO SPECTRAL-ANALYSIS MEASUREMENT THEORY

While the representation of a randomly time-spaced velocity data train is suggestive of the counter-type LV processor, the analysis developed in this study is also applicable to the frequency tracker type of processor. The counter-type processor measures the time of particle passage over adjacent interference fringes in the scattering volume. An analog divider and sample-and-hold circuits generate the analog of the "continuous" velocity data signal.

For the frequency tracker type of processor, the frequency of particle passage is measured directly. To do this in a stable manner, larger particle concentrations and associated rates are required. Electronic damping is also provided, to bridge the gap where particle passages may run low for a short time (hundreds of microseconds). In such a case, this damping acts as a system low-pass filter, thus reducing its overall frequency response. Assuming this damping is low and the tracker can remain stable while the following rapid changes in velocity, the output from a tracker can be sampled at the time of particle passage, to provide an identical signal as the counter system. With these restraints in mind, the power spectra could be deduced in the manner previously presented here.

Nonetheless, the use of a frequency tracker processor may be expected to be particularly less than desirable for routine power spectra measurements in gas flows of a wind tunnel. For such cases, the minimum duty cycle (percent of time at least one particle resides in the scattering volume) of 15 percent for operation of the frequency tracker processor is difficult to attain even in flows of relatively high seeding concentrations. By working at the lower end of this duty cycle, then, tracker processor stability is reduced and more electronic damping is required. The overall result would then be an undesirable LV system with a low turbulence frequency response.

Section 5

EXPERIMENTAL CONFIRMATION OF LASER-VELOCIMETER SPECTRAL
ANALYSIS THEORYVERIFICATION OF SAMPLING PROBABILITY DISTRIBUTION
ASSUMPTION

Experiments were conducted to verify the assumption that the interarrival times of the particles were exponentially distributed. Several records of the particle sampling sequence were captured at a moderately high particle rate (100,000 particles per second).

These records were subjected to the analysis described below, to determine whether the interarrival time was, in fact, an exponentially distributed random variable. The autocorrelation function and spectra of the sampling sequence were computed and were shown to be in good agreement with the theoretical determinations.

The records of the sampling sequence were obtained in the following manner (Figure 28). The output of the photodetector of the laser velocimeter was

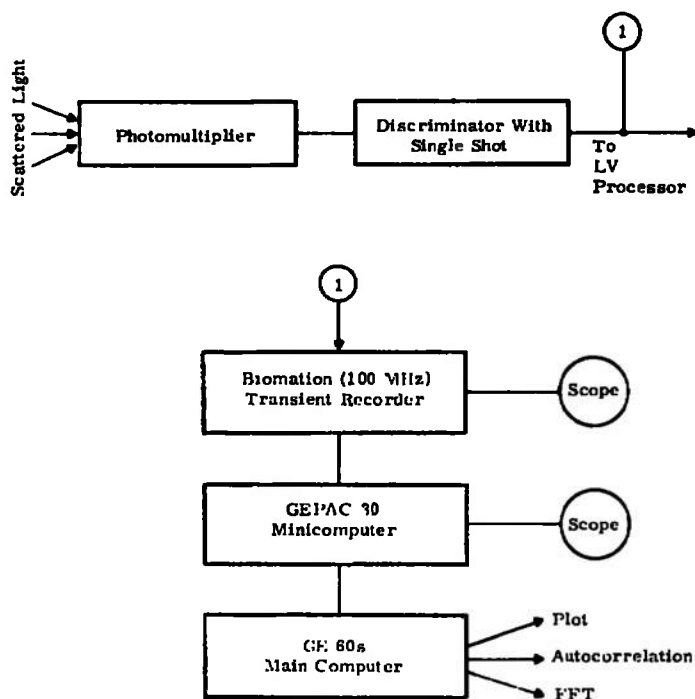


Figure 28. Schematic of Instrumentation for Experimental Verification of Random Sampling Assumption

connected to an amplifier/discriminator (SSR Instruments Company Model No. 1120), which was used to sense the presence of a particle in the probe volume. The discriminator output pulse was then stretched by a Fairchild Model 9601 one-shot multivibrator to 0.75 microsecond. The resulting pulse stream was sampled at a rate of 2 megahertz and stored by the Biomation Corporation transient recorder used in the burst spectra experiment. For a particle rate of 100,000 particles per second, and utilizing the full 1024-point storage capacity of the Biomation recorder, one obtains a record with an expected content of 101 particle occurrences and a mean interarrival time of twenty 0.5 microsecond divisions. Although this population is less than ideal, it was the largest which could be recorded with available equipment and does prove adequate to verify the theory. The records were transferred from the Biomation recorder to a GEPAC 30-2E minicomputer and, by telephone, to the Research and Development Center's GE 600 time-sharing computer. The following tests were then applied to the data records:

- "WE" Test. This is a test to show whether a data record may be attributed to an exponential distribution with arbitrary starting point (Note: the finite width of the event creates a dead time in which no other occurrences may be measured). This test is performed as described by Shapiro and Hahn (Ref. 15), as follows:

1. Compute WE for the first 35 points of the data as

$$WE = \frac{(\bar{x} - x_1)^2}{\sum_{m=1}^{35} (x - \bar{x})^2}$$

where \bar{x} is the sample mean and x_1 is the smallest element of the 35-point array.

2. If WE is such that

$$0.018 < WE < 0.045$$

then the distribution lies in a class of 90 percent of all exponential distributions containing those points.

For the four data records captured,

$$\begin{array}{ll} WE_1 = 0.0274 & WE_3 = 0.0371 \\ WE_2 = 0.0118 & WE_4 = 0.0371 \end{array}$$

all of which are within the limits. Therefore there is reason to believe the data are exponentially distributed.

- Uniform Distribution Transformation. As a further test of the exponential assumption, the distribution function is transformed to the

uniform distribution under an exponential transformation. If the random variable X is the assumed exponential variable, then

$$F_x(x) = P(X < x) = \left(1 - e^{-\lambda(x - x_0)}\right) \quad (63)$$

If Y becomes the transformed variable, so that

$$Y = e^{-\lambda(x - x_0)}$$

then, since

$$P(X > x) = 1 - F_x(x) = e^{-\lambda(x - x_0)} \quad (64)$$

one obtains

$$P\left(\frac{-1}{\lambda} \ln(Ye^{-\lambda x_0}) > x\right) = e^{-\lambda(x - x_0)} \quad (65)$$

or

$$P(Y < e^{-\lambda(x - x_0)}) = -\lambda(x - x_0) \quad (66)$$

If $y = e^{-\lambda(x - x_0)}$, then

$$P(Y < y) = y = F_y(y) \quad (67)$$

which is identified as the uniform distribution function. The transformed data records are plotted in Figures 29a through 29d, with $x_0 = 1$ microsecond and λ optimized for the best mean-square fit to the uniform distribution. As can be seen by examining the data, the curves fit well. In all cases the best-fit value of λ is greater than the measured rate of 100,000 particles per second. This is necessary to correct for the particles which theoretically occur in the dead time between particles.

The sample autocorrelation functions and spectra functions were also computed for the sampling records. These are shown as Figures 30a through 30c and 31a through 31c. According to the theory both the autocorrelation function and the spectra should consist of the sum of a broadband level and an impulse at the origin. In the discrete analysis, the ratio of the "height" of the impulse to the broadband level, μ , should be

$$\mu = 1/\lambda\Delta T \approx 20$$

This agrees favorably with the data. In addition, if the velocity spectra are to be successfully recovered using these sampling sequences, then the broadband component should be reasonably flat and, in particular, contain no high "spikes," as this component convolved with the original turbulence spectra determines the broadband noise in the output. Again examination of the spectra indicates a reasonable flatness; it may therefore be assumed that the noise added to the turbulence velocity spectra will probably be near the theoretical value.

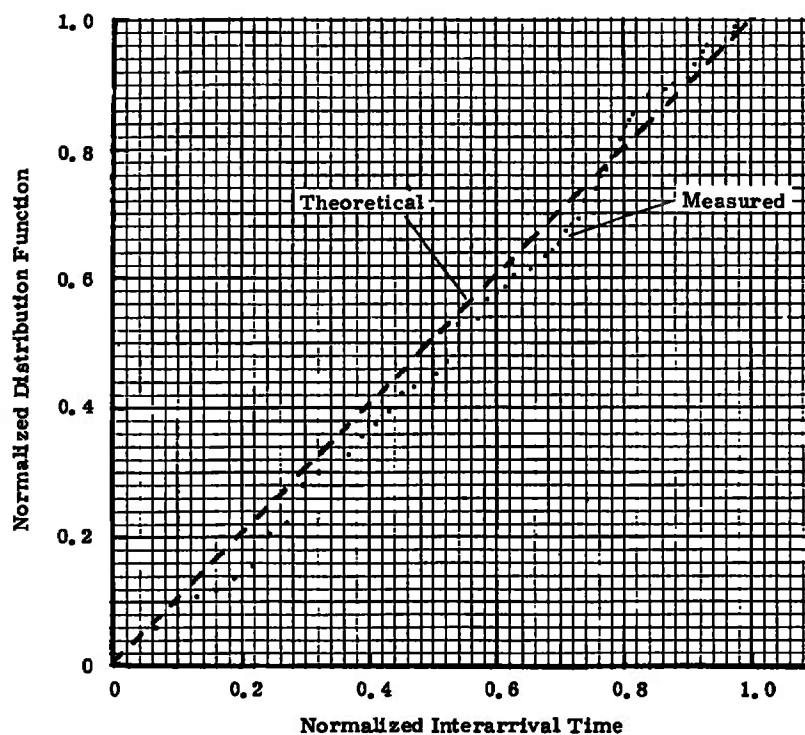


Figure 29a. Exponential Transformation of Particle Interarrival Time
($\tau = 1 \mu\text{sec}$; $\lambda = 143.3 \text{ K/sec}$)

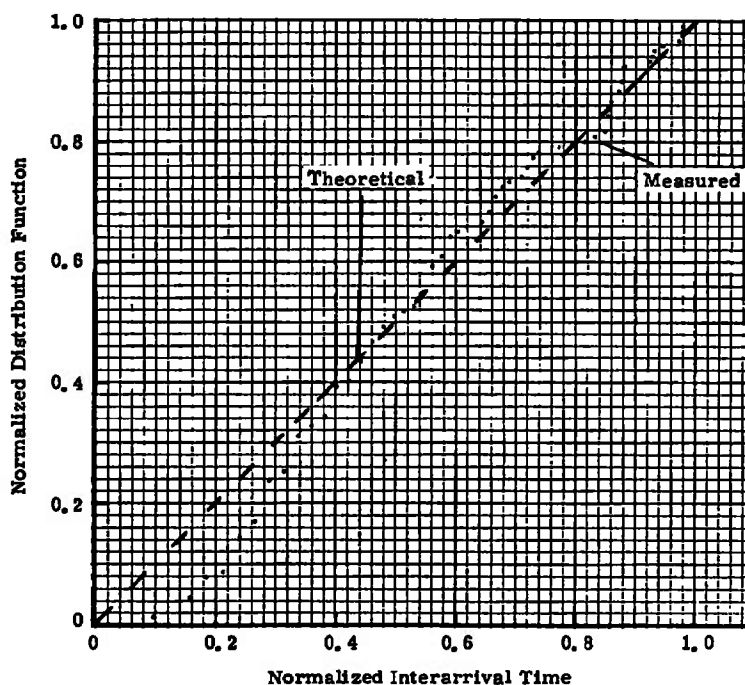


Figure 29b. Exponential Transformation of Particle Interarrival Time
($\tau = 1 \mu\text{sec}$; $\lambda = 138.6 \text{ K/sec}$)

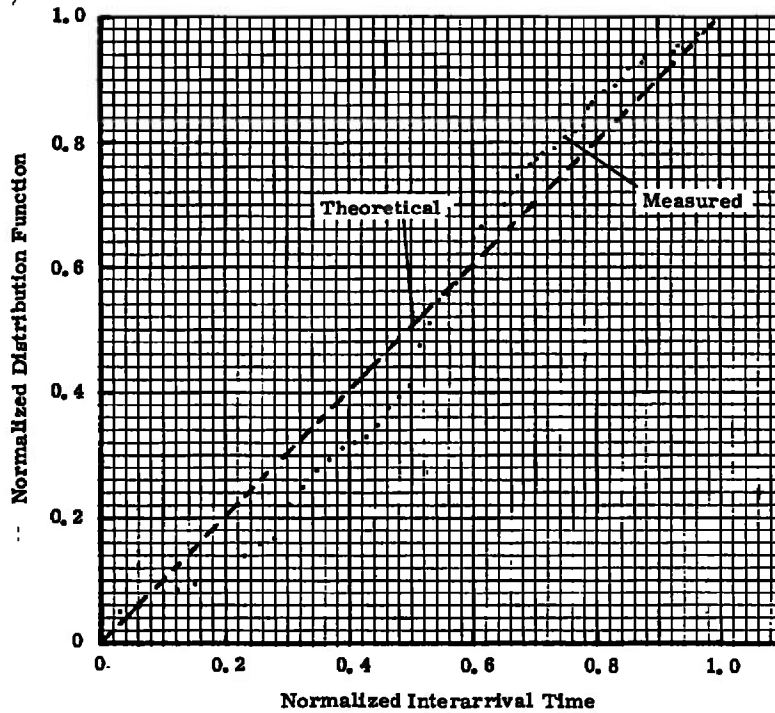


Figure 29c. Exponential Transformation of Particle Interarrival Time
($\tau = 1 \mu\text{sec}$; $\lambda = 132.4 \text{ K/sec}$)

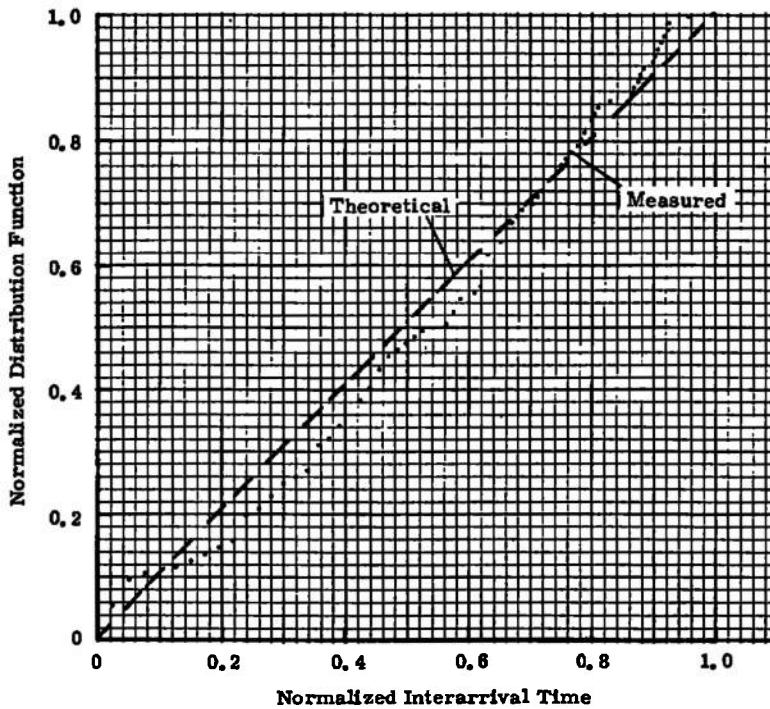


Figure 29d. Exponential Transformation of Particle Interarrival Time
($\tau = 1 \mu\text{sec}$; $\lambda = 112.0 \text{ K/sec}$)

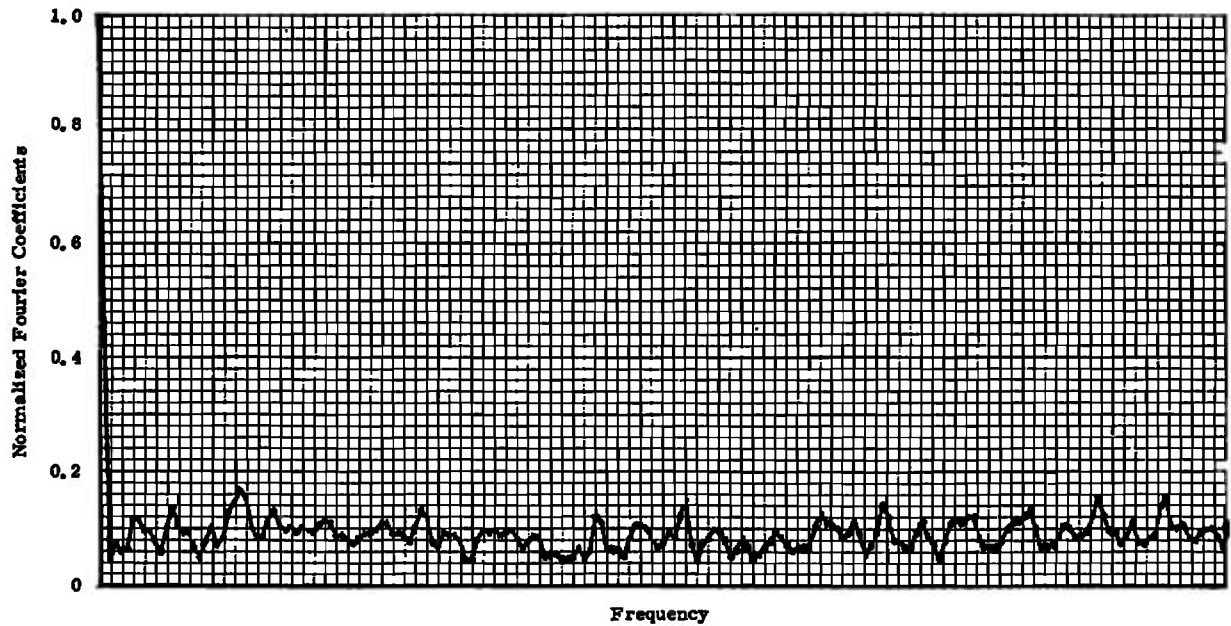


Figure 30a. Autocorrelation of Particle Interarrival for Record in Figure 29a.

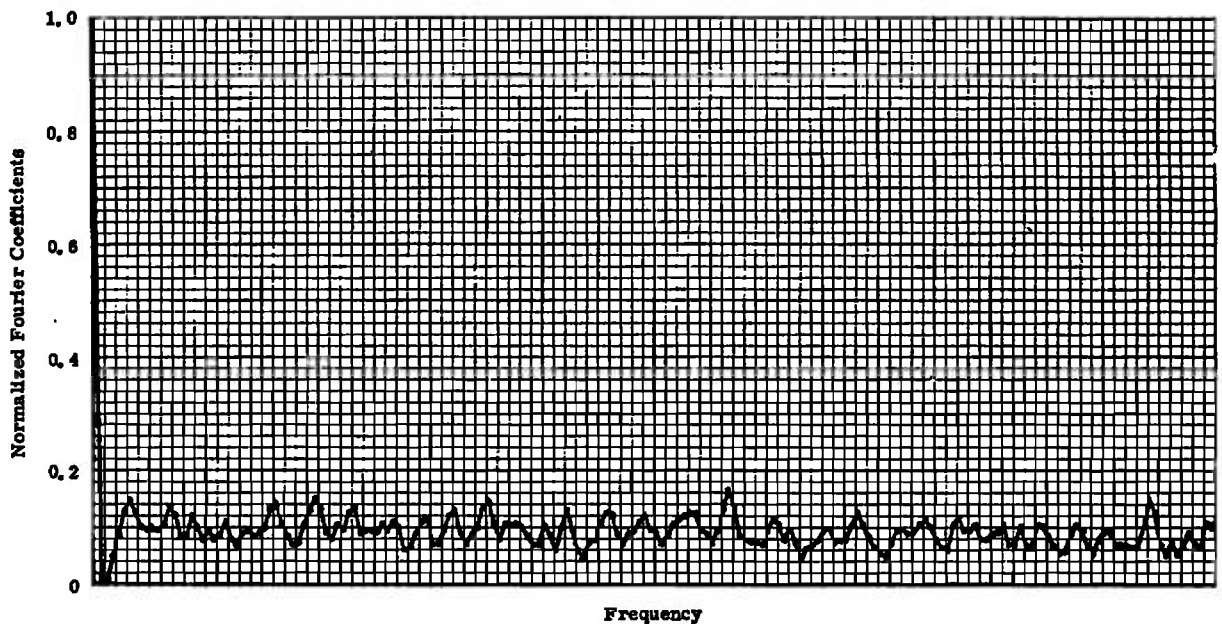


Figure 30b. Autocorrelation of Particle Interarrival for Record in Figure 29b.

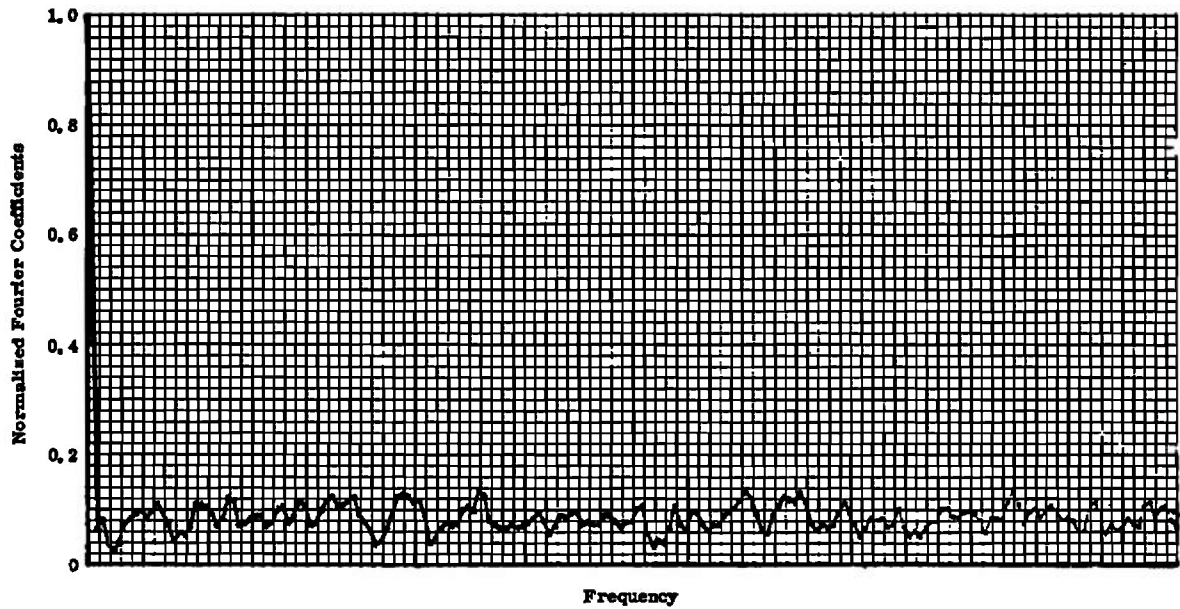


Figure 30c. Autocorrelation of Particle Interarrival for Record in Figure 29c.

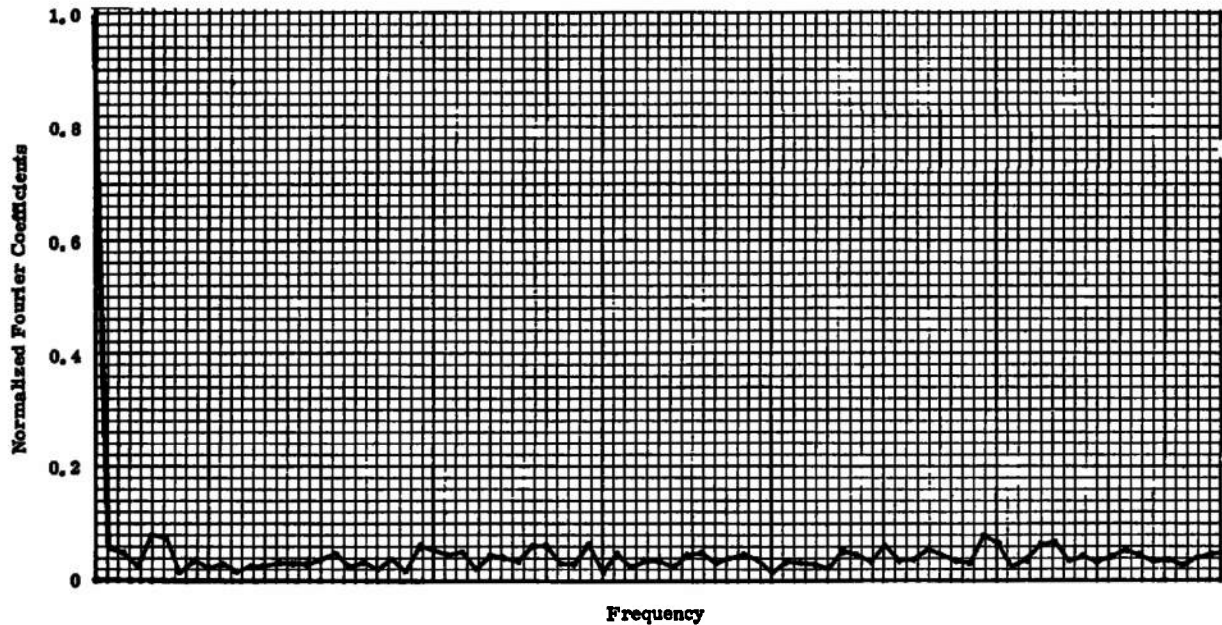


Figure 31a. Spectra of Particle Interarrival Times for Record in Figure 29a.

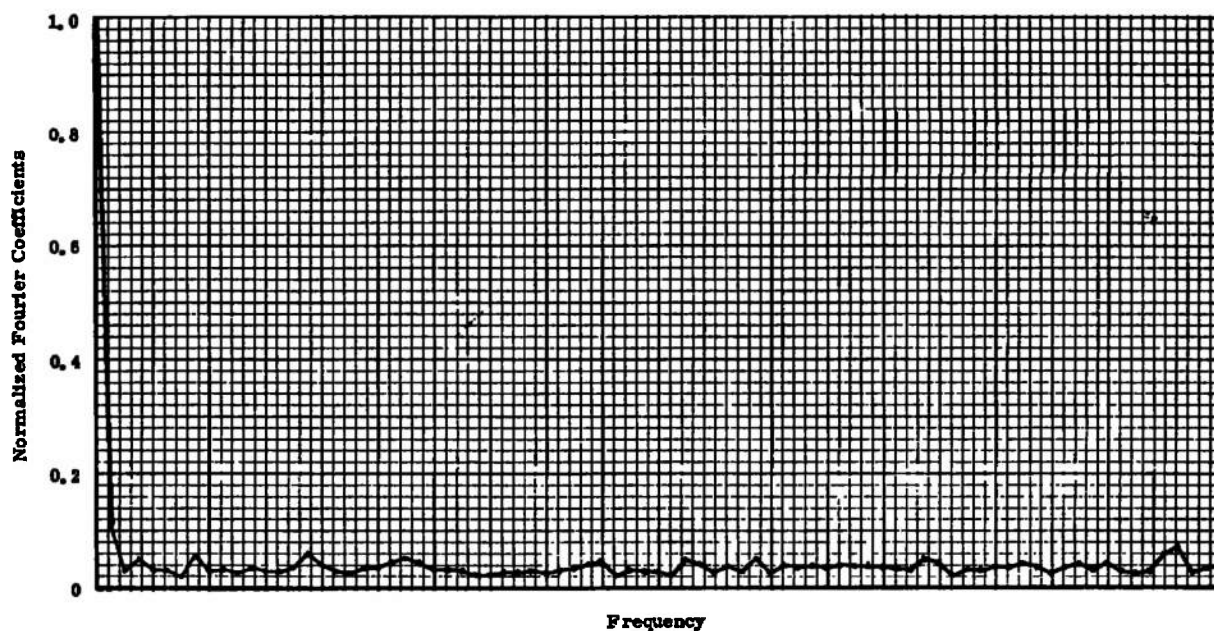


Figure 31b. Spectra of Particle Interarrival Times for Record in Figure 29b.

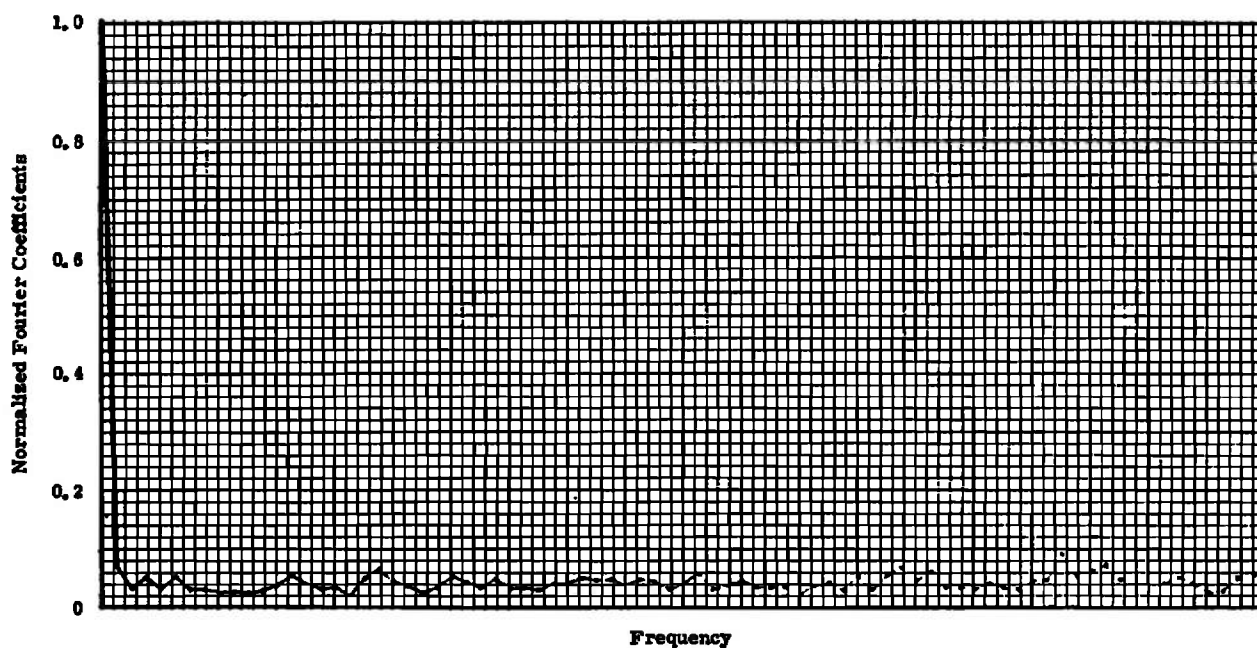


Figure 31c. Spectra of Particle Interarrival Times for Record in Figure 29d.

The outcome of these experiments verifies to a certain degree the model of the spectra generation process.

EXPERIMENTAL DETERMINATION OF SIGNAL PROPERTIES OF DOPPLER BURST

The validity of Equation 46 and Equation 50 in predicting the waveshape and Fourier spectra of the Doppler bursts was experimentally investigated. To accomplish this, a Biomation Model transient recorder was used for capturing the bursts from the photomultiplier preamplifier output. The bursts were sampled at a 100-megahertz sampling rate and stored in the Biomation recorder's internal memory. This information was then transferred, at a slower rate, to a GEPAC 30 minicomputer, which reformatted and sent it by telephone line to the Research and Development Center's General Electric 600 time-sharing computer. The records were normalized to a length of 512 points, and the GE 600 was then used to compute the magnitudes of the Fourier transform coefficients through the autocorrelation function of the data. The relations used in this analysis are, for the autocorrelation function,

$$R_{xx}(N) = \frac{\sum_{K=N}^{511} x(K-N) x(K)}{\sum_{K=0}^{511} x^2(K)} \quad (68)$$

and for the power spectra,

$$S_x(J) = \frac{\sum_{K=0}^{511} R_{xx}(K) \cos(2\pi JK/512)}{\sum_{K=0}^{511} R_{xx}(K)} \quad (69)$$

The magnitudes of the Fourier coefficients were then found from

$$F_x(J) = \sqrt{S_x(J)} \quad (70)$$

Two sets of data are shown in Figures 32a through 32c and Figures 33a through 33c. In the first case, Figures 32a to 32c, a small, single particle passes through the scattering volume, yielding a Doppler signature of high contrast. The second signature, Figures 33a to 33c, probably results from the passage of a larger particle with a smaller particle entering the scattering volume as the large seed is leaving.

Although there is moderate superimposed high-frequency noise associated with the input traces (Figures 32a and 33a), the autocorrelation function and the spectra clearly indicate the predominant Doppler time and frequency, respectively. The general transient pulse shapes of Figures 32a and 33a are

similar to those derived from the analytical model previously presented as Equation 16.

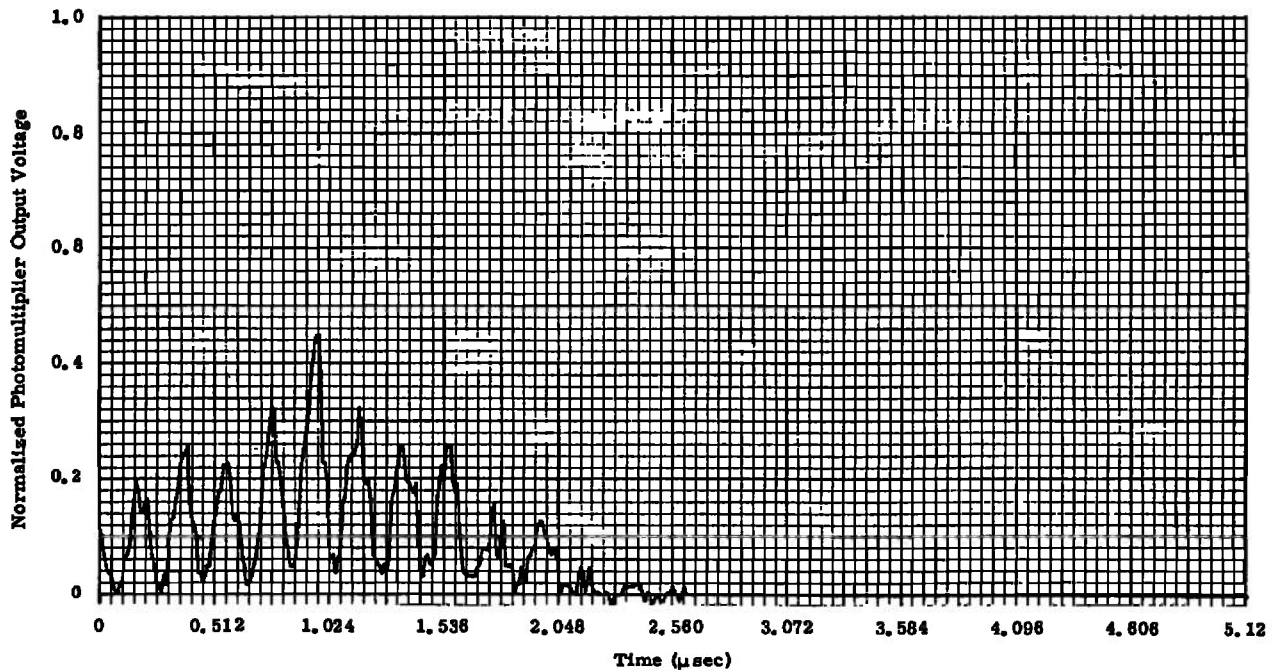


Figure 32a. Transient Recorder Output of a Doppler Burst with High Contrast (Single Small Particle)

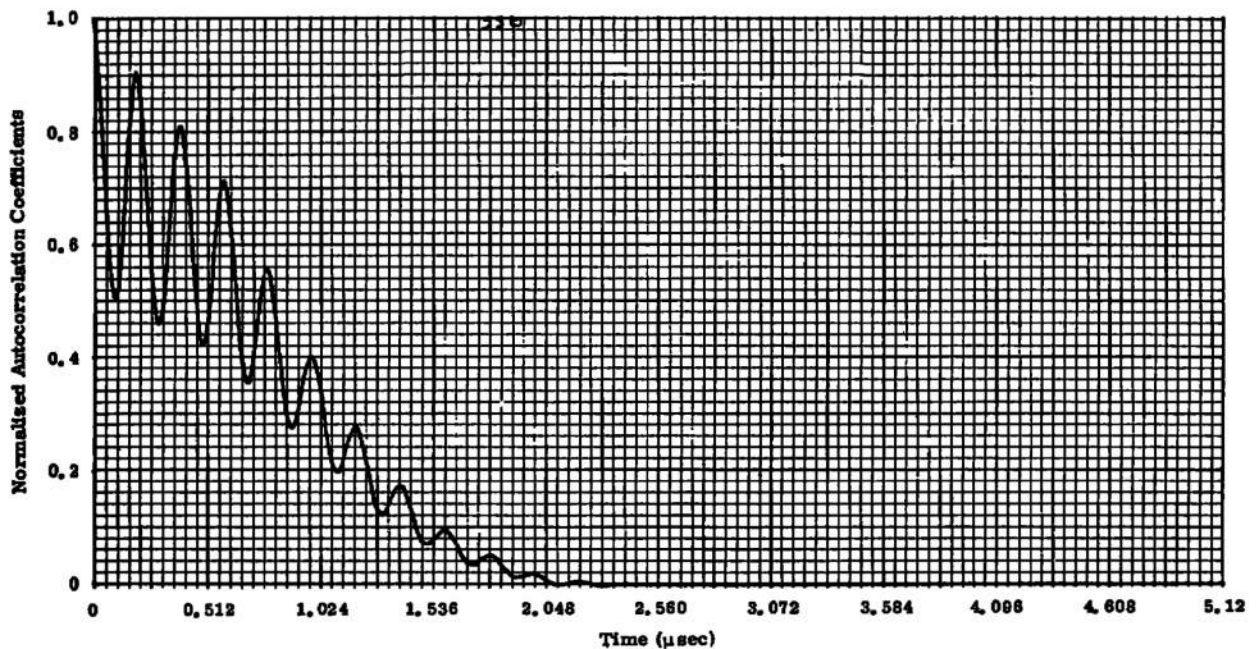


Figure 32b. Autocorrelation of Doppler Burst with High Contrast

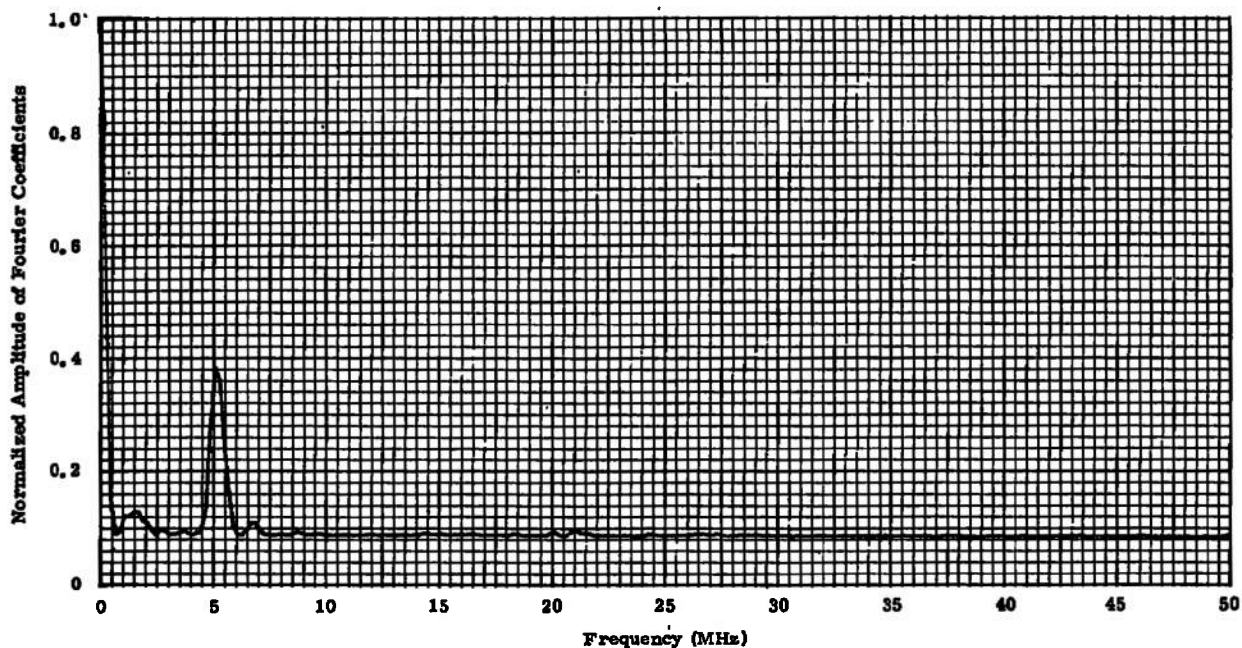


Figure 32c. Magnitude of Fourier Coefficients with Doppler Burst of High Contrast

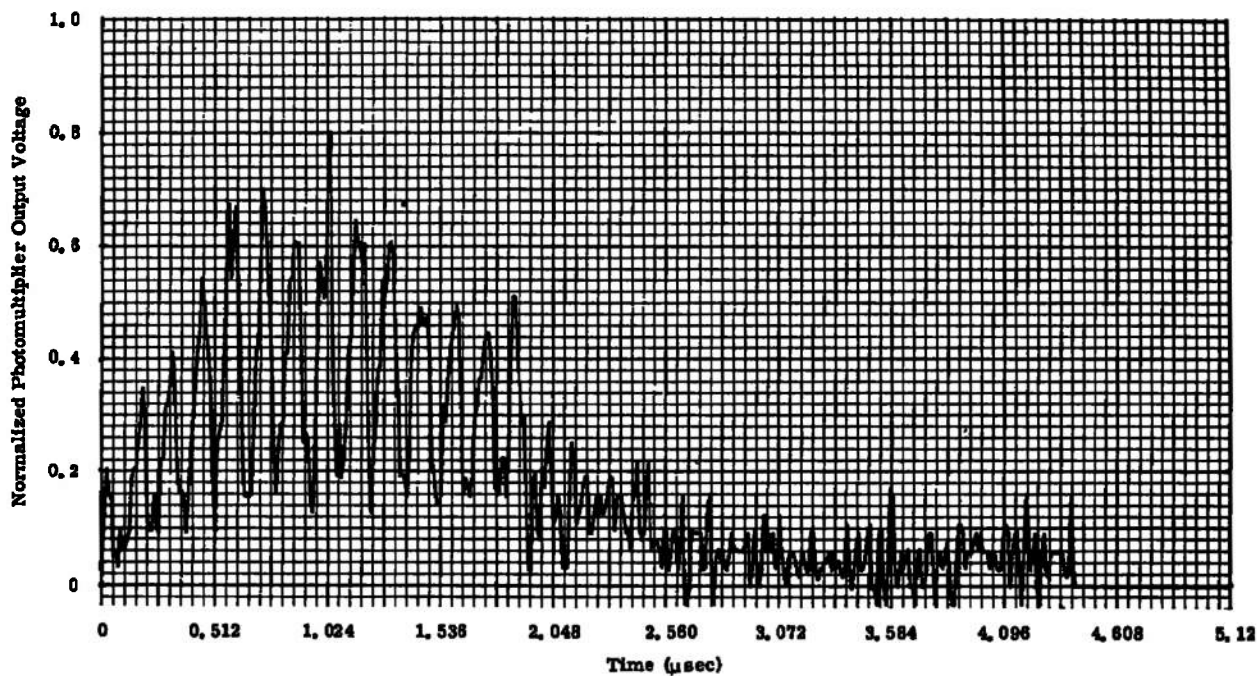


Figure 33a. Transient Recorder Output of a Doppler Burst with Fair Contrast

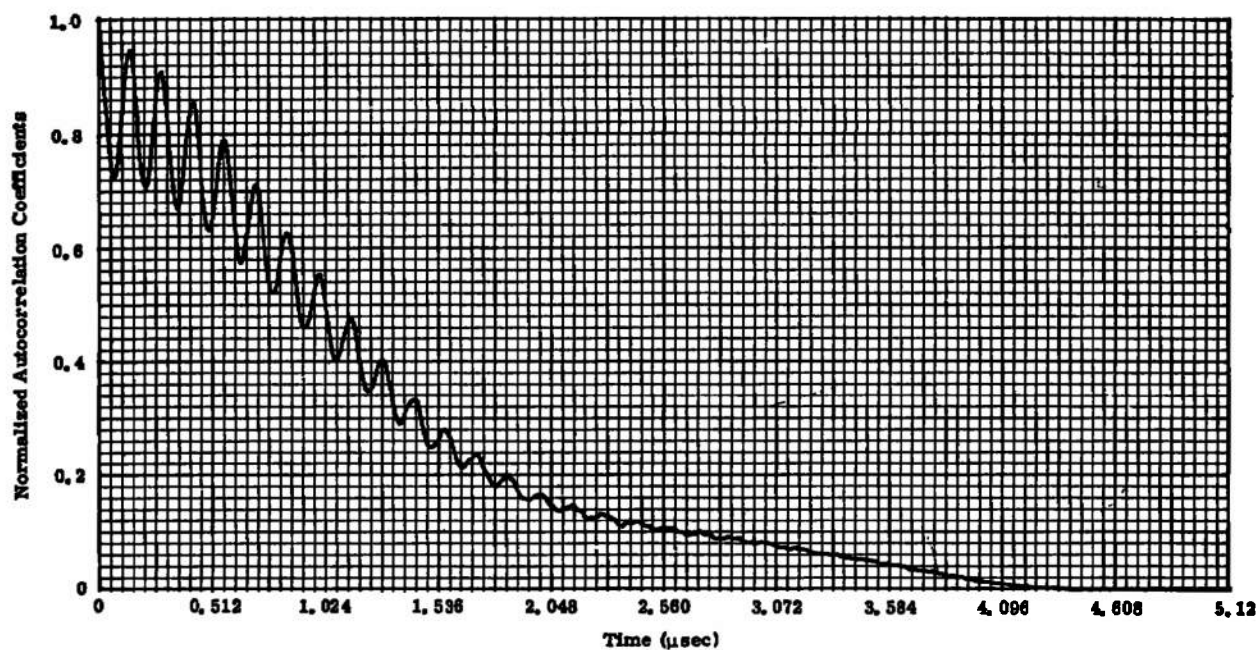


Figure 33b. Autocorrelation of Doppler Burst with Fair Contrast

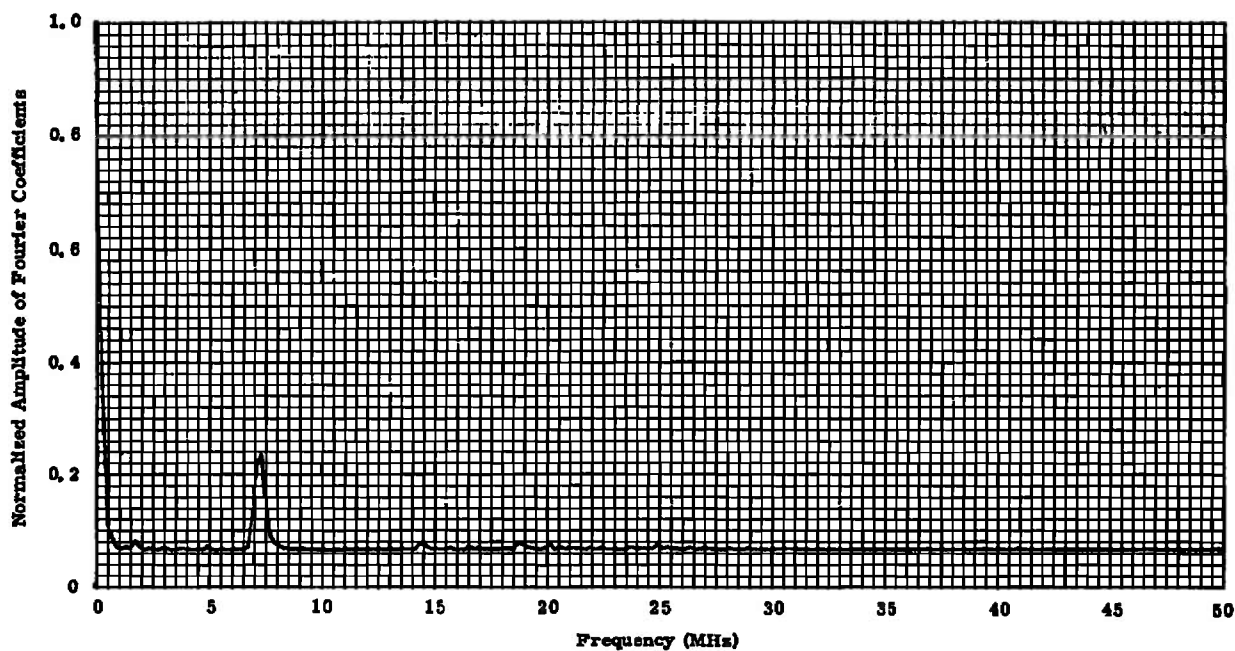


Figure 33c. Magnitude of Fourier Coefficients with Doppler Burst of Fair Contrast

ELECTRONIC SIMULATION OF SPECTRA ANALYSIS BY RANDOM SAMPLING

An electronic simulation was conducted to verify the developed theoretical analysis for laser-velocimeter spectral measurements. In this experiment, electronically generated noise with known bandwidths was sampled, using pre-recorded particle-arrival information from a typical test run obtained from the LV counter-type processor detailed in Appendix I, "Laser-Velocimeter Optical Setup and Processor" (Figure 34). The data or particle arrival rate was 60

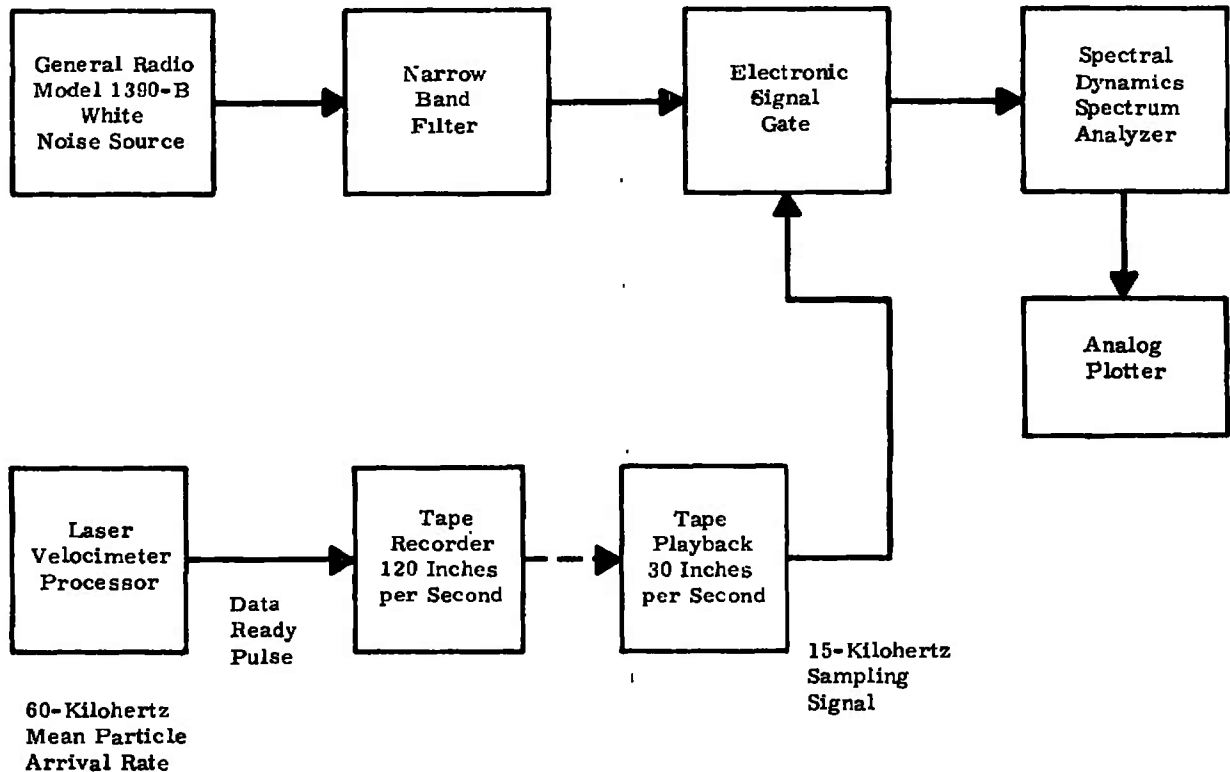


Figure 34. Experimental Setup

kilohertz. This tape was then played back at one-fourth the recording speed so that a 15-kilohertz mean sampling rate was obtained. Five analog narrowband filters were constructed and their bandwidths verified experimentally. A white-noise generator (Model No. 1390-B, made by the General Radio Company) was used to excite the filters; the combination provided a source of narrowband noise with known statistics. This noise was then gated by the 15-kilohertz sampling signal and fed to a Spectral Dynamics spectrum analyzer.

As previously derived, the sampling process is expected to add a white noise to the source signal. The magnitude of the noise should be related to the mean sampling rate and the bandwidth of the source signal. Specifically, if μ is defined to be the ratio of the maximum of the signal-spectra-plus-sampling-noise to the sampling noise, then:

$$\mu = \frac{\text{Max Source Spectra} + \text{Sampling Noise}}{\text{Sampling Noise}}$$

$$\mu = 1 + \frac{\lambda}{f_{3dB}}$$

where λ = mean sampling rate = 15 kilohertz and f_{3dB} = the 3-decibel bandwidth of the source signal. This ratio is calculated for each of the filtered noise and source signals in Table 3.

The output spectra from the Spectral Dynamics analyzer were used to determine experimental values of μ . These values, tabulated in Table 3, were found to be within 4 decibels of the predicted values. The sampled spectra were also estimated from the original filtered-noise source spectra. These are submitted, together with the measured spectra of the sampled process, in Figures 35 through 39. The output spectra may be seen to be in good agreement with predictions.

This experiment extends confidence that LV spectra may be derived in a similar manner, and that the theoretical results presented in this report may be successfully used to predict the effects of the sampling on the turbulence velocity spectra.

EXPERIMENTAL ATTEMPT TO OBTAIN LASER-VELOCIMETER TURBULENCE SPECTRA MEASUREMENTS

As mentioned previously, the desired comparisons of LV and hot-wire power spectra measurements were originally planned at the conclusion of this investigation. In spite of a significant effort, this proof-testing of the LV spectra measurement theory was not satisfactorily completed. Since the electronic simulation did show conclusively that the theory is valid, sources of error in experimental technique for these comparisons were sought. The following problems were isolated and overcome by the end of the study:

- Sample-and-hold circuit bias accentuated low-frequency spectra.
- Monitoring of the data acquisition rate for a time slice of data undergoing spectra analysis is necessary.

The difficulties encountered should be viewed as the normal debugging of a newly integrated and complex system (which includes the flow, LV optics and processor, and spectra analyzer) rather than a reflection on the validity of the developed spectral theory. While the hot-wire and LV comparisons need to be made before routine spectral measurements can be obtained with confidence, there remains little doubt that the LV spectral measurement theory is correct.

The remaining parts of Section 5 document the insights developed during this proof test.

Table 3
TABULATION OF FILTERED NOISE DATA

Filtered Noise Number	Bandwidth (Hz)	Maximum Filtered Noise Spectra + Sampling Noise	
		Predicted (dB)	Measured (dB)
1	158	14.9	15
2	468	10.4	14
3	1651	5.89	9
4	6485	2.39	6
5	25700	0.737	3

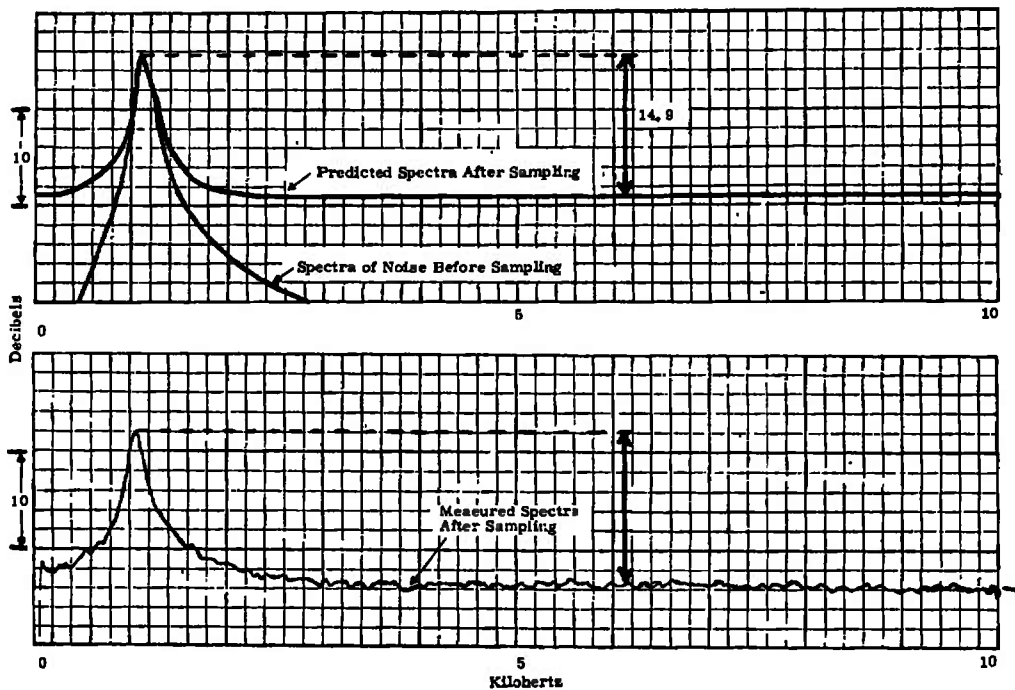


Figure 35. Electronic Simulation of Laser-Velocimeter Spectra Measurements from Random-Time Sampled White Noise of Bandwidth 158 Hertz

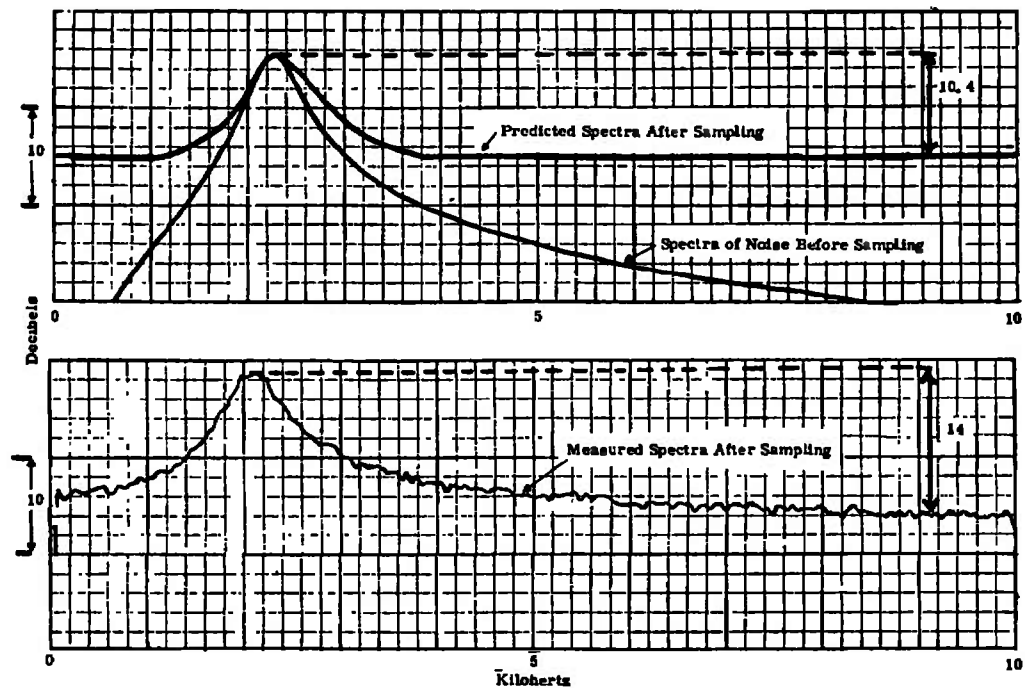


Figure 36. Electronic Simulation of Laser-Velocimeter Spectra Measurements from Random-Time Sampled White Noise of Bandwidth 468 Hertz

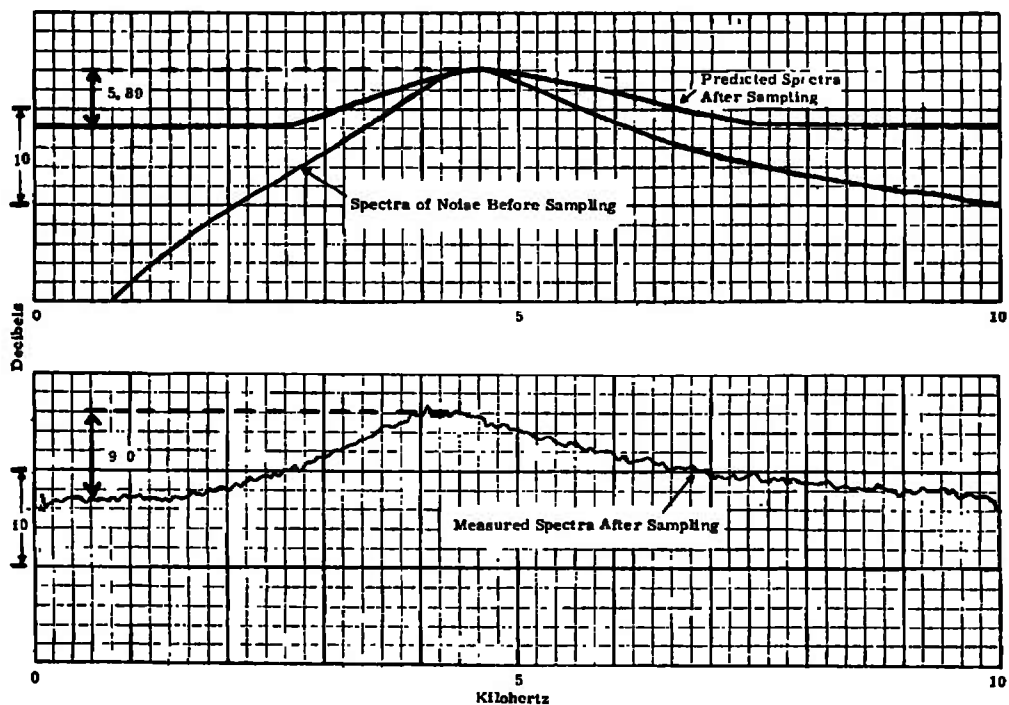


Figure 37. Electronic Simulation of Laser-Velocimeter Spectra Measurements from Random-Time Sampled White Noise of Bandwidth 1651 Hertz

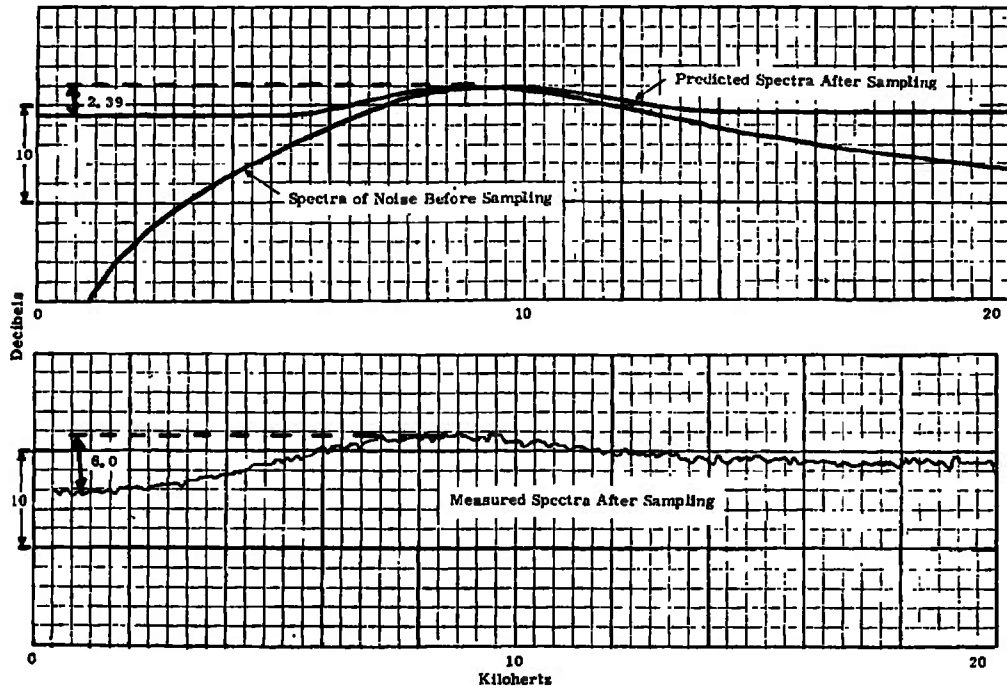


Figure 38. Electronic Simulation of Laser-Velocimeter Spectra Measurements from Random-Time Sampled White Noise of Bandwidth 6485 Hertz

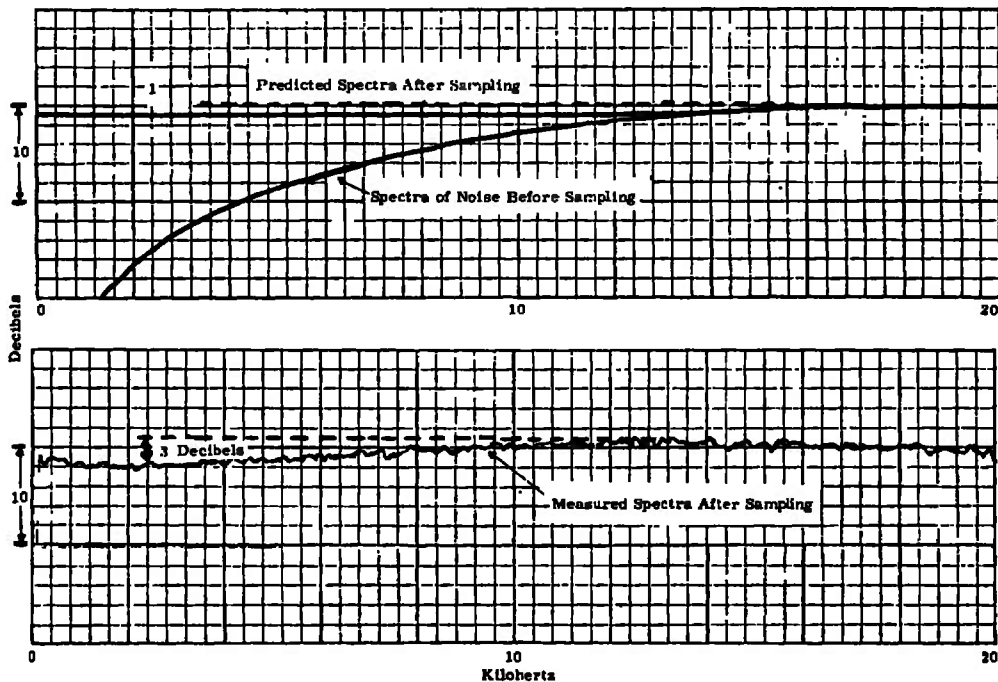
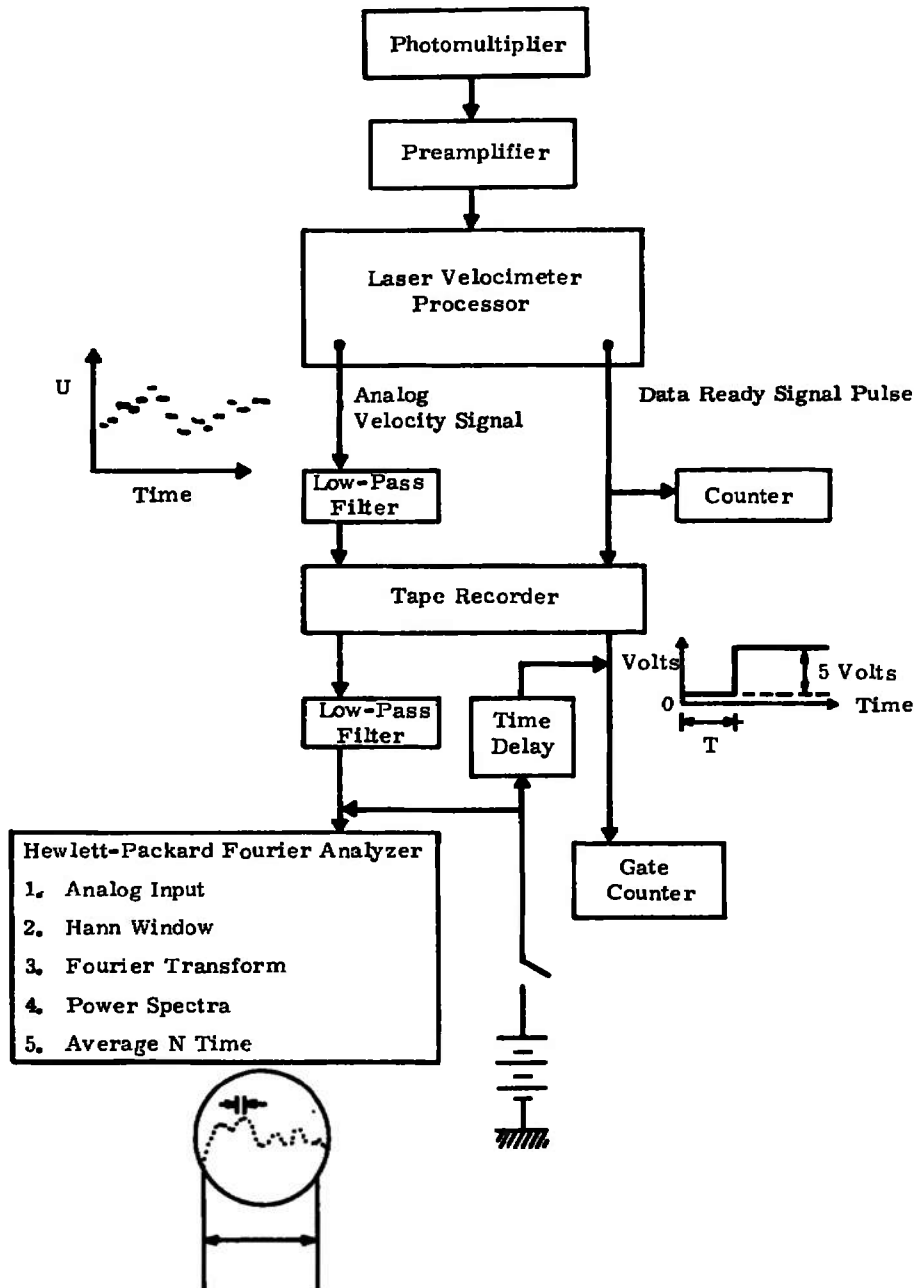


Figure 39. Electronic Simulation of Laser-Velocimeter Spectra Measurements from Random-Time Sampled White Noise of Bandwidth 25,700 Hertz

EXPERIMENTAL SETUP FOR SPECTRA ANALYSIS

A subsonic jet facility 3/4 inch in diameter was utilized in the attempt to obtain a power spectra measurement comparison between the hot wire and laser velocimeter. This facility was the same as that used previously for the experimental particle dynamics study. Figure 40 is a schematic diagram of the experimental setup and the data analyzing procedure.



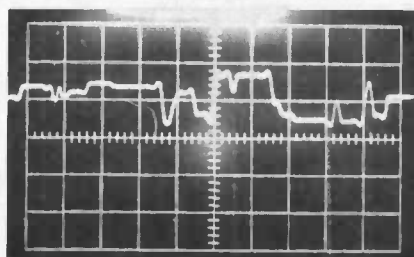
$$T = N \Delta T \text{ (e.g., } N = 256, \Delta T = 50 \mu\text{sec, } T = 12.8 \text{ msec)}$$

Figure 40. Schematic Diagram of Laser-Velocimeter Turbulence Spectra Measurements Setup

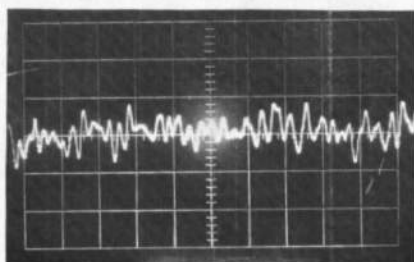
When a valid seeding particle was detected at the photomultiplier, an analog voltage directly proportional to the velocity of that particle was fed from the General Electric counter-type LV processor. The sample-and-hold circuit for this output held the preceding value of velocity until the next valid seeding particle was detected. This analog velocity signal passed through a low-pass filter (set at 8 kilohertz) and was recorded on a magnetic tape for future spectra analysis.

With the arrival of a particle passage and the output of its associated valid analog velocity, a "data ready" pulse is simultaneously generated. Normally this pulse of 2-microsecond width is used to strobe the pulse height analyzer (when in the "coincidence mode") and is also fed to a pulse counter to determine the data acquisition rate. In this case, the pulse height analyzer, which is used for the measurement of time-averaged mean and turbulence velocities, was not employed. The pulse counter was utilized in its normal manner and was found to be misleading in providing realistic data acquisition rates. This matter will be discussed in the next part of this section.

The "data ready" pulse was analog-tape-recorded on an adjacent track with the analog velocity information. Velocity measurements at data rates between 2000 and 80,000 velocities per second were obtained for a jet flow at Mach number 0.15. Typical LV processor outputs at two data rates are shown in Figure 41. The recorded LV analog-velocity signal was analyzed on a



Velocity Time Trace at Low Seeding
Rate (≈ 2000 Particles per Second)



Velocity Time Trace at High Seeding
Rate ($\approx 80,000$ Particles per Second)

Figure 41. Typical Laser-Velocimeter Sample-and-Hold Output at Two Data Acquisition Rates

Hewlett-Packard 5451 marrowband Fourier analyzer and on a General Radio 1/3-octave-band spectrum analyzer.

Using the same jet facility and spectrum analyzers, a hot-wire amplifier (product of Thermo-Systems Inc.) with a linearized output was used to obtain the power spectra measurements of an $M = 0.15$ jet flow. The results are shown in Figures 42 to 47 and are typical of the measurements taken. The

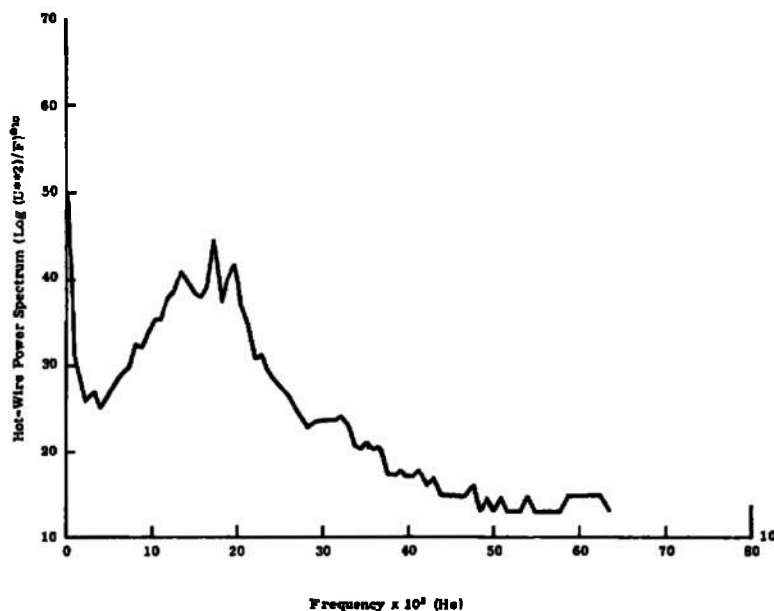


Figure 42. Hot-Wire-Turbulence Power Spectrum Results from 3/4-Inch-Diameter Air Jet ($M = 0.15$; $X/D = 2$; $Y/D = 0.2$)

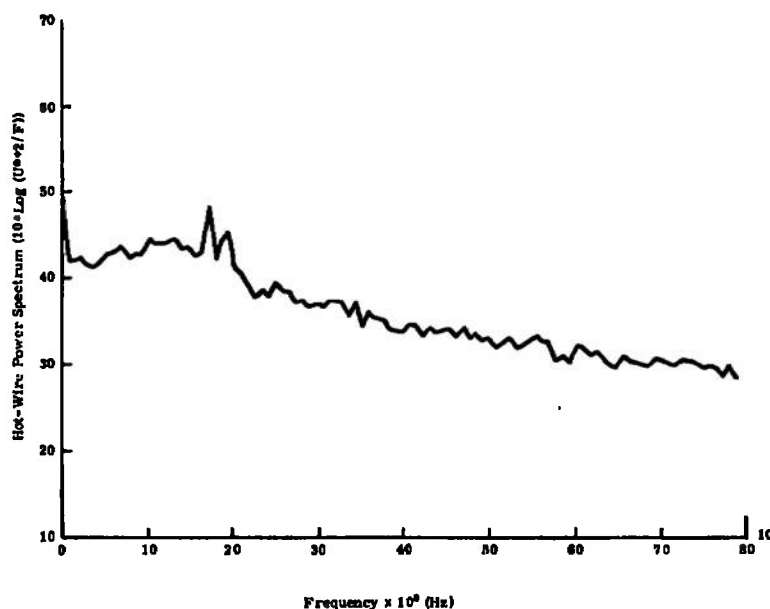


Figure 43. Hot-Wire-Turbulence Power Spectrum Results from 3/4-Inch-Diameter Air Jet ($M = 0.15$; $X/D = 2$; $Y/D = 0.4$)

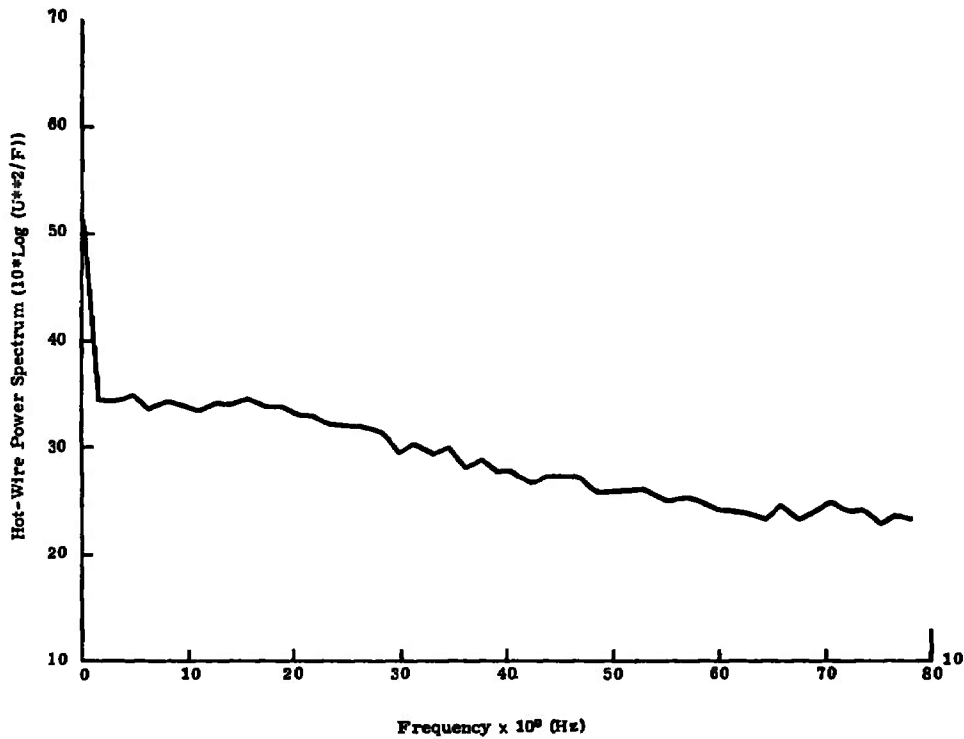


Figure 44. Hot-Wire-Turbulence Power Spectrum Results from 3/4-Inch-Diameter Air Jet ($M = 0.15$; $X/D = 6$; $Y/D = 0$)

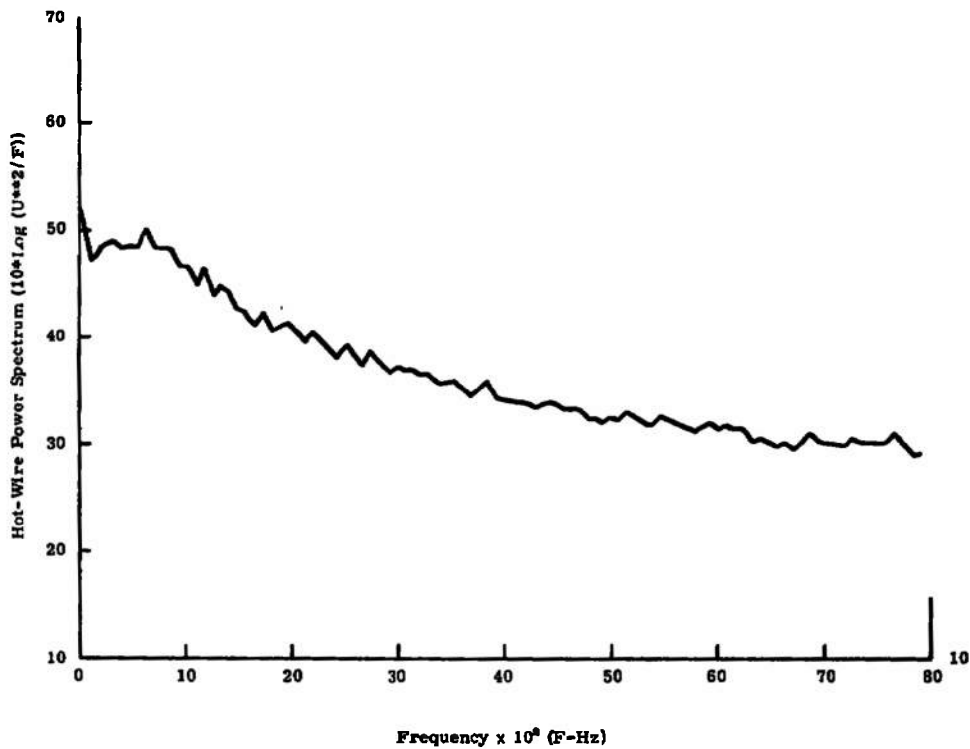


Figure 45. Hot-Wire-Turbulence Power Spectrum Results from 3/4-Inch-Diameter Air Jet ($M = 0.15$; $X/D = 6$; $Y/D = 0.2$)

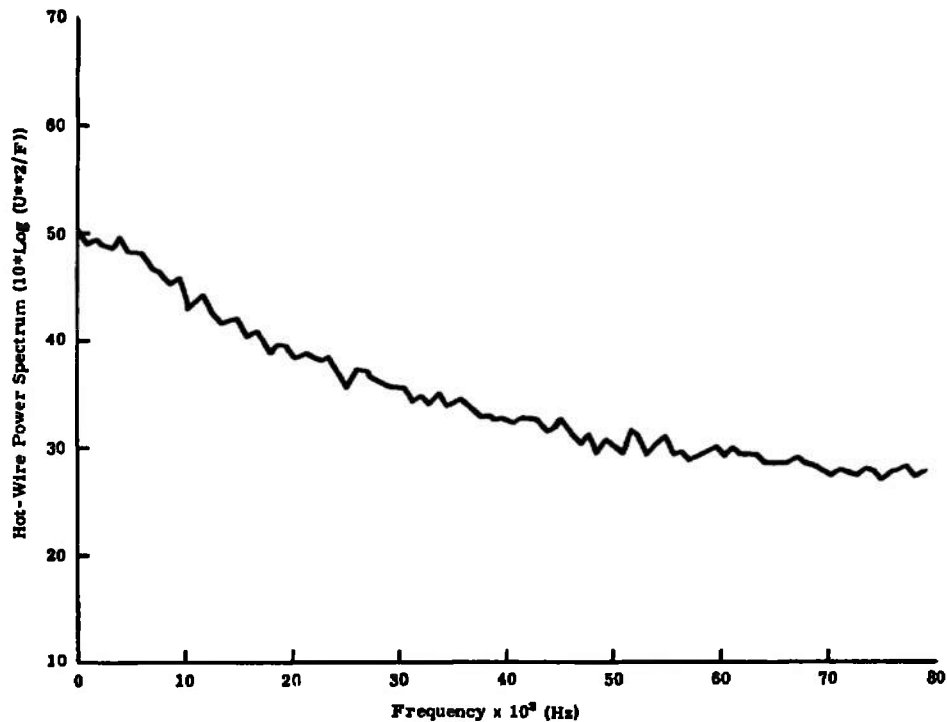


Figure 46. Hot-Wire-Turbulence Power Spectrum Results from 3/4-Inch-Diameter Air Jet ($M = 0.15$; $X/D = 6$; $Y/D = 0.4$)

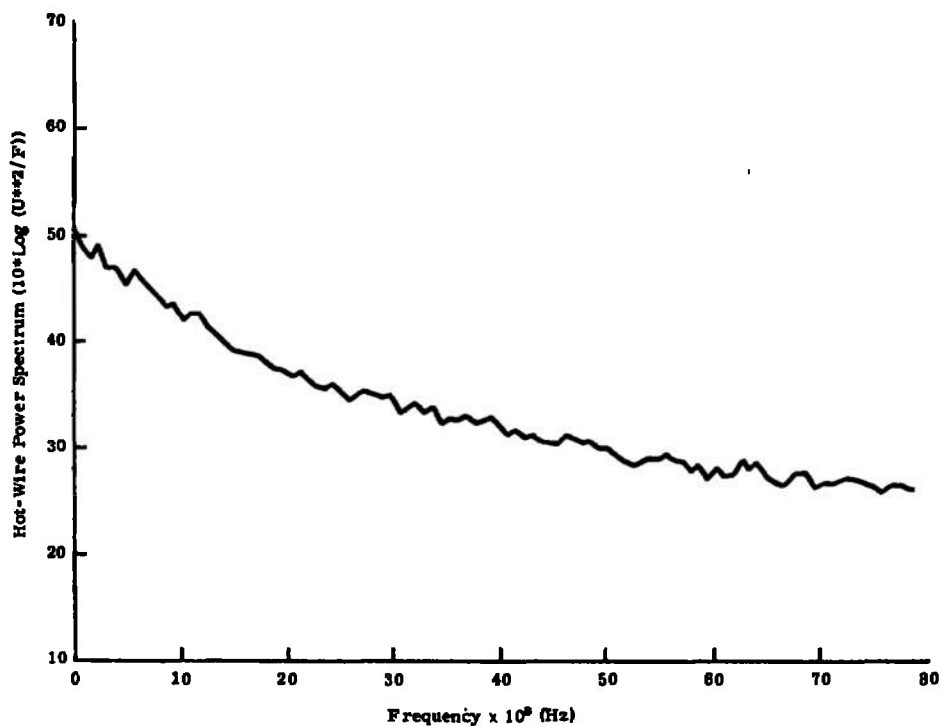


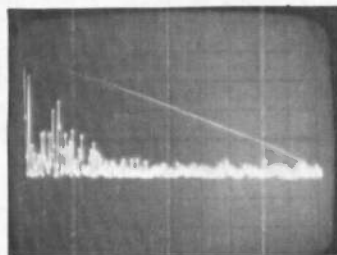
Figure 47. Hot-Wire-Turbulence Power Spectrum Results from 3/4-Inch-Diameter Air Jet ($M = 0.15$; $X/D = 10$; $Y/D = 0$)

potential core region is shown to have a more narrowband spectra associated with the jet Strouhal number. For downstream positions where mixing has taken place, the spectra have flattened out significantly. These results are similar to those reported by Fuller (Ref. 16).

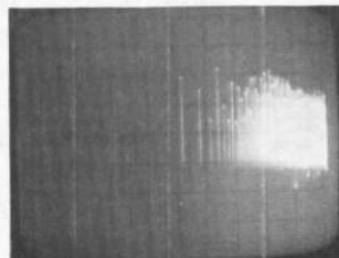
EFFECT OF SAMPLE-AND-HOLD OUTPUT CIRCUIT ON SPECTRA MEASUREMENTS

Inability to achieve satisfactory LV spectra results at the General Electric Research and Development Center may be in part attributable to the sample-and-hold circuit at the LV processor output. The theory presented in this report assumes "impulse type" sampling. It was originally assumed that the output sample-and-hold would provide the same function as in the case of the equispaced sample -- that is, act as a low-pass filter. In the LV data, however, its effect on the spectra is considerably more subtle.

This is best shown in Figures 48 and 49, where the results are those obtained. It may be seen that the peak is close to 800 hertz rather than the expected 1.3 kilohertz, and that there appears to be a superimposed decrease in the power spectra with increasing frequency.



$M = 0.6$, $X/D = 2$, $Y/D = 0$, $n = 25,000$ Particles per Second



Same as Above on Log-Log Scale

Figure 48. Typical Laser-Velocimeter Narrowband Power Spectra Output from HP5451 Fourier Analyzer (Sample-and-Hold Bias Present)

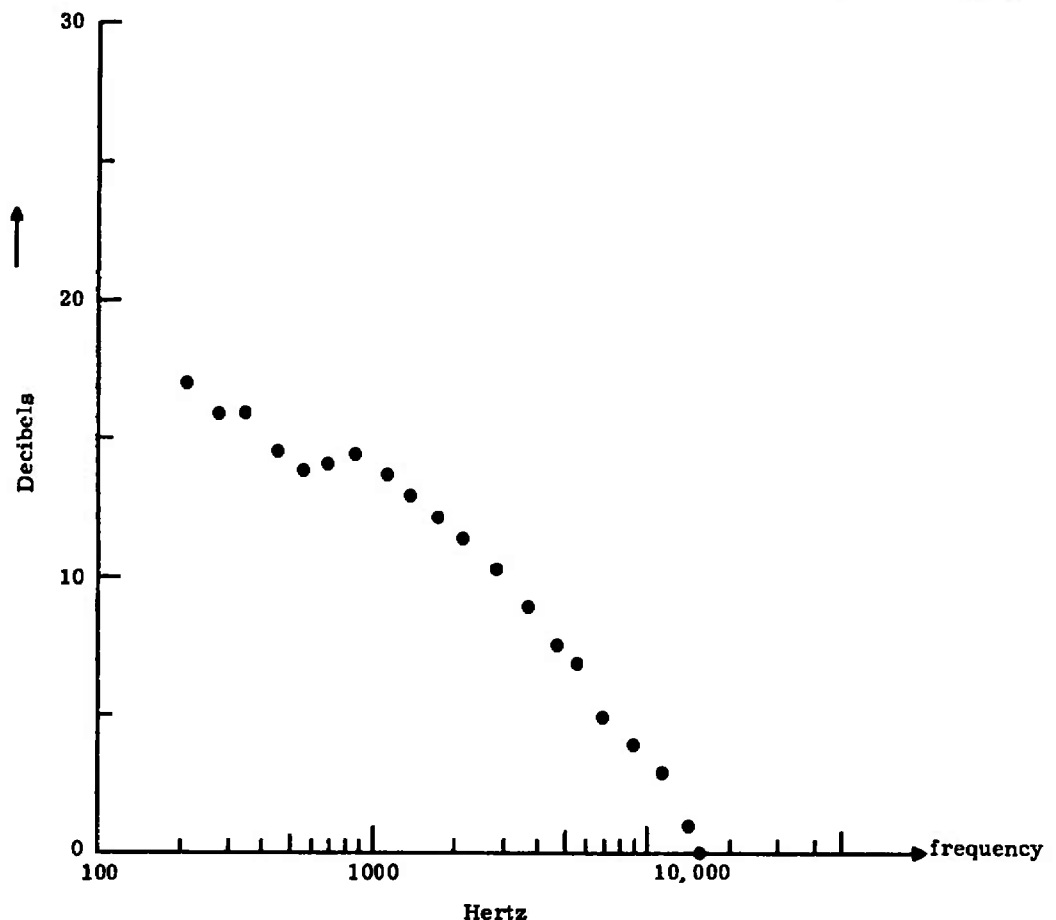


Figure 49. Typical Laser Velocimeter One-Third-Octave Power Spectra Output from General Radio Analyzer (Sample-and-Hold Bias Present)

To prove that these results were associated with the sample-and-hold circuit, a simple electronic simulation was made. Figure 50 shows the output of a narrowband noise source; Figure 51 shows the result of sampling this source by a Poisson type process, using impulse-type sampling -- the output set at zero between samples. A white noise is added to the spectra by the sampling process, as predicted by the theory.

Figure 52 shows the same process sampled by the same sampling sequence; in this case, however, sample-and-hold sampling is used -- the output between samples is set equal to the previous sample value. It may be seen that this latter sampling, by the use of a sample-and-hold simulation, has now added a low-frequency noise to the spectra, and the peak due to the source spectra has almost disappeared. Since the effects of this sampling are difficult to predict and the noise added by the sampling distorts the shape of the source spectra, this type of sampling should be avoided when estimating LV spectra.

Such an estimation may be accomplished if the sample-and-hold is followed by a sampling gate, activated by the "data ready" pulse available on most counter



Figure 50. Spectra of Unsamped Narrowband Process for Study of Sample-and-Hold Bias

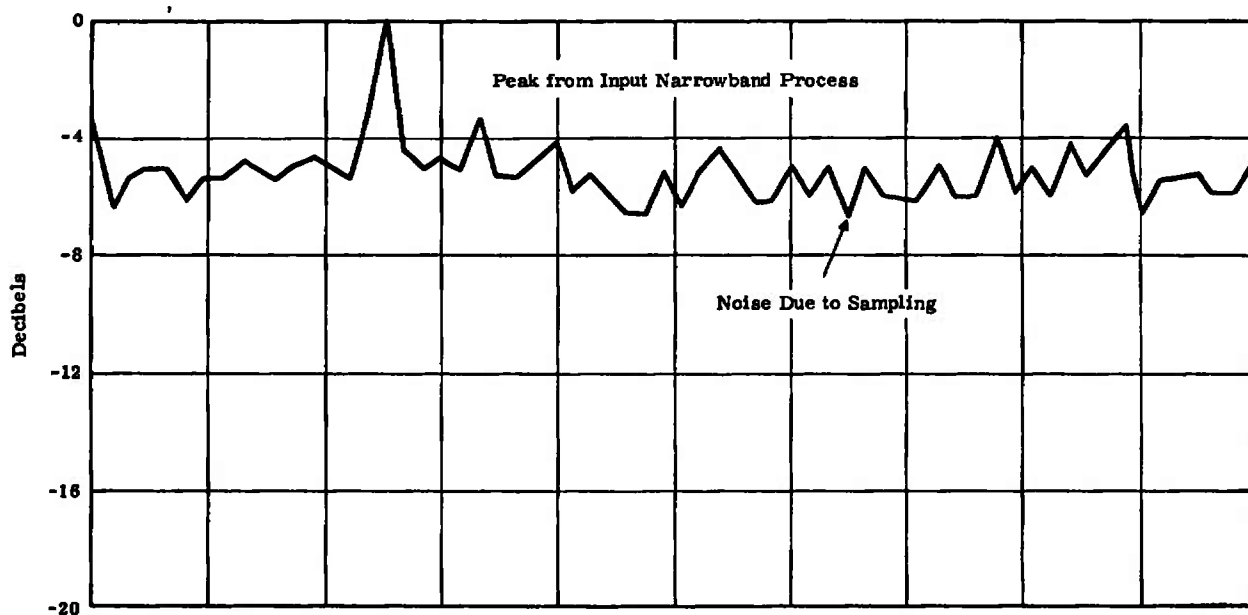


Figure 51. Spectra of Narrowband Process Sampled by a Poisson Impulse Sequence for Study of Sample-and-Hold Bias

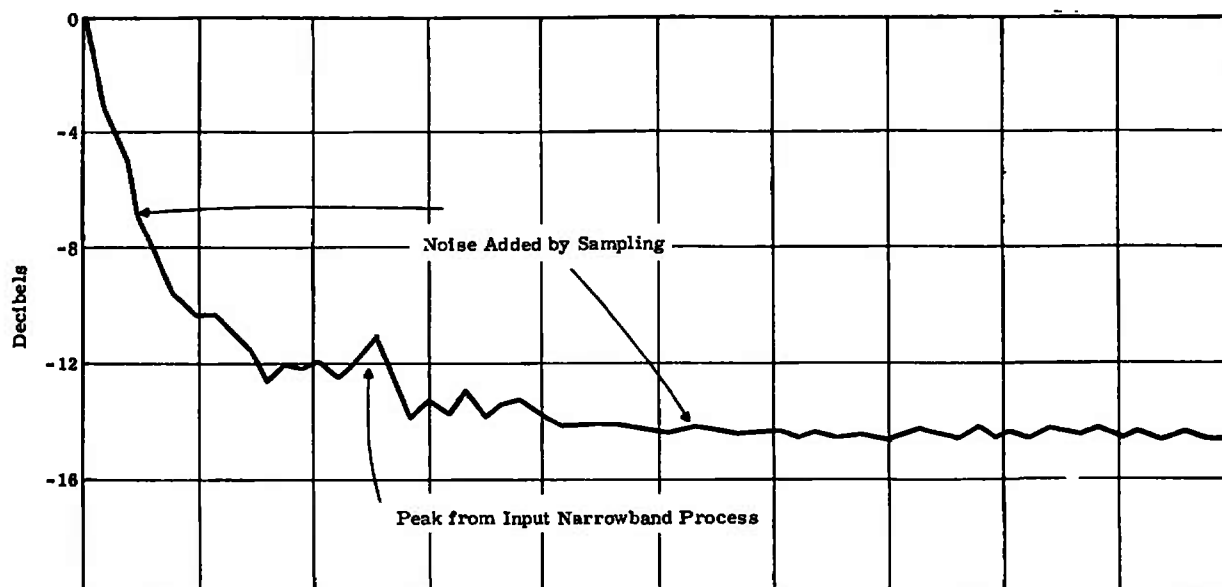


Figure 52. Same Process and Sampling as Figure 51 with the Addition of a Sample-and-Hold Simulation to Study its Low-Frequency Bias of Spectra Data

type LV processors. This will convert the output process to the impulse-sampling case.

MONITORING DATA ACQUISITION RATE

It was seen that accuracy of LV spectra measurements is dictated principally by the data acquisition rate associated with the output of valid velocity data. Monitoring therefore becomes crucial, since a large variance of wide-band noise may unexpectedly result by averaging of the power spectra of data slices of widely varying data rates. This average of many (greater than 50) short records (256- or 512-word block size) is found to minimize the spectra variance rather than the use of long records.

The use of a pulse counter for monitoring this data rate is not sufficiently accurate; it depends on pulse counting over a period of time which is probably not directly associated with the data slice being spectrum-analyzed. These data slices correspond in real time to 25 or 50 milliseconds, and it is normally impractical to gate the counter for such small intervals.

In these experiments the data acquisition rate was found to vary significantly because of the manner in which the high rate of seeding was injected into the flow. The high data rates required for this comparison of hot-wire and LV techniques showed data rate variations of five- or tenfold.

In an effort to quantify the actual data rate of the data slice being spectrum-analyzed, the following solutions were identified:

- Using the Hewlett-Packard analog-to-digital converter in the multiplex mode, both the velocity and data feed pulse were simultaneously input from the tape recorder. Visual inspection or computer manipulation of the data then yielded superpositions of spectra data at a data rate which was within the desired limits.
- Another method, which is perhaps most viable in the use of readily available equipment, employs the pulse counter in an externally strobed mode. As seen in Figure 53 a circuit may be added which defines the data rate at the same time the data are played back, for the precise time interval that the data are being digitally converted (Block Size \times Sample Time Increment). This is obtained by the use of a scope sweep gate pulse that is preset to provide a 5-volt peak during sweep. This voltage is converted by a simple gate to provide a logic 0 (zero voltage), thus enabling the counter during sweep, and a logic 1 (5 volts) during the time the scope is not sweeping. The Fourier analyzer and scope are started simultaneously by a pushbutton.

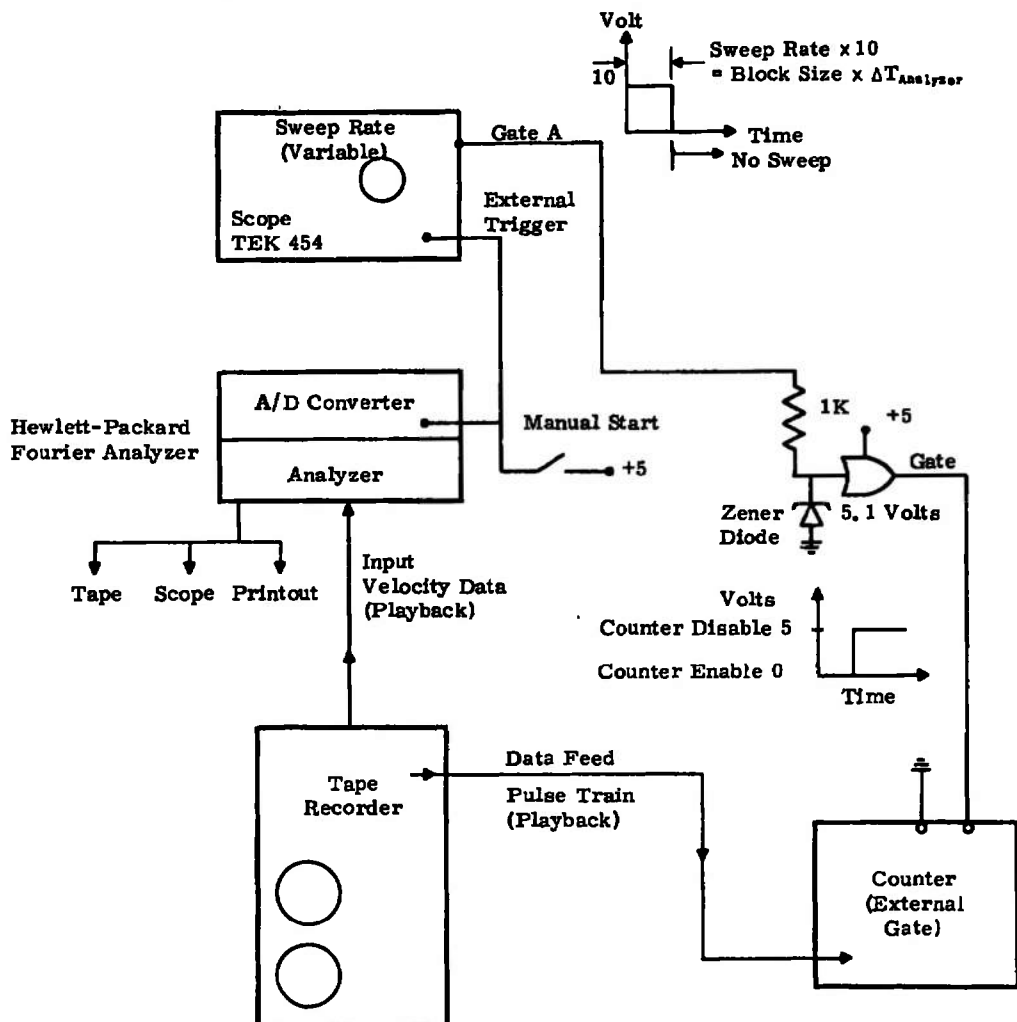


Figure 53. Schematic Setup of Turbulence-Power Spectra System

Section 6

SUMMARY AND CONCLUSIONS

The purpose of this investigation was to study the parameters which affect the feasibility of using the laser velocimeter optical technique for the measurement of turbulence power spectra. Based on this work, the following major results may be summarized:

1. From a theoretical and experimental standpoint, the particle relaxation time (turbulence- and shock-particle interactions) must be minimal for accurately measuring time-average and spectral properties of the fluid. Agglomeration or particles of a large size range were found to be significant factors in distorting these measurements.
2. Error by the counter-type processor may be generated by the use of a Schmitt trigger, or other electronic limiter circuit, as a result of the inherent amplitude modulation of the Doppler burst signature. Errors can also be traced to the use of a high-pass filter.
3. The spectra theory developed for random particle passages through the scattering volume indicates that wideband noise is superimposed on the true spectra. The magnitude of this noise is indirectly proportional to the mean particle arrival time or data acquisition rate.
4. At present, the theory has been confirmed by an electronic simulation at high data rates. A method for extending this analysis for obtaining laser-velocimeter turbulence spectra data at low data rates has been eluded to in this report. While this method was not explored in detail, it may be expected that a greater system complexity and investment, and significantly longer analysis times, would be required to obtain such spectra.*
5. The use of a sample-and-hold output circuit was shown to cause a spectral bias to low frequencies. This was overcome by an electronic gating circuit.
6. Monitoring of the actual data rate for a data slice being spectrum-analyzed was found to be critical. Two methods for accomplishing this were given.

*Recent work by the General Electric and Lockheed-Georgia Companies have shown this lower data rate approach to be feasible. This work was done in the Supersonic Jet Exhaust Noise program, which is jointly supported by the Department of the Air Force Aero Propulsion Laboratory (P. Shahady, Project Engineer) and the Department of Transportation.

Section 7

REFERENCES

1. W.B. Jones, Laser Fluid Sensor, paper presented at the Fluids Engineering Conference, American Society of Mechanical Engineers, Pittsburgh, Pa., May 9-14, 1971.
2. W. T. Petit, III, The Laser Doppler Velocimeter for Measuring Turbulence in Gas Flows, Masters Thesis, Polytechnic Institute of Brooklyn, Brooklyn, N.Y., June 1970.
3. J. A. Asher, Laser Doppler Velocimeter System Development and Testing, Report No. 72-CRD-295, General Electric Company, Schenectady, N. Y., October 1972; soon to be published in Progress in Astronautics and Aeronautics series, American Institute of Aeronautics and Astronautics.
4. J. C. F. Wang and J. A. Asher, Three-Dimensional Diagnostical Techniques -- Laser Velocimeter Hypersonic Velocity Measurements, Final Report, Aerospace Research Laboratories, Wright-Patterson Air Force Base, Ohio, Contract No. F33615-71-C-1867, Project No. 7065, General Electric Company, Schenectady, N. Y., May 1973.
5. P. W. Mossey, J. A. Asher, and P. R. Knott, "Differential Laser Doppler Velocimeter Investigation," Supersonic Jet Exhaust Noise (M. J. Benzakein and P. R. Knott, eds.), Technical Report No. AFAPL-TR-72-52, Air Force Aero Propulsion Laboratory, Wright-Patterson Air Force Base, Ohio, August 1972.
6. D. C. Wisler and P. W. Mossey, Gas Velocity Measurements Within a Compressor Rotor Passage Using the Laser Doppler Velocimeter, Report No. 72-AEG-287, General Electric Company, Cincinnati, Ohio, September 1972.
7. M. Lapp, C. M. Penney, and J. A. Asher, Application of Light Scattering Techniques for Measurements of Density, Temperature and Velocity in Gas Dynamics, Final Report No. ARL-TR-72-0045, Aerospace Research Laboratories, Wright-Patterson Air Force Base, Ohio; or Report No. SRD-72-085, General Electric Company, Schenectady, N. Y., July 1972.
8. A. E. Lennert, et al., Summary Report of the Development of a Laser Velocimeter to be Use in AEDC Wind Tunnels, Report No. AEDC-TR-70-101, ARO Inc., Arnold Air Force Station, Tenn., July 1970.
9. Arnold Engineering Development Center, Test Facilities Handbook, 9th ed., Arnold Air Force Station, Tenn., July 1971.
10. H. A. Becker, H. C. Hottel, and G. C. Williams, "On the Light-Scatter Technique for the Study of Turbulence and Mixing," Journal of Fluid Mechanics, Vol. 30, Part 2, 1967, pp. 259-284.

11. J. Loeffler, Experimental Investigation of Underexpanded Axisymmetric Jet Flows Interacting with Transversely Impinging Radial Converging Jet Flows, Masters Thesis, Syracuse University, Syracuse, N. Y., August 1967.
12. W.M. Farmer, On the Measurement of Particle Size, Number Density and Velocity Using a Laser Interferometer, report on Contract No. F40600-72-C-0003, Arnold Research Organization, Arnold Engineering Development Center, Arnold Air Force Station, Tenn.
13. C.S. Lorens, "Recovery of Randomly Sampled Time Sequences," IRE Transactions on Communications Systems, Vol. CS-10, June 1962, pp. 214-216.
14. Y.W. Lee, Statistical Theory of Communication, John Wiley and Sons, Inc., New York, N. Y., 1960.
15. G.J. Hahn and S.S. Shapiro, Statistical Models in Engineering, John Wiley and Sons, Inc., New York, N. Y., 1967.
16. C.E. Fuller, Development Testing and Application of a Three-Dimensional Laser Doppler Velocimeter for the Measurement of Gas Flows, Engineering Report No. 1678 (CR-102948), National Aeronautics and Space Administration Contracts No. NAS8-21527 and NAS8-21162, Hayes International Corporation, Birmingham, Ala., April 1970.

Appendix I

LASER VELOCIMETER OPTICAL SETUP AND PROCESSOR

To provide a better basis for the subsequent discussion of the parameters affecting laser-velocimeter power spectra measurements, this appendix should offer a brief background of the optical setup and processor used during the experimental portions of this study.

DUAL-SCATTER OPTICAL METHOD

Two basic optical techniques are used in laser velocimetry: 1) reference beam, and 2) dual-scatter. The dual-scatter (Figure 54), compared with the reference beam, has been shown to be easily aligned and relatively vibration-free, and results in a scattering light with a greater signal-to-noise ratio. These attributes have made the dual-scatter configuration predominant in the recent literature.

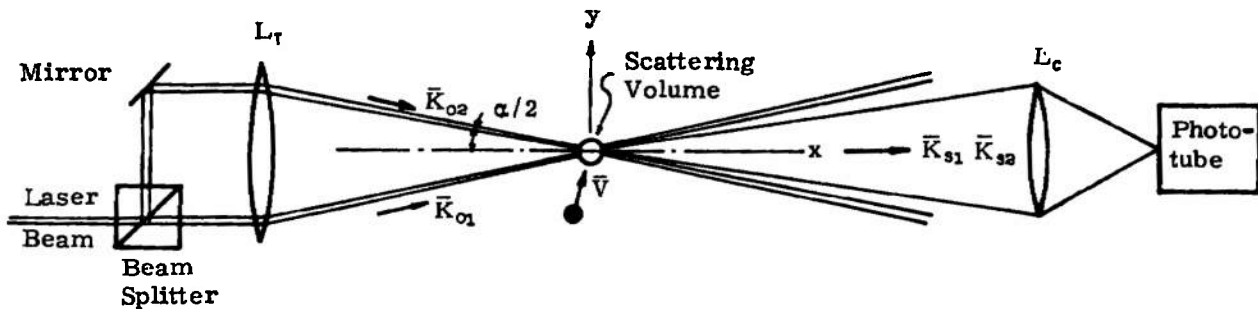


Figure 54. Dual-Scatter or Differential Doppler Arrangement

An analysis of the dual-scatter method can perhaps be most easily understood by considering the interference pattern created by two intersecting beams of coherent radiation, each having a wavelength λ_0 . Referring to Figure 55, at the scattering volume formed by the cross beams, constructive interference occurs when the optical path length, Δ , between the two beams differs by an amount $n\lambda_0/2$, or n odd. Similarly, destructive interference occurs when $\Delta = n\lambda_0/2$ for n even. Planes of constant optical path-length difference between the two beams are parallel to the plane that bisects the two beams. Thus, the fringe spacing, s , is given by

$$s = \frac{\lambda_0}{2} \left(\frac{1}{\sin \frac{\alpha}{2}} \right) \quad (71)$$

As the particle passes through these fringes at velocity v , light is scattered only when it is in a bright fringe; hence, the scattering frequency, $\Delta\nu$, is simply

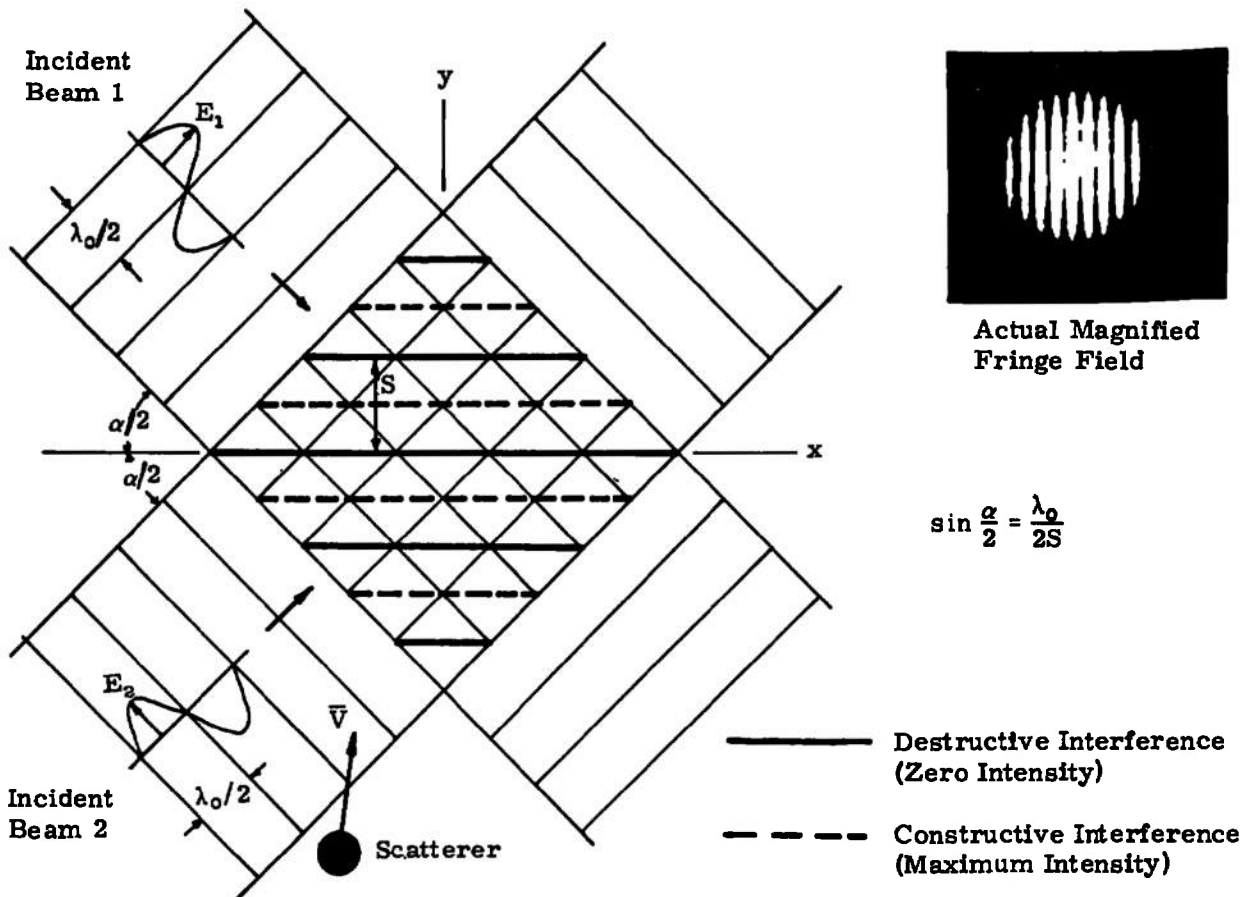


Figure 55. Interference Fringes Formed by Two Coherent Crossed Beams

$$\Delta v = \frac{\Delta \omega}{2\pi} = \frac{v_y}{S} = \frac{2v_y}{\lambda_o} \sin \frac{\alpha}{2} \quad (72)$$

where v_y is the velocity component perpendicular to the fringes. The interference pattern considerations are easier to visualize when analyzing the LV as a velocity measuring device, since the pattern can be thought of as a light grid placed in the flow to define an accurate displacement increment, s . Then the local velocity normal to the fringes is simply s/t , where t is the transit time between bright fringes.

LASER-VELOCIMETER COUNTER PROCESSOR

A series of electronic circuits has been designed at the General Electric Research and Development Center which translates the average Doppler frequency of a particle going through the data probe volume into an analog voltage proportional to the average Doppler transit time (Ref. 3). This direct counting approach is similar to that adopted by the Arnold Engineering Development Center, except that it does not use pulse stretching (Ref. 8). A block diagram of the complete signal processor is shown in Figure 56.

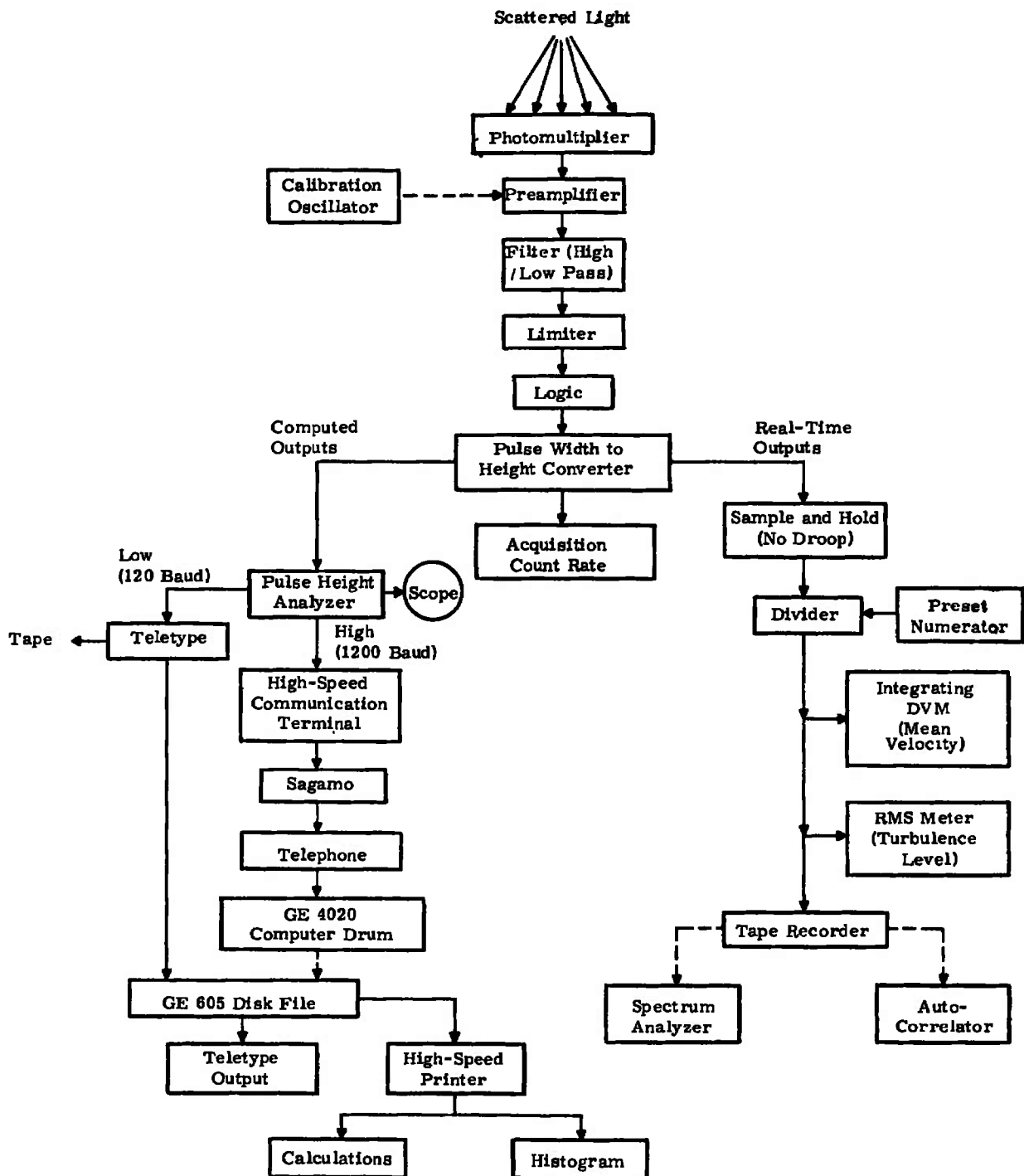


Figure 56. Laser Velocimeter Data Reduction

The LV-counter-processor system consists of three major components:

- Front-end detector module (FED)
- Logic output and display module (LOD)
- Waveform generator module (WG)

This system differs from the conventional frequency-tracker system in that it measures the velocity of individual particles. As such, the counter system is not degraded in accuracy for lightly seeded flows. This is a distinct advantage in the case of gas flows where high-density seeding is not easily obtained. Other advantages include:

1. Reduced signal-to-noise ratio requirements.
2. A high data rate, limited primarily by peripheral storage devices external to this system.
3. Absence of ambiguities due to multiple particles and finite passage time.

The processing of a scattered light signature from the particle passage across the scattering or probe volume begins by the amplification of the photomultiplier output. To prevent signal distortion, this first amplifier is mounted close to the photomultiplier (RCA 8645) and remote from the main processing unit. The Doppler burst presented at the input of the front-end detector (FED) module is again amplified by a FED input amplifier. It is passed through a selectable high-pass filter to remove the superimposed lower-frequency pedestal waveform which acts as an envelope to the Doppler burst signature (Figure 57). The resulting signal is then electronically limited about the zero crossing point (subject to the hysteresis added to eliminate switching due to noise by the Schmitt trigger). Prior to the high-pass filtering, the amplified Doppler burst is passed through a buffer amplifier and presented to a comparator to determine whether or not it exceeds a preset threshold height. If the threshold is exceeded, the overload output is driven to ground, indicating to the LOD that the data being processed should be ignored.

The TTL compatible square-wave pulse train, corresponding to the passage of a particle by adjacent interference fringes from the FED module, is then fed to the logic output and display (LOD) module.

The LOD module consists of two timers, validation circuitry, and control logic. It is entirely digital, with the exception of a portion of the validation and output translation circuitry. At the occurrence of the first pulse, a 100-megahertz clock is gated to two counters. When 5 pulses have occurred, the first counter is stopped. When 8 pulses have occurred, the second counter is stopped.

Although each counter consists of 16 bits, only eight bits are selected, depending on the scale setting. When the counters are stopped, the eight bits

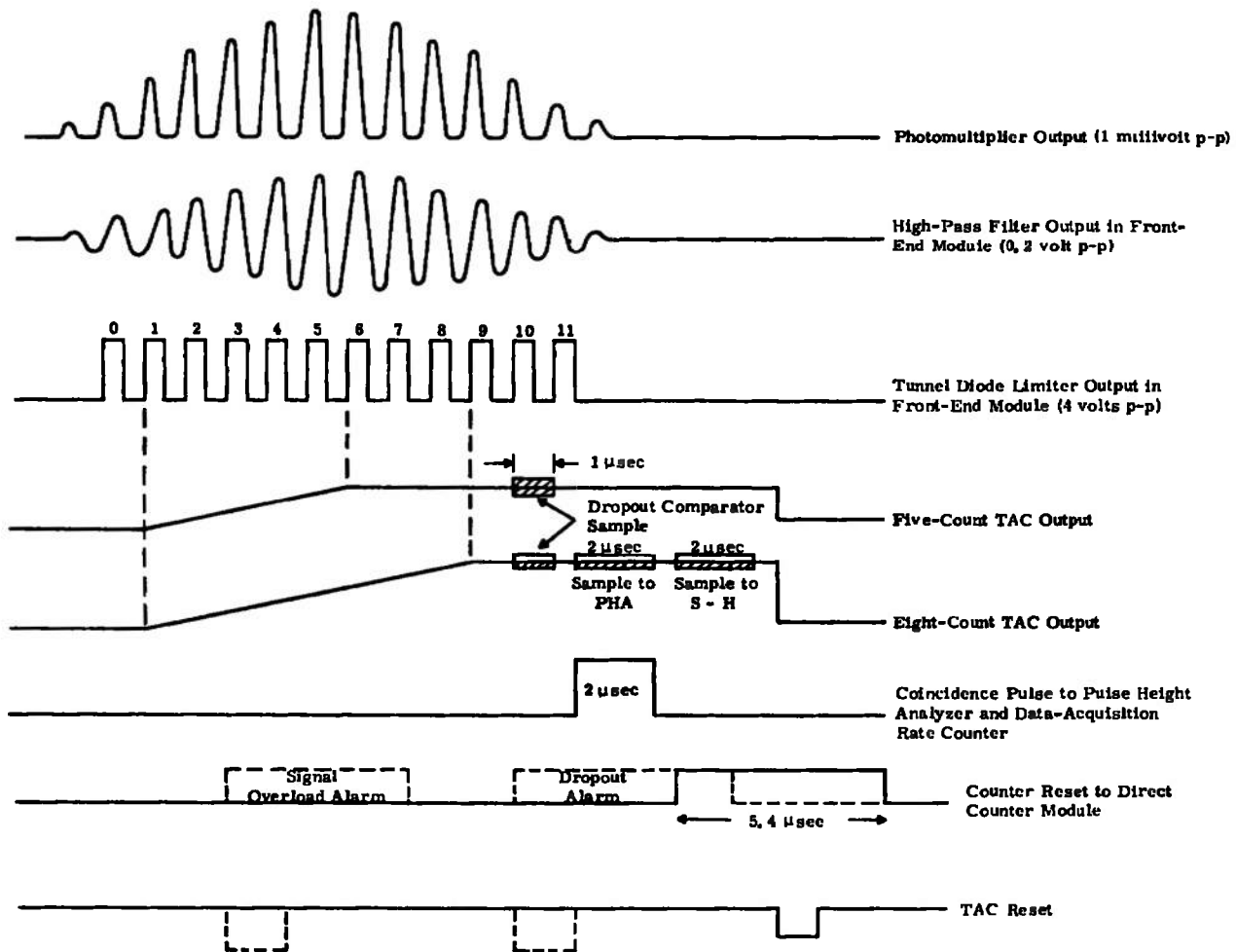


Figure 57. Timing Diagram for Laser Velocimeter Processor

from each counter are passed through a digital-to-analog converter. The outputs are compared, for the proper 5:8 ratio. The allowable error is set by a front panel adjustment. If the allowable error is exceeded, the data are ignored, the counters are reset, and the input circuit is enabled to begin another reading. If the readings are validated (within set error limits), the output from the eight-pulse counter is strobed into a storage register.

The data obtained are then presented, along with the scale, to a digital output located on the rear panel, where it is converted to an analog signal. When the D/A converter has settled, the "data ready" line, which was brought to the high state as the data were strobed to the storage register, is lowered, indicating the validity of the data. The analog signal is passed through a divider to convert the time measurement to frequency; either time or frequency may then be selected at the front panel. In the case of power spectra measurements the output is taken directly, as an instantaneous velocity which goes to an analog tape recorder and/or a spectrum analyzer. Other optional readouts include an eight-bit digital output and a display meter where the velocity signal has been low-pass-filtered.

With each new output of data, the result of the comparison is stored. The ten most recent samples at any one time are stored in a shift register. The parallel outputs are summed, filtered, and the resulting voltage is applied to a front panel meter to yield the percentage of data validated. At any time prior to data validation; the counters will be reset and the input circuitry will be enabled for the next measurement. If the counters exceed the selected eight-bit range, an overflow will be detected and the circuitry will be reset.

One of the most important aspects of this processor is the use of the 5:8 counter output comparison (Ref. 3). This provides an inhibit of the measured output velocity where one or both counters has missed a pulse. This may occur because of the trajectory of the particle through the scattering volume and/or because of a large particle size. In either of these cases, significant amplitude modulation of the scattered light may exist as the particle passes through the scattering volume. The analog voltage representing this Doppler burst will mirror this amplitude modulation and, as a result, the fixed threshold limiter and counters may miss one or more pulses. This difficulty, called "Doppler dropout,"* is a common occurrence during the use of counter processors. Generally speaking, the use of small particles, large fringe spacing, and viewing of only a small portion of the scattering volume near the beam intersection point tends to minimize the probability of Doppler dropout.

To calibrate the LV signal processor, a calibration waveform generator is used. The unit produces a signal of known frequency (0.1 to 25 megahertz) for data acquisition rates up to 200 kilohertz and for contrast ratios (the Doppler/Doppler plus pedestal height) of 0 to 100 percent. Furthermore, it is possible to scan or modulate by FM the preset center Doppler frequency by ± 10 percent, for a complete, unbiased assessment of the LV signal processor's accuracy in turbulent media, without having to provide a known flow for comparison.

As shown in Figure 56, two alternative paths presently exist for measuring the mean and fluctuating velocities. For the computed output, the voltage signal, which is inversely proportional to the particle velocity, is fed into a Northern Minicon 256-channel, pulse-height analyzer for sorting, V , and a small incremental voltage interval, ΔV . Thus, the memory for each channel contains a count of the number of signals at voltage V in the interval ΔV , and the memory output for all the channels then gives the probability of V [$P(V)$ as a function of V]. This probability factor can easily be converted into a probability distribution in the velocity.

All channels have an equal time interval, Δt ; a two-point calibration is put on the display to define the horizontal time axis and, hence, the time interval between channels. If u is the velocity normal to the fringes of spacing, s , then

*Not to be confused with the same nomenclature for frequency trackers, where this means loss of signal acquisition due to low duty cycle.

$$u = S\Delta\nu$$

where $\Delta\nu$ is the Doppler frequency (fringes per second) of the photomultiplier output signal. It can be shown that the mean velocity is the centroid and the turbulence velocity is the standard deviation of the velocity probability distribution. Other moments of this distribution are likewise easily computed.

The dump of the pulse-height analyzer memory is done at low (120 baud) or high speeds (1200 baud, which implies a dump of 15 seconds' duration) by the use of normal telephone lines. A sample computer readout (calculations and velocity probability distribution) is shown in Figure 58.

This LV processor system has a bandwidth of Doppler frequencies from 100 kilohertz to 25 megahertz. The instantaneous accuracy of the system (single-particle measurement) is 1 percent, up to 8 megahertz and drops to 3 percent at 25 megahertz. The maximum data acquisition rates are 188,000 and 760,000 velocities per second for analog and digital outputs, respectively.

RUN NO.=101 X/D= 3.000 Y/D= 0. SAMPLE TIME(SFC)= 49.

NOZZLE DIA.(INCH)	PRINGF SPACING(MICRO.FT)	CHAN.OEL T (MICROSEC)	TEMP 1(F)	ROOM PR. (MM, MG)	NOZ.PR (IN, W20)
0.500	98.804	0.001712	79.0	757.000	19.912

EXIT-CORP(F/S)= 291.06 EXIT MACH NO.= 0.260 REYN NO.= 75421.

U-MEAN VEL. (F/S)	U/UEX-TH	MEAN FREQ.	U PRIME (F/S)	U PRIME/UEX-TH	U PRIME/U
279.78	0.961	2.8317F=06	11.786	0.040	0.042

CT MAX= 3338. CT MAX/TOT. COUNT= 0.062 TOTAL COUNT= 54087.

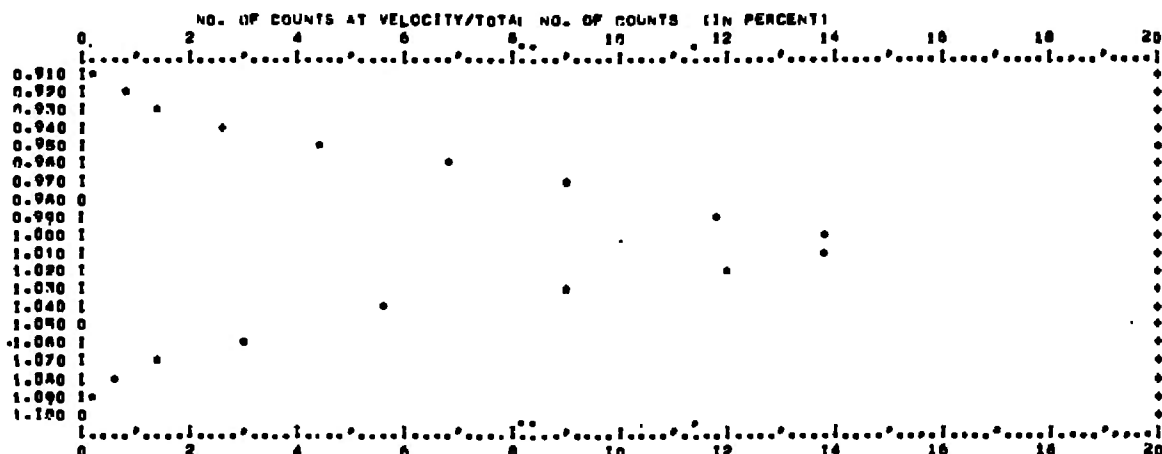


Figure 58. Typical Computer Readout from a Laser Doppler Velocimeter Signal Processor

NOMENCLATURE

SYMBOLS

a	Particle radius
A	Height of sampling signal
d, d_p	Particle diameter
D_j	Jet exit diameter
D_{NB}	Discernibility (linear scale) for narrowband process
D_{WB}	Discernibility (linear scale) for wideband process
E	Electromagnetic field vector of laser beam
f	Frequency
F	Magnitude of Fourier coefficients
g	Sampled velocity signal from laser velocimeter measurement
H	Gain due to optics and particle scattering cross section
Int	Integer value
K	Wave number of laser lights; number of random particle arrivals; constant = 1.8 (Section 2); ratio of specific heats
M	Mach number
$m(t)$	Continuous velocity signal
N	Number of Doppler pulses required by counter-type processor; independent trial number
p	Probability
P	Pressure (psia); probability
R_A	Pedestal ripple of high-pass Doppler burst
R_N	Distance perpendicular to axis of laser beam
R_{xx}	Correlation coefficient
s	Sampling signal due to discrete random passage of particle through scattering volume
S	Fourier coefficients
t	Time
T	Temperature ($^{\circ}R$); time period for integration
T_ℓ	Data record length
ΔT	Time separation for independent trial or particle passage

u, U	Velocity
v	Velocity
V	Area-averaged (over particle) voltage output from photodetector due to particle light scattering
V_p	Voltage output from photodetector due to particle light scattering
X_N	Distance along axis of laser beam

GREEK LETTERS

α	Ratio of voltages -- limiter threshold/minimum acceptable signal amplitude
β	Half the e^{-1} location of center of scattering volume
γ	Inverse of relaxation time
θ	Half laser-beam intersection angle
λ	Time-averaged seed rate
μ	Height of impulse to broadband level; defined as $\sqrt{2} \theta KB$; dynamic viscosity
$\mu_o(\omega)$	Set of impulses
ρ	Density
ω	Natural frequency of light, $2\pi C/\lambda$; also generalized frequency, $2\pi t/f$
ω_o	Filter cutoff frequency

SUBSCRIPTS

3db	Three-decibel or half power point
f	Fluid property
g	Related to measured value
j	Related to air-jet exit diameter or theoretical velocity
l	Low
m	Related to true value
N	Intersecting laser beam designation; $N = 1$ or 2
o	Stagnation conditions; filter cutoff; cutoff frequency of wideband process
p	Related to particle or photodetector

r Associated with relaxation phenomena
STP Related to standard temperature and pressure

SUPERSCRIPTS

— Average value
' Rms fluctuation
^ Estimated value